Joint Monitoring Programme for Ambient Noise North Sea

2018 – 2020

Jomopans model benchmarking and sensitivity studies

WP 4

Deliverable/Task: T4.2

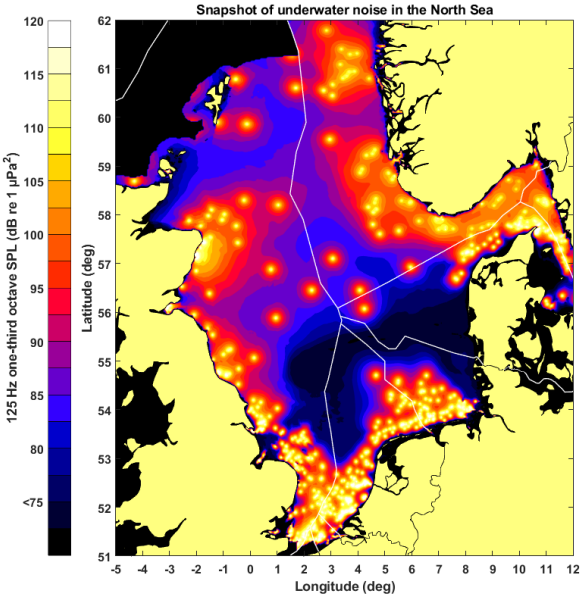

Authors: Christ de Jong (TNO), Bas Binnerts (TNO), Martin Östberg (FOI), Ilkka Karasalo (FOI), Thomas Folegot (QO), Dominique Clorennec (QO), Michael Ainslie (JASCO), Alex MacGillivray (JASCO), Graham Warner (JASCO), Lian Wang (NPL)

Affiliations: TNO (NL), FOI (SE), QO and JASCO (for RWS, NL)

Date: June 2021

Project Full Title	Joint Monitoring Programme for Ambient Noise North Sea
Project Acronym	Jomopans
Programme	Interreg North Region Programme
Programme Priority	Priority 3 Sustainable North Sea Region

Colophon	
Name	Christ de Jong (WP4 lead)
Organization Name	TNO
Email	christ.dejong@tno.nl

This report should be cited:

de Jong, CAF, Binnerts, B, Östberg, M, Karasalo, I, Folegot, T, Clorennec, D, Ainslie, MA, MacGillivray, A, Warner, G, Wang, L (2021) Jomopans model benchmarking and sensitivity studies. Report of the EU INTERREG Joint Monitoring Programme for Ambient Noise North Sea (JOMOPANS)

Cover picture: Snapshot of modelled underwater noise from ships and wind in the North Sea, produced by TNO

Table of contents

1 Introduction 6

2 Propagation model benchmarking 7

2.1 Previous benchmark studies for propagation loss models 7

2.2 Overview of benchmarked propagation models for ship noise 8

2.3 Test case 1: Range-independent environment 9

2.4 Test case 2: upslope bathymetry 17

2.5 Test case 3: wind noise source and propagation model 22

2.6 Discussion 23

3 Model parametrization – sensitivity studies 25

3.1 Spectral resolution 25

3.2 Spatial resolution 27

3.3 Spatial processing for sound maps 29

3.4 Temporal resolution 30

3.5 Spatial source gridding 32

3.6 Configuration of propagation models 34

4 Sensitivity scenarios 36

4.1 Seabed loss 36

4.2 Surface loss 40

4.3 Sound speed profile 44

5 Ship source level model and statistics 48

5.1 Wales & Heitmeyer (2002) 48

5.2 RANDI 3.1 (Ross, 1978, Breeding et al, 1996) 48

5.3 ECHO Source Level data (MacGillivray & Li, 2018) 49

5.4 RANDI 3.1 model versus the ECHO data set 50

5.5 Ship source model update RANDI 3.1a 51

5.6 Ship source model update RANDI 3.1b 52

5.7 Ship source model update RANDI 3.1c 52

5.8 Updated RANDI 3.1c model compared with SHEBA dataset 56

6 Statistical modelling 60

6.1 Acoustic modelling for ambient noise maps (ships and wind) 60

6.2 Uncertainty in the percentiles 61

6.3 Uncertainty in SPL (or level difference) time series 61

6.4 'Monte Carlo' approach 62

6.5 Gervaise et al [2015] approach 62

6.6 Source level statistics 62

6.7 Acoustic metric statistics 63

7 Conclusions and way ahead 64

7.1 Model verification: 64

7.2 Model sensitivity studies 64

7.3 Way forward 64

8 Acknowledgement 66

9 References 67

Summary

The aim of the Jomopans project is to develop a framework for a fully operational joint monitoring programme for ambient noise in the North Sea. Output will be the tools necessary for managers, planners and other stakeholders to incorporate the effects of ambient noise in their assessment of the environmental status of the North Sea, and to evaluate measures to improve the environment.

Sound is omnipresent in the underwater environment and can be produced by natural (e.g. waves, weather, animals) and anthropogenic (e.g. shipping, construction) sources. International concern increasingly focuses on the potential negative effects of anthropogenic underwater noise on sensitive marine fauna. Sound sources, sound transmission, and the distributions of vulnerable species in the North Sea are all transnational questions which must be tackled transnationally, as specifically required by the Marine Strategy Framework Directive.

The project will deliver an innovative combination of state of art acoustic modelling and high-quality measurements at sea for an operational joint monitoring programme for ambient noise in the North Sea. The use of consistent measurement standards and interpretation tools will enable marine managers, planners and other stakeholders internationally to identify, for the first time, where noise may adversely affect the North Sea. Next, we will explore the effectiveness of various options for reducing these environmental impacts through coordinated management measures across the North Sea basin.

This report provides a description of the benchmarking and sensitivity studies for the acoustic models selected in WP4, as deliverable of task 4.2

1 Introduction

The primary objective of the modelling work package (WP4) is to develop and demonstrate verified and validated[1] modelling methods applicable for generating maps of ambient noise in the North Sea, as input for assessment of the environmental status. Based on the guidance provided by WP3 (standardization), appropriate modelling approaches are selected and implemented for the most important sound sources (such as ships and wind) and for underwater sound propagation in the North Sea. A secondary objective is to use the proposed modelling method to generate maps of the ambient noise in the North Sea for the year 2019. WP6 will evaluate the uncertainty of the modelling results using the measurements from the Jomopans stations coordinated by WP5.

An inventory of models and data sources was made in Jomopans task 4.1 [de Jong et al, 2018].

In chapter 2 the acoustic propagation model and wind noise model implementations available to the Jomopans partners are verified via benchmark scenarios, developed in collaboration with WP3. Different propagation modelling methods are tested and compared, in order to provide insight in their suitability for acoustic modelling of underwater noise in the North Sea. These results have been published and presented at the 5th Underwater Acoustics Conference and Exhibition UACE2019, Hersonissos, Crete, Greece [Binnerts et al, 2019].

In chapter 3, the propagation models considered suitable for producing noise maps in the North Sea are optimised for operational use by means of finding a balance between achieving sufficient numerical convergence and minimising the computational complexity. Furthermore, additional parameters required for making noise maps are investigated and studied and initial recommendations are given.

In chapter 4, various sensitivity studies are carried out to investigate (and where possible quantify) the uncertainty associated with available environmental information used for making underwater sound maps.

In chapter 5, various updates are presented of the source level model for ships, based on the parameters provided in AIS, and adapted to match with statistics of vessel measurement data from the Port of Vancouver's Enhancing Cetacean Habitat and Observation (ECHO) programme.

In chapter 6, statistical modelling methods are described and their added value in the context of the Jomopans project is discussed.

Finally, in chapter 7, conclusions from previous chapters are summarized and the next steps in the development of the North Sea sound mapping capability described.

[1] See the WP3 terminology standard [Wang & Robinson, 2020] for the definitions of the terms ‘verified’ and ‘validated’, as used in Jomopans.

2 Propagation model benchmarking

The accuracy of the underwater noise model predictions depends on the quality of the applied models and of the input data. Selection of the appropriate propagation model depends on the environment and frequency range of interest. The benchmarking described in this report is aimed at quantifying the differences between various models for synthetic test cases representative for modelling ambient noise due to shipping and wind in the North Sea. No criteria are yet specified for the modelling accuracy, but the benchmarks provide a preliminary assessment on the precision that can be achieved for typical North Sea ambient noise scenarios with different models. The results provide insight in the uncertainty associated with the choice of the propagation model as a function of frequency and local environment.

Using the validation results that will come available later in the project (T4.3), guidelines will be designed by WP3 that can be used in future studies to assess the suitability of models for the application of making large scale – monthly and yearly statistical sound maps. The uncertainty associated with the environmental input, the source, and the computational complexity of the problem will be taken into consideration.

In section 2.1, previous benchmark studies for shallow water propagation loss models are summarized. In section 2.2, the propagation loss models available to the WP4 partners for this study are introduced. In sections 2.3 and 2.4 a range-independent and a range-dependent modelling scenario are introduced. The models described in section 2.2 are tested for these scenarios. In section 2.5, two versions of a semi-empirical wind noise model are compared to test their correct implementation. In section 2.6 the results from the model verification are discussed and preliminary conclusions are drawn on the suitability of the models investigated for generating noise maps for the North Sea region.

2.1 Previous benchmark studies for propagation loss models

2.1.1 Weston Memorial Workshop

The purpose of the Weston Memorial Workshop (WMW) [Ainslie, 2010a], held at the University of Cambridge in April 2010, was to improve understanding of signal to noise ratio and signal to reverberation ratio for simple sonar performance problems based on the 2006 ONR Reverberation Modelling Workshop [Perkins & Thorsos, 2007]. Although WMW was organized for sonar performance problems, its test cases were later used for model verification studies for other sources such as ships, see the following sections.

2.1.2 AQUO-SONIC workshop

The Jomopans partners have been involved in a prior joint effort of two research projects in the scope of the 7th Framework Program, theme "Sustainable Surface Transport", topic coordinated with the "Oceans of Tomorrow", in answer to the FP7-SST-2012-RTD-1 call on "Assessment and mitigation of noise impacts of the maritime transport on the marine environment":

- AQUO - Achieve QUieter Oceans by shipping noise footprint reduction
- SONIC - Suppression Of underwater Noise Induced by Cavitation

In March 2014, the two projects organised an ‘AQUO–SONIC workshop on Underwater Acoustic Propagation Modelling’. The purpose of the workshop was to gain confidence in the different modelling approaches for generating shipping sound maps. For this purpose, a set of five test cases was defined for which each model was applied. The test cases had an increased complexity, ranging from computation of propagation loss in a range-independent shallow water (Pekeris) waveguide at multiple frequencies to the computation of a multiple ship sound map in a synthetic shallow water environment representing a part of the Skagerrak. The scenarios were published in [Colin et al, 2015] in the hope to ‘stimulate other researchers to produce results for the same test cases or similar ones in order to build confidence in the model solutions, and thus provide high-fidelity solutions against which to compare the accuracy of faster models’.

2.1.3 PHD research Özkan Sertlek

In his PhD study [Sertlek, 2016], Özkan Sertlek developed a new analytical formulation for the calculation of the range and depth-dependence of propagation loss in shallow water. He used three test cases derived from Scenarios A.2.I and A.2.IV from the Weston Memorial Workshop (§2.1.1) to benchmark the implementation of this formulation in his “SOPRANO” code against various other propagation loss codes (KrakenC, Bellhop, and Ram). Results of this comparison have been published in [Sertlek & Ainslie, 2014] and [Sertlek et al, 2018].

2.1.4 Dublin workshop

The International Airgun Modelling Workshop (IAMW) [Ainslie et al, 2019] took place in Dublin, Ireland on 16 July 2016 as a follow-on to the 4th International Conference on the Effects of Noise on Aquatic Life that was held 10-15 July. The aim of the IAMW was to provide insight into the reliability and accuracy of source and propagation models describing the sound field at different ranges from airgun

arrays. The propagation loss scenario was adapted from the Weston Memorial Workshop benchmark, with an extension towards lower frequencies (water depth 50 m and source depth 5 m, for frequencies 1, 10, 15, 25, 50, 100, 250, 500 Hz). Propagation loss results for this scenario have been published in [Küsel & Siderius, 2019].

2.2 Overview of benchmarked propagation models for ship noise

Table 2.1 introduces the propagation models included in the WP4 benchmark studies for ship noise modelling, for two test cases (range-independent[2] test case 1, see §2.3, and range-dependent test case 2, see §2.4). For each of the models, the frequency range is specified at which the models are considered applicable. For the benchmark also models with a high computational complexity (not directly suitable for making monthly sound maps of the North Sea area) are considered, to provide a reference solution for model benchmarking. More information about a selection of these models is described in [Binnerts et al, 2019]

Table 2.1: overview of models that have been compared for test case 1 and 2, a description of the model type and an indication of the frequency range of applicability (for test cases 1 and 2)

	Model name	Model type	Frequency range	Remark
TNO	Aquarius 3	Range-dependent hybrid analytical mode sum + flux integral model	32 Hz-20 kHz	High precision configuration used for benchmarking
	Aquarius 4	Range-dependent numerical mode model using mode lookup table	10 Hz-20 kHz	Contribution from leaky modes neglected
	RAM	Range-dependent split-step Padé PE	10-500 Hz	Double precision
QO	RAM-Surf	Range-dependent split-step Padé PE	10 Hz - 2 kHz	High precision configuration used for benchmarking. Bellhop used for 2 kHz one-third octave band.
	Bellhop	Range-dependent coherent Gaussian rays	2 kHz - 20 kHz	
	Quonops	Hybrid RAM-Surf & Bellhop	10 Hz – 20kHz	
FOI	JEPE	Range-dependent Jeltsch energy-conserving PE	32 Hz - 10 kHz	
	XRAY	2D hybrid raytracing and plane wave	200 Hz - 20 kHz	
	REV3D	3D hybrid raytracing and plane wave	200 Hz - 20 kHz	Coherent and Incoherent
	XFEM	range-independent, wave number integration/ normal modes	10 Hz - 20 kHz	
	RPRESS	range-independent, wave number integration/ normal modes	10 Hz -10 kHz	
NPL	OASES	Wavenumber integration	10 Hz - ~20 kHz	Range-dependent version limited to ≤1 kHz (test case 2)
JASCO	Marine Operations Noise Model (MONM)	Range-dependent split-step Padé PE	10 Hz - ~20 kHz	

Note that all of these models have their own specific implementations of the acoustic wave equations and their own specific settings. For example: normal mode model settings include the number of modes and the root finding algorithm applied to find these modes, ray model settings include the number of rays and the type of rays and parabolic equation model settings include number of Padé terms [Jensen et al, 2011]. In the JOMOPANS model benchmarking, the selection of model settings was left to the model operators, see also section 3.6. Several model settings were adapted after a first iteration of comparing the results for the two test cases described below, generally leading to a reduction of the differences between the model results.

[2] In the context of underwater acoustics, the term 'range-independent' indicates that the environmental parameters (water depth, sound speed, sediment parameters, etc.) are uniform over all distances ('ranges') from the source.

2.3 Test case 1: Range-independent environment

The basic test case 1 is adapted from the 'single ship' scenario from the AQUO-SONIC workshop [Colin et al, 2015]. The scope of the model benchmark and sensitivity studies in Jomopans WP4 is wider than that of the AQUO-SONIC workshop. The objective is not only to gain confidence in the different sound propagation modelling approaches and implementations, but also to get a quantitative assessment of the error associated with the various simplifications that need to be made to be able to make large scale shipping sound maps, as well as the uncertainties associated with the source and environmental modelling.

The 'single ship' scenario from the AQUO-SONIC workshop [Colin et al, 2015] was based on a test case defined in the Weston sonar performance modelling workshop (WMW) [Zampolli et al, 2010], see also [Sertlek & Ainslie, 2014] and [Sertlek et al, 2018]. The test case involves the two-dimensional (axisymmetric) modelling of propagation loss in a 'range-independent' shallow water (Pekeris) waveguide and the calculation of sound pressure levels due to the sound spectrum radiated by a ship, represented by an omnidirectional point source at 5 m below the sea surface. The scenario is sketched in Figure 1. This scenario deviates from the original WMW scenario by a different source depth (5 m instead of 30 m) and water depth (50 m instead of 100 m) and by an extension towards lower frequencies (down to the 10 Hz frequency band). This makes the scenario more representative for ship noise (source close to sea surface and low frequency noise) and for the North Sea environment (mainly shallow water). Although no benchmark results are available for this altered scenario, wave number integration and normal modes, such as RPRESS, XFEM and OASES, have been sufficiently tested for this range independent environment, to have confidence that these provide a "trusted solution".

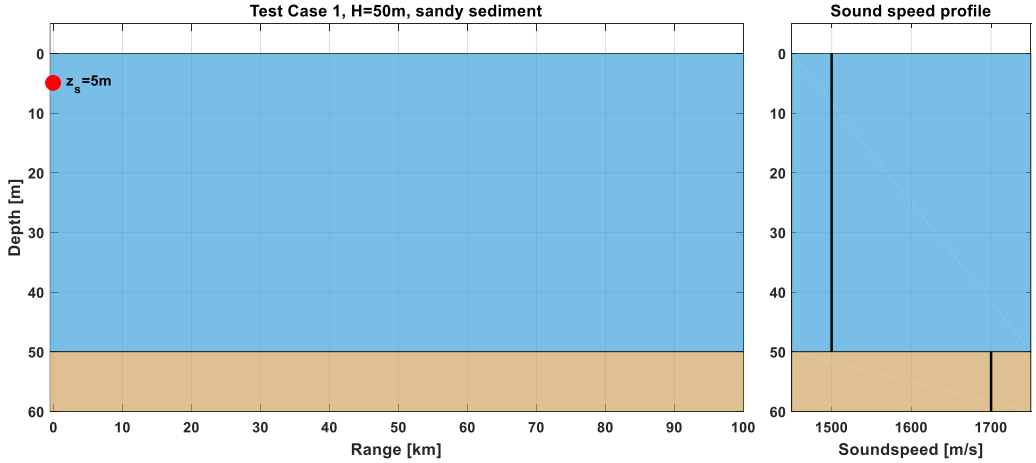

Figure 1 Schematic representation of the Test Case 1 environment. The red dot indicates the source position at 5 m depth

2.3.1 Parameter definition

Azimuthal symmetry is assumed for all parameters of the test case. A single two-dimensional radial section of this range-independent problem is considered.

Sea surface

- Smooth (perfectly compliant) sea surface.
  - Zero wind speed
  - Zero surface roughness

Water:

- Iso-velocity water
  - uniform sound speed $c_0 = 1500\,\mathrm{m/s}$
  - uniform fluid density $\rho_0 = 1000\,\mathrm{kg/m^3}$
- Absorption α_0 in sea water, in dB/km, (Ainslie-McColm model, from [Ainslie, 2010], p 29):

$$\alpha_0 = \frac{20\,dB}{ln10}\left(\alpha_1 \frac{\hat{f}^2}{\hat{f}^2 + \hat{f}_1^2} + \alpha_2 \frac{\hat{f}^2}{\hat{f}^2 + \hat{f}_2^2} + \alpha_3 \hat{f}^2\right)$$

– Here $\hat{f}$ is the frequency in kHz, and $\hat{f}_1 = 1.15$ and $\hat{f}_2 = 75.6$ are relaxation frequencies in kHz. The coefficients α_i are: $\alpha_1 = 1.40 \times 10^{-2}$, $\alpha_2 = 5.58$ and $\alpha_3 = 3.90 \times 10^{-5}$.

Sea floor:

- Uniform water depth $H = 50$ m.
- Homogeneous half space, sandy sediment
  - Fluid model for the sediment: only compression, no shear
  - Compressional wave velocity $c_s = 1700\,\mathrm{m/s}$ (sound speed ratio $c_s/c_0 = 1.1333$)
  - Density $\rho_s = 2000\,\mathrm{kg/m^3}$ (density ratio $\rho_s/\rho_0 = 2$)
  - The sediment absorption coefficient (β), in units of decibels per wavelength, is 0.5, corresponding to an absorption coefficient per unit frequency (β/c_s) of 0.294118 dB/(m kHz). The sediment absorption coefficient is related to fractional imaginary part ϵ of the complex sediment wave number $k_s(1 + \mathrm{i}\epsilon)$ by means of $\epsilon = \beta \ln(10)/40\pi$ [Sertlek et al, 2018].

Source

- Source depth $z_s = 5$ m
- Source directivity: omnidirectional (monopole)
- Average shipping source level spectrum as suggested by [Colin et al, 2016] based on [Wales & Heitmeyer, 2002], extrapolated outside its range of validity below 30 Hz and above 1.2 kHz, see Figure 2, using the following formula for the mean monopole source spectral density level (in $\mathrm{dB\ re\ 1\ \mu Pa^2\,m^2/Hz}$)

$$L_{S,f}(f) = 230\ dB - 10log_{10}\left(\left(\frac{f}{1\ Hz}\right)^{3.594}\right)\ dB + 10log_{10}\left(\left(1 + \left(\frac{f}{340\ Hz}\right)^2\right)^{0.917}\right)\ dB \quad \text{(2-1)}$$

  – At frequencies of 30 Hz and below, a constant value of $L_{S,f}(f)$ is used, equal to the right hand side of Eq. (2), evaluated at 30 Hz.

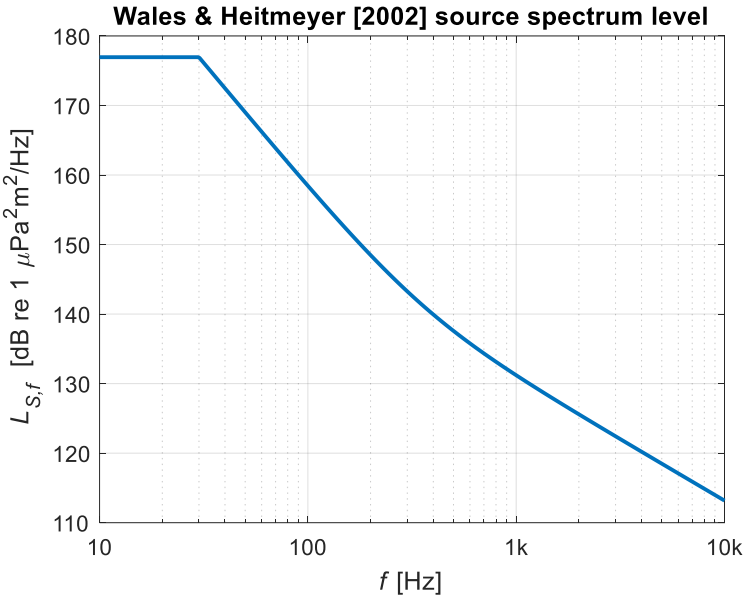

Figure 2 Monopole source spectral density level for a merchant ship based on [Wales & Heitmeyer, 2002], extrapolated at low frequency to 10 Hz and at high frequency to 10 kHz as explained in the text

- The quantity of interest is the band level in one-third octave (base 10)[3] bands as defined by IEC 61260-1 and ISO 18405) in the range from 10 Hz to 20 kHz, with centre frequencies:

$$f_n = 10^{\frac{n}{10}} \times 1\ kHz, \quad \text{for} \quad n = -20{:}1{:}13 \quad \text{(2-2)}$$

- The one-third octave ('OTO') band source level $L_{S,\mathrm{OTO}}$ is defined by integration of the spectral density over the bandwidth, but can be approximated by the level of the product of the spectral density at the centre frequency and the bandwidth of each band:

$$L_{S,OTO}(f_n) \approx L_{S,f}(f_n) + 10\,log_{10}\left(0.231\,\frac{f_n}{1\ Hz}\right) dB \quad \text{(2-3)}$$

[3] JOMOPANS always uses the one-third octave (base 10) bands, i.e., decidecade (or one-tenth decade) bands, even when the '(base 10)' is not mentioned explicitly.

- Figure 3 shows that this approximation is very good for the smooth average shipping source level spectrum considered here. The maximum difference between the integration (approximated by a power sum over in each band over the calculated levels at a frequency resolution of 1 Hz) and the approximation based on the level at the centre frequency is 0.1 dB. The difference in the calculated SPL may be larger if the propagation loss exhibits a less smooth spectrum.
- As an additional check, the band levels have been calculated (on the basis of the levels at the centre frequencies) in one-third octave (base 2) bands. The maximum difference between the base-10 and base-2 band levels (in the range from 10 Hz to 10 kHz) is 0.17 dB for the Wales-Heitmeyer source level spectrum.
- Of course, these differences may be larger in the calculated sound pressure level spectra, where the propagation loss increases the spectral slope in individual one-third octave bands.

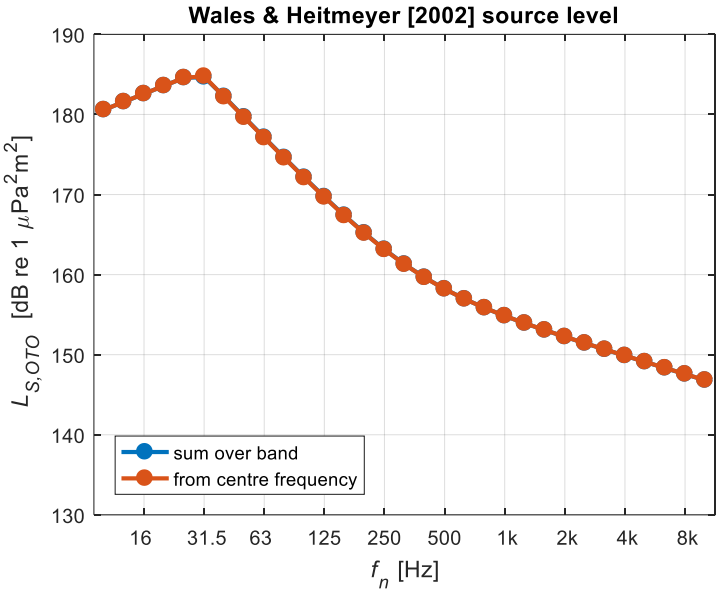

Figure 3 Monopole source level in one-third octave (base 10) bands for a commercial ship based on [Wales & Heitmeyer, 2002], extrapolated at low frequency to 10 Hz and at high frequency to 10 kHz as explained in the text. The 'sum over band' is obtained from narrowband calculations with a spectral resolution of 1 Hz.

2.3.2 Output specification

The quantity to be calculated is the sound pressure level (SPL) spectrum $L_{p,\mathrm{OTO}}(f_n, r, z)$ in one-third octave bands, with f_n the centre frequency of the n-th band, in Hz, and (r, z) the range and depth of the receiver positions, in m.

- The SPL is calculated as the difference of the single ship source level and the calculated propagation loss (PL) between the reference position of the source and the receiver positions:

$$L_{p,OTO}(f_n, r, z) = L_{S,OTO}(f_n) - N_{PL}(f_n, r, z) \tag{2-4}$$

- Calculations for the Test Case 1 scenario are compared at the band centre frequency with calculations for a single frequency. To quantify the uncertainty associated with this approximation, a sensitivity study is carried out (section 3.1).
- A minimum requirement is to calculate the SPL at 63 Hz ($n = -12$), 125 Hz ($n = -9$) and 2 kHz ($n = +3$), but if possible, all 34 frequency bands (in the range from 10 Hz to 20 kHz) are calculated.
- A quantity of interest is the total broadband SPL in the 10 Hz to 8 kHz one-third octave bands (ADEON band BD – see [Ainslie et al, 2018]). This can be done by summation of the spectral contributions:

$$L_{p,BD}(r, z) \approx 10\, log_{10}\left(\sum_{n=-20}^{n=9} 10^{\frac{L_{p,OTO}(f_n, r, z)}{10\, dB}}\right) dB \tag{2-5}$$

  However, in the benchmark studies described in this report the comparisons have been made for the full broadband SPL in the 10 Hz to 20 kHz bands ($n = -20$ to $n = 13$). Since the lower frequency bands dominate the spectrum, the difference with the SPL in the ADEON BD band is negligible.
- The receiver ranges r of interest are between 100 m and 100 km from the source. A minimum requirement is to calculate the SPL at ranges of 0.1, 0.2, 0.5, 1, 2, 5, 10, 20, 50 and 100 km. If

possible, a higher range resolution may be useful, e.g. to produce continuous graphs of SPL versus distance with a 100 m receiver range resolution.
- A minimum requirement is to calculate the depth averaged value of the squared sound pressure over the local water depth H at the receiver. The user defines and reports the depth resolution in the calculations. If the acoustic indicators (defined by WP6 and WP7) require multiple depth intervals these will be added later in the project.

2.3.3 Test Case 1 results

In this section the model results for the first test case are compared. Both the broadband and the one-third octave (OTO) band sound pressure levels are compared to assess their agreement and where possible their expected accuracy.

Broadband results

Figure 4 (upper) shows the model predictions of the depth averaged broadband SPL as a function of range. The lower figure show the same results, but normalised against a 'reference' solution obtained from the Weston incoherent energy flux model (eq.(4) from [Harrison, 2003]), as done in [Sertlek, 2016; Sertlek et al, 2018]. Figure 5 shows an alternative normalization of the same results, with the **Aq3 (TNO)** model as the reference solution, to improve the illustration of the agreement between the various model results at greater distances (beyond 10 km). Note that the choice for the reference model is arbitrary, and does not say anything about the accuracy of the reference model itself.

The following is observed with respect to the broadband SPL calculations:
- The incoherent models (Weston flux '**reference**' and **incoherent REV3D** (FOI)) do not incorporate the effect of coherent interference due to surface reflections (known as the Lloyd Mirror effect in underwater acoustics, see e.g. [Carey, 2009]). This results in a large (>10 dB) overestimation of the broadband SPL, which indicates that the tested incoherent models are not suitable for the test case 1 benchmark scenario, nor for broadband shipping noise modelling in general. Nevertheless, the close agreement between the results from these two different incoherent models indicates that the models are implemented correctly.
- With respect to this ensemble of modelling predictions: The maximum observed difference between the ensemble of **Aq4 (KrakenC)** (TNO), **XFEM** (FOI), **RPRESS** (FOI), **JEPE** (FOI), **MONM** (JASCO), **OASES** (NPL) and **RAM-SURF + Bellhop** (QO) model predictions is smaller than 0.2 dB at distances greater than about 500 m from the source.
- At distances smaller than 500 m from the source, the **Aq4 (KrakenC)** (TNO) and **JEPE** (FOI) predictions are similar in their deviation from the other models in this ensemble up to a difference of -2 dB at 100 m.
- The **Aq3** (TNO) model, using normal modes which are estimated from an 'effective depth' approximation [Sertlek & Ainslie, 2014], underestimates the ensemble of model predictions by 2 dB at 500 m from the source. The deviation decreases with distance towards distances larger than 500 m and increases towards shorter distances.
- The coherent **REV3D** (FOI) model predicts levels 3 dB higher than the ensemble of models at 500 m from the source. The deviation decreases towards larger distances.

Spectral results

Figure 6 and Figure 7 show the one-third octave band spectra of the SPL as a function of frequency at 10 km and 40 km distance from the source for test case 1 predicted by the various models.

The following is observed:
- The overestimation of the broadband SPL by the incoherent models (Weston flux '**reference**' and **incoherent REV3D** (FOI)) and the **coherent REV3D** (FOI) ray model occurs mainly at low frequencies (<~500 Hz at 10 km and <~1 kHz at 40 km).
- The ensemble of **Aq4 (KrakenC)** (TNO), **XFEM** (FOI), **RPRESS** (FOI), **JEPE** (FOI), **OASES** (NPL) and **RAM-SURF + Bellhop** (QO-Quonops) model predictions agree within 0.2 dB at the selected ranges (10 and 40 km) in all frequency bands, starting from the 20 Hz band, below which there are no propagating modes.
- The **MONM** (JASCO) model predictions also agree within 0.2 dB (at 10 and 40 km distance) in all frequency bands up to 1 kHz, and within 1 dB at higher frequencies (at 10 km).
- The 1-2 dB lower estimation of the SPL by the **Aq3** (TNO) model occurs mainly in the dominant 32 Hz band. The Aq3 model predictions give a significant overestimation (irrelevant for the broadband SPL) in lowest frequency bands considered.

Conclusion

The results for test case 1 benchmark show that an agreement of the broadband SPL (<1 dB) can be achieved by using the correct model configuration at ranges beyond 500 m. An uncertainty of 1 dB in the implementation of the propagation loss model for the relevant frequency is considered acceptable given that the uncertainty in the propagation loss modelling associated with uncertainties in the model

input parameters is expected to be significantly larger. This is further investigated in a variety of sensitivity studies in chapter 4.

It should be noted that this quantitative assessment of the model agreement is specific for the considered synthetic environment of test case 1. In order to gain more confidence that the applied models are valid for making noise maps in the North Sea, an additional scenario that includes a range-dependent bathymetry is considered in section 2.4.

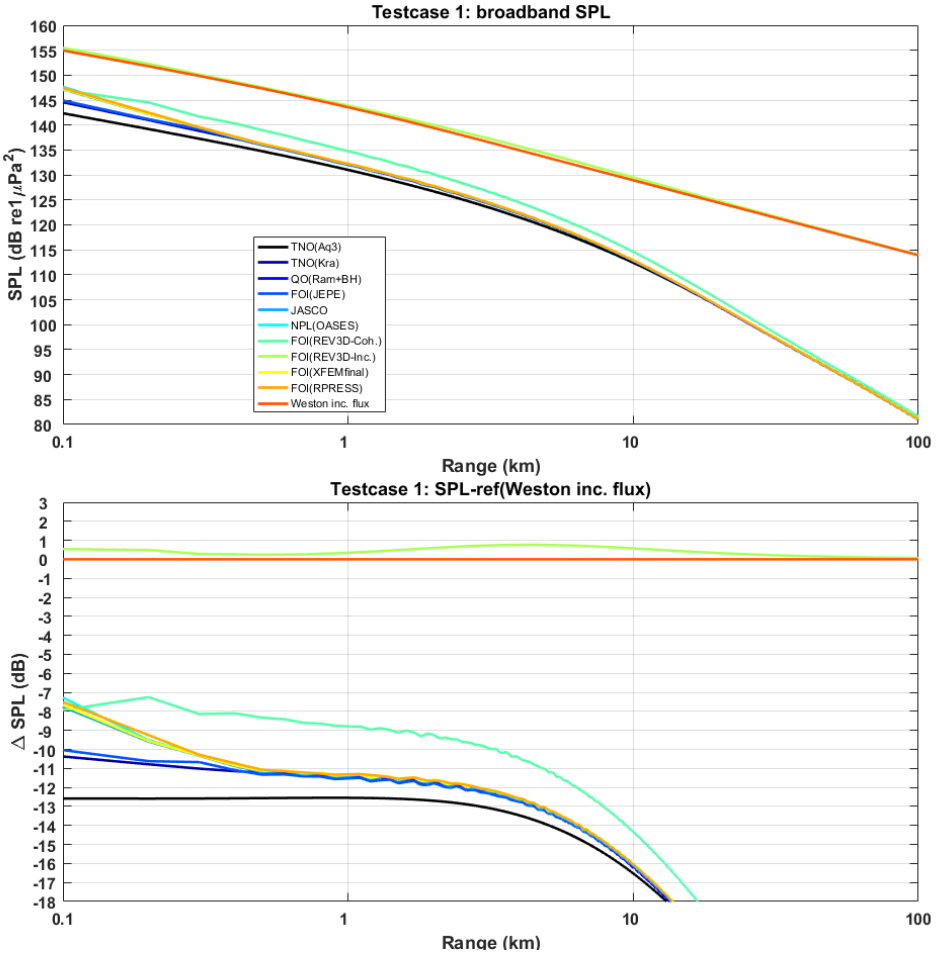

Figure 4 Calculated depth-averaged broadband SPL in dB re 1 μPa^2 as a function of range (horizontal distance to the source) for test case 1 (upper) for the various models (see legend) and difference (lower) between the various model solutions and the Weston incoherent energy flux reference solution (see text).

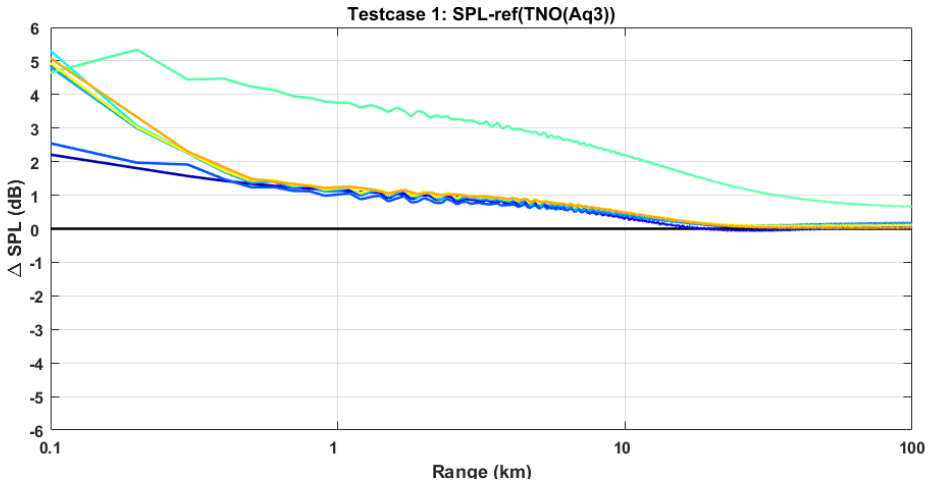

Figure 5 Difference between the depth-averaged broadband SPL for test case 1 for the various models (see legend in Figure 4) and the TNO Aquarius 3 as the reference solution

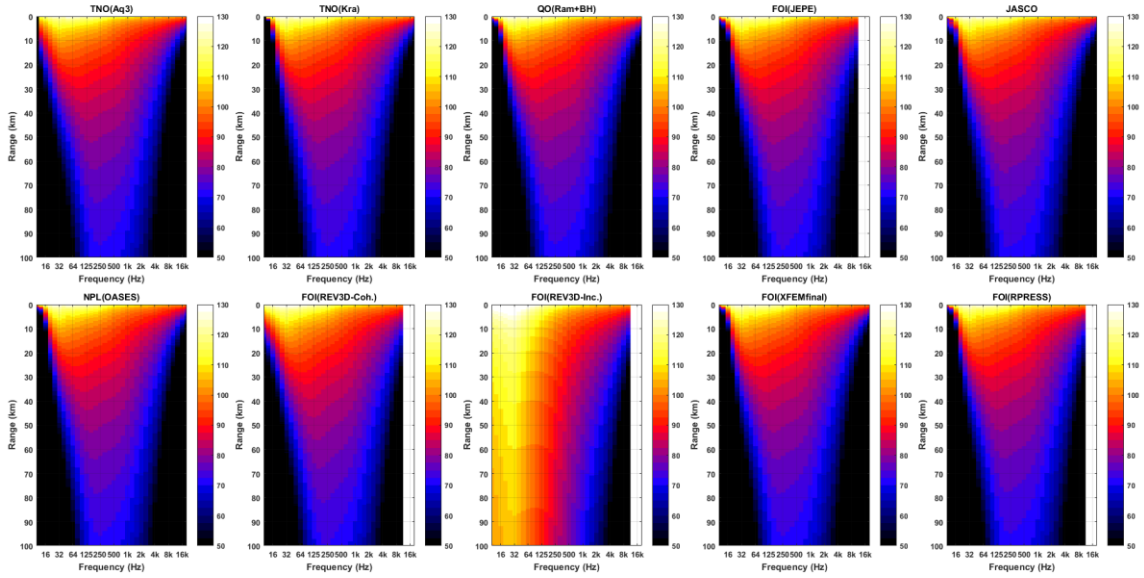

Figure 6 Depth-averaged SPL in dB re 1 μPa^2 as a function of frequency (one-third octave bands) and range, as calculated by the various models for test case 1.

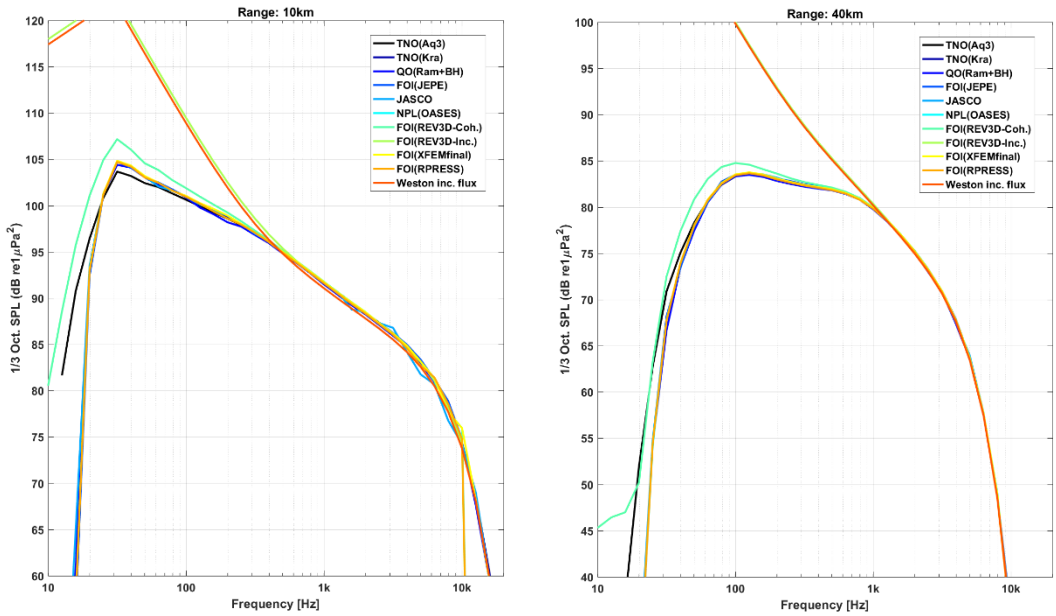

Figure 7 One-third octave band spectra of the depth-averaged SPL in dB re 1 μPa^2 at 10 km (left) and 40 km (right) range, as calculated by the various models for test case 1. (no RPRESS results above 10 kHz)

2.3.4 Test Case 1 – Küsel & Siderius [2019]

Point to point propagation loss results for the range-independent scenario have been published in [Küsel & Siderius, 2019] for a single receiver depth of 15 m, at frequencies 10, 15, 25, 50, 100, 250 and 500 Hz. These were calculated for the Dublin workshop (§2.1.4) scenario which is equal to the Jomopans T4.2 test case 1 scenario. These results are compared with various modelling results obtained by TNO, using the Aq3 and Aq4 (KrakenC) models and a Matlab RAM model implementation in Figure 8 (linear range scale) and Figure 9 (logarithmic range scale).

The agreement between the various models is generally good, except at the lowest frequencies (<50 Hz). Due to the choice for an incoherent mode sum, the normal mode models Aq3 and Aq4(KrakenC) do not predict the details of the frequency-dependent interference patterns observed at frequencies at 50 Hz and above, but their prediction of the average trend of the range-dependent propagation loss agrees quite well with the results from the detailed coherent models.
The Aq4 solution agrees with the Küsel and Siderius results at 25 Hz and above, but no mode and therefore no solution was obtained at 10 and 15 Hz. The Aquarius 3 model, which uses an analytical method to determine the modal eigenvalues and mode shape, deviates from the KrakenC solution at 15 and 25 Hz, and is expected to be less accurate at these frequencies. The TNO-RAM model predictions agree with the K&S-RAM predictions at 25 Hz up to the maximum tested range of 30 km. At 10 and 15 Hz, the TNO-RAM model deviates from the K&S-OASES and K&S-RAM results, but only after the PL reaches high values. The observed interference patterns suggest that the down going wave in the sediment is insufficiently damped by the absorbing seabed boundary condition. This effect is not investigated further, as the errors caused at these larger ranges at these low frequencies is assumed to have a negligible effect on the computation of the selected acoustic metric in Jomopans.

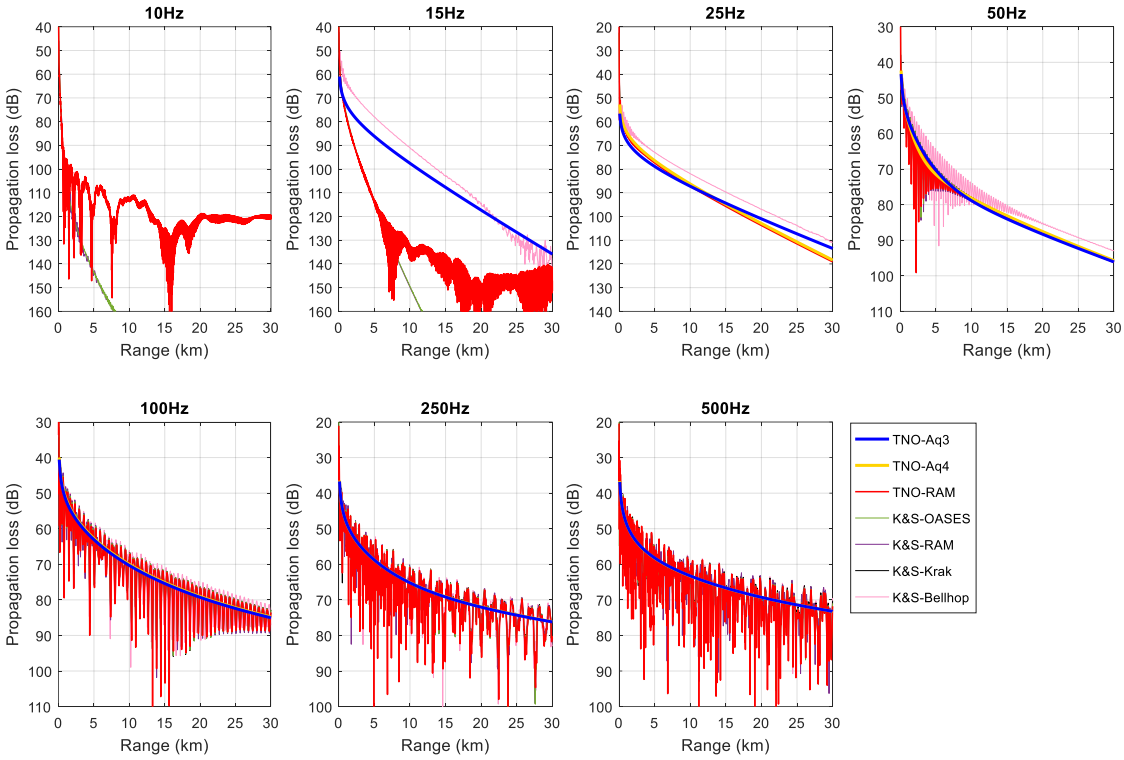

Figure 8 Calculated propagation loss in dB re 1 m^2 as a function of range for a single receiver depth of 15 m for the test case 1 scenario at frequencies 10, 15, 25, 50, 100, 250 and 500 Hz. Results from three TNO models (Aquarius 3 (Aq3), Aquarius 4 (KrakenC) and a RAM implementation) compared with results (K&S) from four different models from [Küsel & Siderius, 2019]

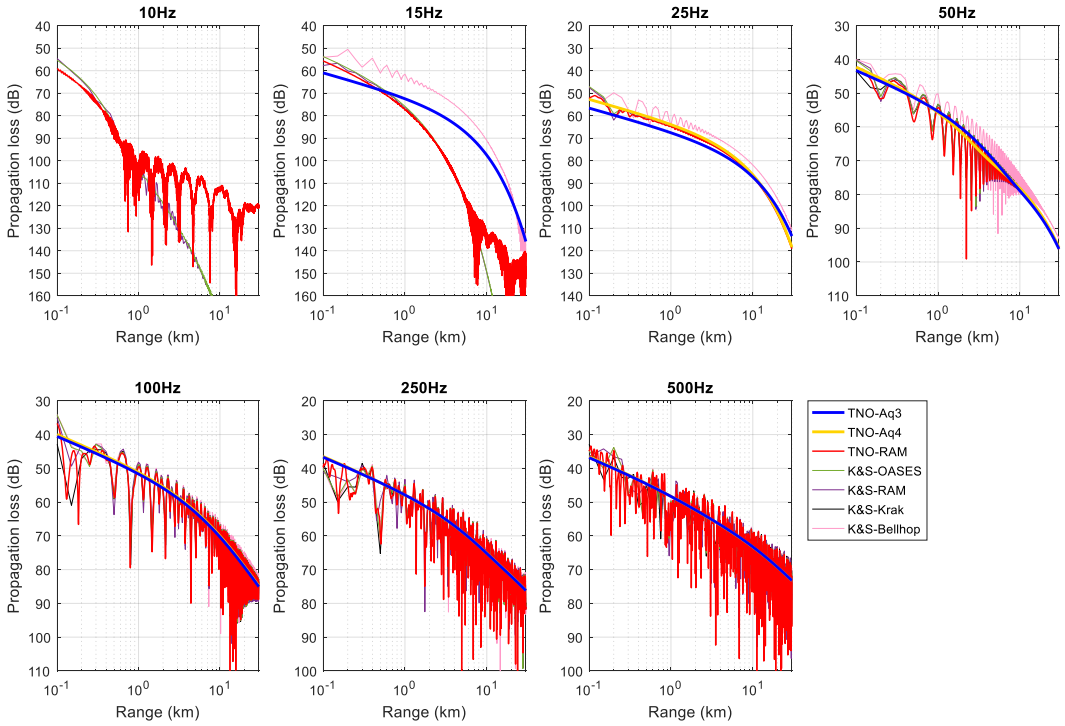

Figure 9 The same information as given in Figure 8 but with a logarithmic instead of linear horizontal (range) axis.

2.4 Test case 2: upslope bathymetry

The acoustic models for generating North Sea sound maps must be range-dependent, i.e. able to incorporate (at least) the effects of the varying water depth (bathymetry) on sound propagation. To test this ability, a range-dependent benchmark scenario is considered. Details on the origin of the scenario can be found in [Sertlek et al, 2018, Case 4]. The geometry is shown in Figure 10. The source depth for this scenario deviates from the original (5 m instead of 30 m) to be more representative for ship generated noise. The other input parameters and the output specification are identical to test case 1.

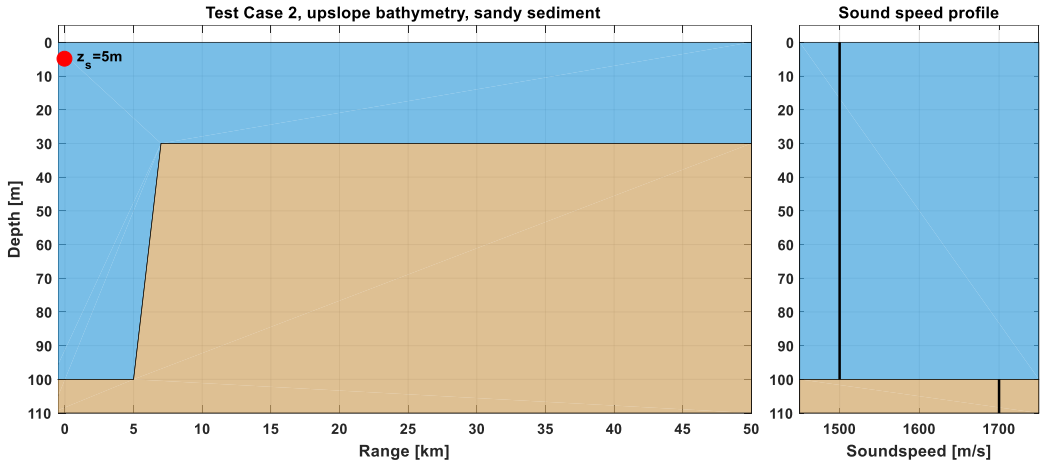

Figure 10 Schematic representations of the test case 2 environment with a 5 m source depth (red dot) to be representative for ship generated noise and an iso-velocity sound speed gradient, similar to the testcase 1 environment

2.4.1 Results

In this section the model results for the range-dependent test case 2 are compared. For this comparison both the broadband and one-third octave band sound pressure levels are compared, to gain confidence in the accuracy of the models. The objective of this test case is to investigate if the models correctly take into account the effect of the upslope bathymetry on the sound propagation. A second objective is to study the effect of the shallower water depth of 30m, resulting in a higher cut-off frequency, on the sound propagation.

Broadband results

Figure 11 (upper) shows the model predictions of the depth averaged broadband SPL as a function of range. The lower figure shows the same results, but normalised against a 'reference' solution obtained from the Weston incoherent energy flux model (in the formulation from [Harrison, 2003]), as done in [Sertlek, 2016; Sertlek et al, 2018].

The following is observed with respect to the broadband SPL calculations:

- The incoherent models (Weston flux '**reference**' and **incoherent REV3D** (FOI)) do not incorporate the effect of coherent interference due to surface reflections (known as the Lloyd Mirror effect in underwater acoustics, see e.g. [Carey, 2009]). This results in a large (>10 dB) overestimation of the SPL, which indicates that incoherent models are not suitable for broadband shipping noise modelling. Nevertheless, the close agreement between the results from these two different incoherent models indicates that the models are implemented correctly.
- At distances up to 5 km (where the upslope bathymetry starts) the **RAM-SURF + Bellhop** (QO), **JEPE** (FOI) and **MONM** (JASCO) model predictions show a larger spread than for test case 1, in which the water depth was half that of test case 2. In this case the **RAM-SURF + Bellhop** (QO) and **MONM** (JASCO) results overlap. The **OASES** (NPL) results are 1 dB higher.
- At ranges between 1 km and 5 km, the **JEPE** (FOI) and **Aq4**(**KrakenC)** (TNO) model predictions deviate at maximum 1 dB from the **RAM-SURF + Bellhop** (QO) and **MONM** (JASCO) results. The difference between the model predictions increases towards shorter ranges. Beyond 5 km (where the range-dependence starts) the difference between the PE models is less than 0.5 dB.
- Beyond 5 km, the **Aq3** & **Aq4(KrakenC)** models by TNO diverge from the other (PE) models up to 4 dB estimation at 50 km. The adiabatic mode coupling approximation assumed by the Aquarius models is likely contributing to this observed bias.
- The **coherent REV3D** (FOI) ray model predictions are about 2 dB above the results of these models for distances up to 5 km, where the start of the slope of the water depth starts. In the shallow region the discrepancies increase. This is expected since the high frequency approximation of ray-based methods makes such methods a poor choice for small water depths and low frequencies.

- The range-dependent version of the **OASES** (NPL) model is limited to a maximum frequency of 1 kHz. The resulting broadband SPL is close (within 2 dB) to the results of the **Aq3** (TNO), **Kraken** (TNO-Aq4)), **RAM-SURF + Bellhop** (QO), **JEPE** (FOI) and **MONM** (JASCO) models for distances between 1 km and 7 km. At shorter and larger distances, the deviations are significantly greater.

Spectral results
Figure 13 and Figure 14 show the one-third octave band spectra of the SPL as a function of frequency at 10 km and 40 km distance from the source for test case 2 for the various models.

The following is observed:
- The overestimation of the broadband SPL by the incoherent models (Weston flux '**reference**' and **incoherent REV3D** (FOI)) seems to occur mainly at low frequencies (<~1 kHz at 10 km and <~3 kHz at 40 km).
- The **RAM-SURF + Bellhop** (QO), **JEPE** (FOI) and **MONM** (JASCO) model predictions are similar (with a maximum deviation of 5 dB in individual frequency bands at 40 km) over the whole frequency range (starting at 32 Hz).
- Below 1 kHz the range-dependent **OASES** (NPL) model agrees with the PE models within about 5 dB.
- At 2 kz and above, the **Bellhop** (QO) model uses a ray approach, which lead to the same results as the **JEPE** (FOI) and **MONM** (JASCO) PE models.
- The **Aq3** (TNO), **Aq4**(**KrakenC)** (TNO) results are similar to the to the PE models at 10 km, but are about 5 dB lower, at frequencies between 500 Hz and 3 kHz, at 40 km distance. This observed bias may be caused by the adiabatic mode coupling assumption used by these models. A comparison of a coupled mode or a FE simulation would strengthen this hypothesis.
- The **JEPE** (FOI), **MONM** (JASCO) and **OASES** (NPL) models exhibit similar variations of the SPL with frequency (See Figure 13) at ranges beyond 10 km and in the frequency range between 100 Hz and 1 kHz. These variations are not seen in the **Aq3** (TNO) and **Aq4**(**KrakenC)** (TNO) results, in which the range dependence is implemented via an adiabatic mode coupling.
- The **coherent REV3D** (FOI) model predictions deviate from the other model predictions for frequencies below ~1 kHz, where the approximation of ray-based methods is invalid.

Conclusion
The results for test case 2 benchmark show that an agreement of the broadband SPL (<2 dB at ranges beyond about 1 km from the source up to about 20 km) can be achieved for this range-dependent scenario by using the correct model configuration. Also, it is observed that the Aquarius models, that make use of the adiabatic approximation, deviate from the parabolic equation models (RAM, JEPE and MONM), leading to an lower SPL at large distances (up to about 5 dB at 50 km).

It should be noted that this quantitative assessment of the model agreement is specific for the considered synthetic environment of test case 2, and that the model differences will be likely different for different scenarios. Moreover, the choice for the steep slope considered in this scenario was mainly taken to match a previous benchmarking effort [Sertlek et al, 2018, Case 4], and is not representative for most locations in the North Sea. For environment with a less steep bathymetric slope it is expected that the differences between the Aquarius models and the PE models become smaller.

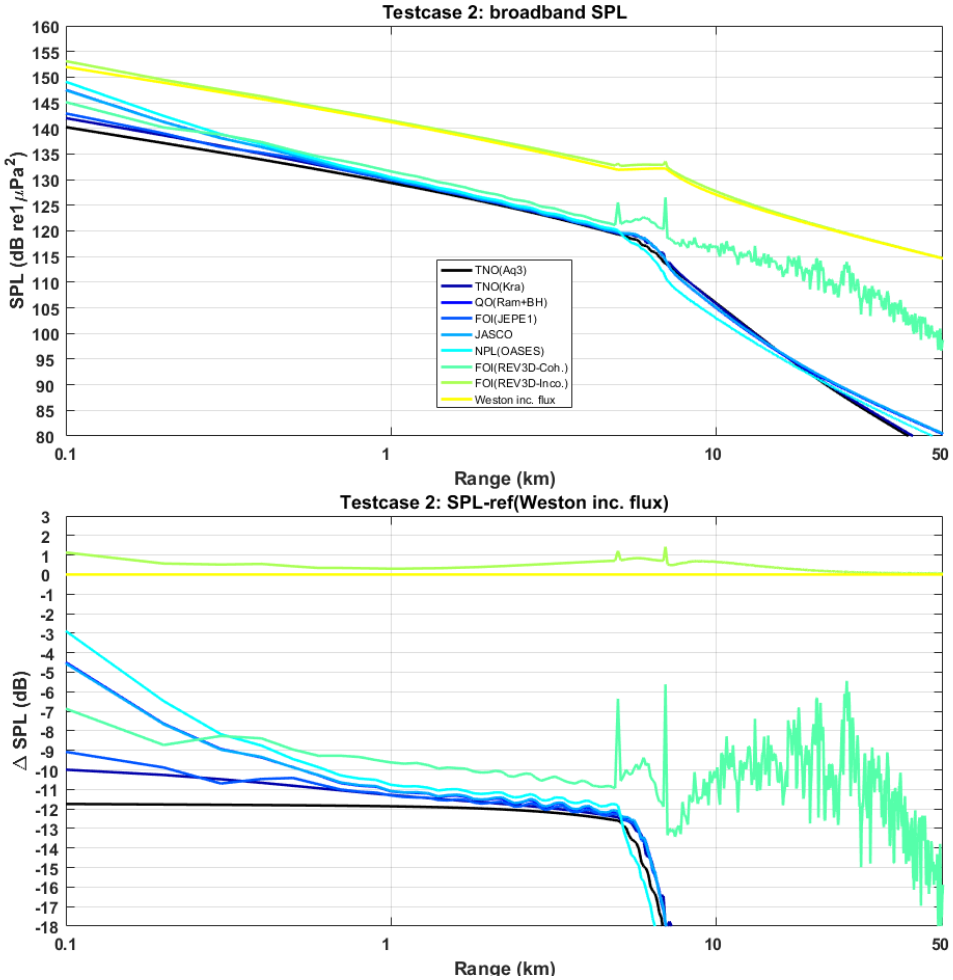

Figure 11 Upper: Calculated depth-averaged broadband SPL in dB re 1 μPa^2 as a function of range (horizontal distance to the source) for test case 2 for the various models (see legend) and Lower: difference between the various model solutions and the Weston incoherent energy flux reference solution.

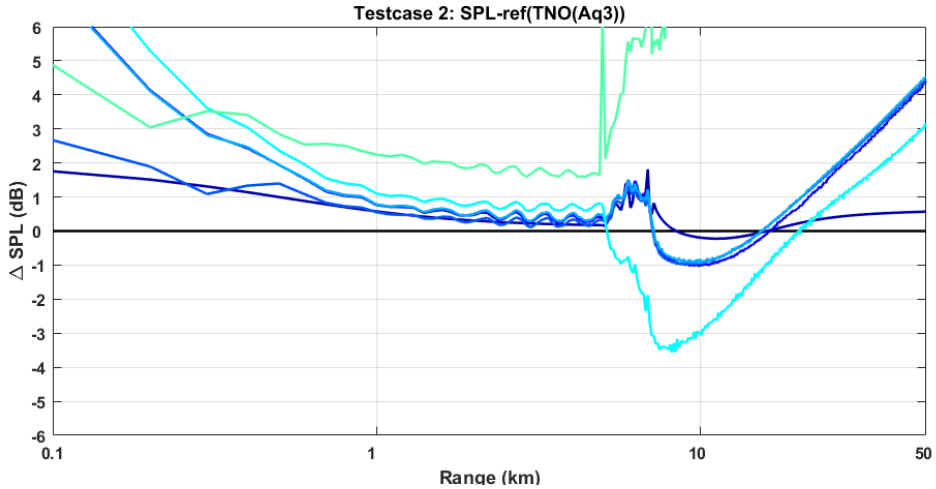

Figure 12 Difference between the depth-averaged broadband SPL for test case 2 for the various models (see legend in Figure 11) and the TNO Aquarius 3 solution

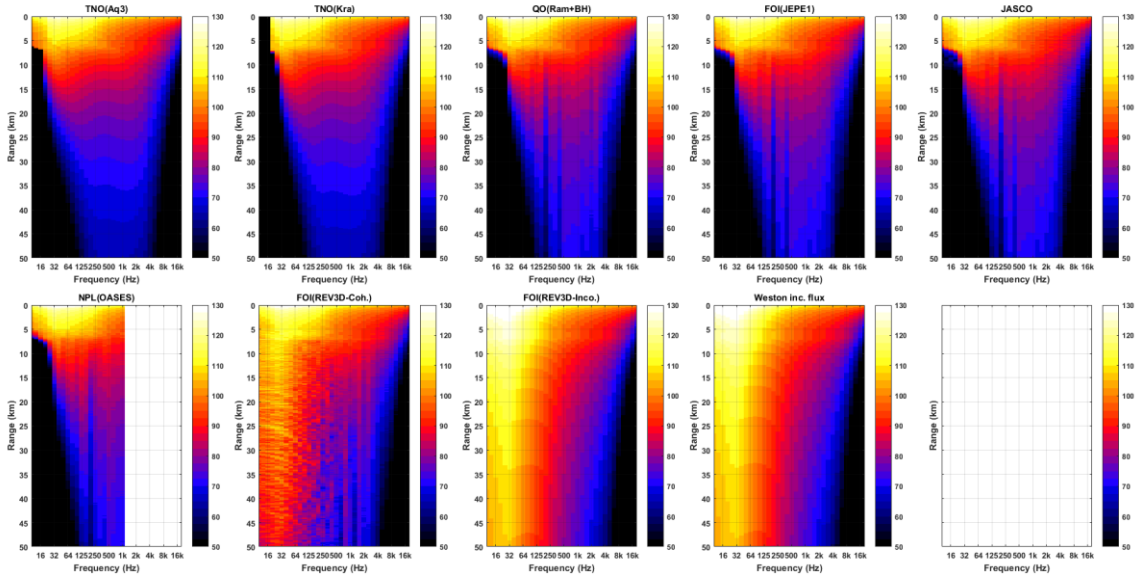

Figure 13 Depth-averaged SPL in dB re 1 μPa^2 as a function of frequency (one-third octave bands) and range, as calculated by the various models for test case 2.

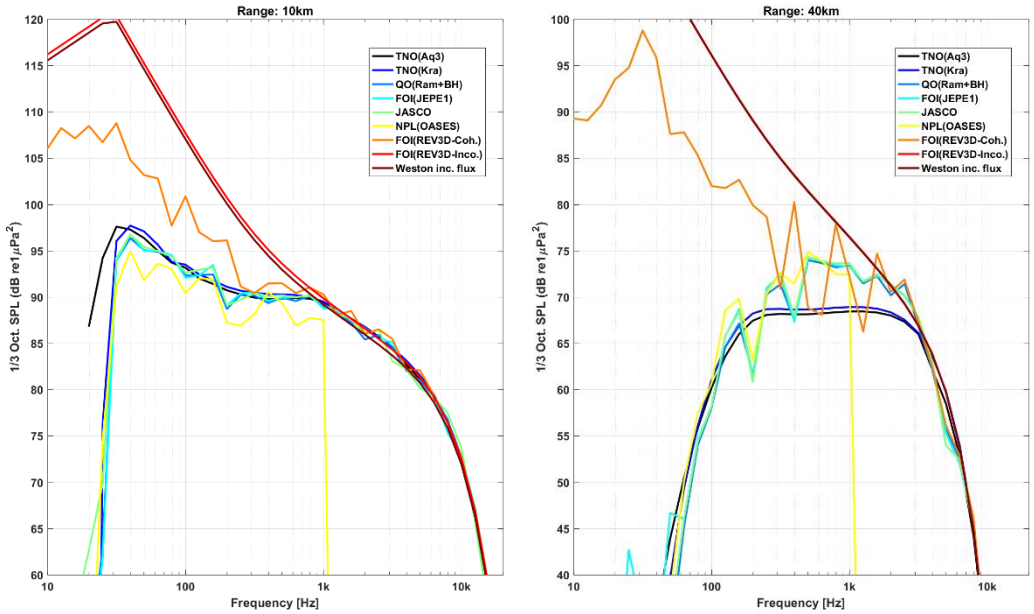

Figure 14 One-third octave band spectra of the depth-averaged SPL in dB re 1 μPa^2 at range 10 km (left) and 40 km (right), as calculated by the various models for test case 2. (no OASES results above 1 kHz)

2.4.2 Range-dependent scenario - Küsel & Siderius [2019]

Point to point propagation loss results for a single receiver depth of 15 m for a range-dependent scenario, at frequencies 50, 100, 250 and 500 Hz have been published in [Küsel & Siderius, 2019]. This scenario is similar to the Jomopans T4.2 test case 2 scenario, but with a slightly different geometry in which the water depth decreases linearly from 250 m at 0 to 5 km ranges to 215 m at 7 km range and beyond (up to 12 km). TNO modelling results (Aq3, Aq4(KrakenC) and RAM) are compared with the published results from [Küsel & Siderius, 2019] in Figure 15.

Similar to what was observed for the range-independent scenario (§2.3.4) from [Küsel & Siderius, 2019], the agreement between the various models is generally good at ranges larger than 1 km (~10 times the water depth at the source). Due to the choice for an incoherent mode sum, the normal mode models Aq3 and Aq4(KrakenC) do not predict the details of the frequency-dependent interference patterns, but their prediction of the average trend of the range-dependent propagation loss agrees quite well with the results from the detailed coherent models. The TNO-RAM predictions predict the same interference patterns as the K&S results for RAM and Bellhop.

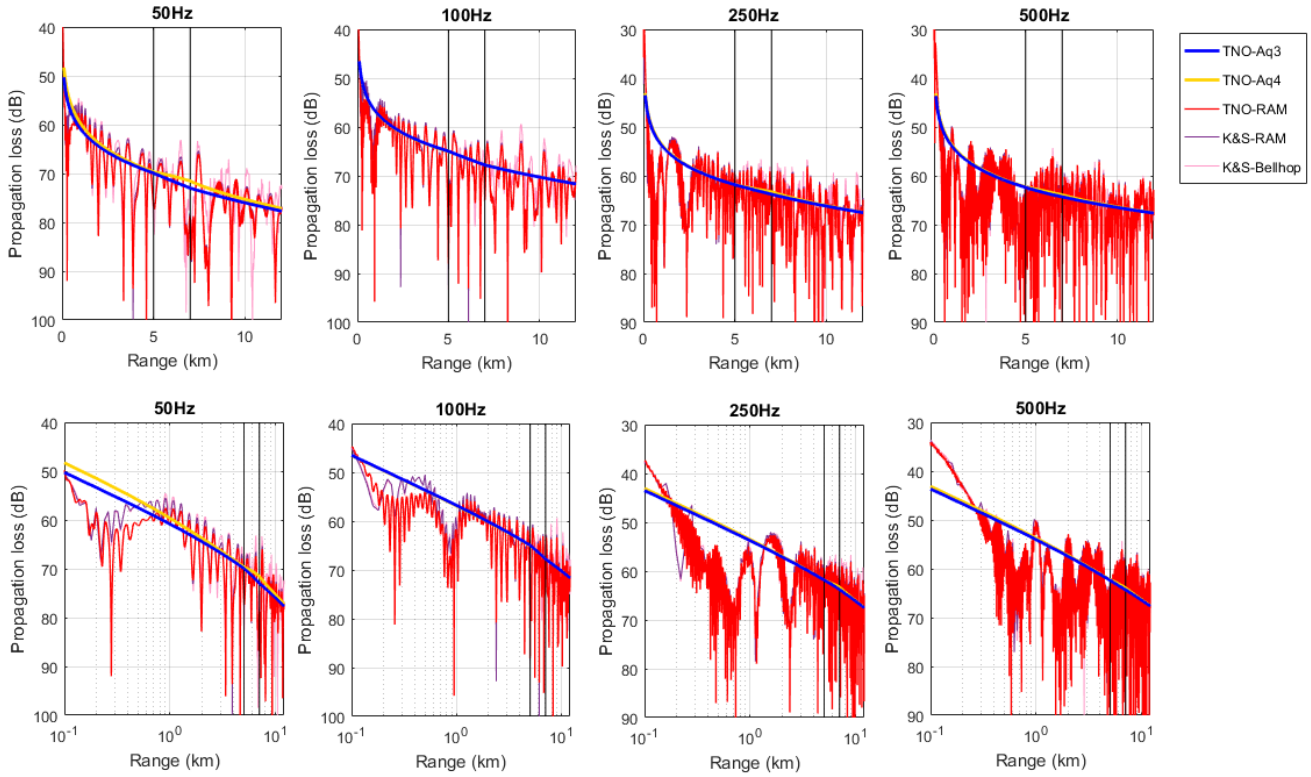

Figure 15 Calculated propagation loss in dB re 1 m^2 as a function of range for a single receiver depth of 15 m for the test case 1 scenario at frequencies 50, 100, 250 and 500 Hz. Results from three TNO models (Aquarius 3 (Aq3), Aquarius 4 (KrakenC) and a RAM matlab implementation) compared with results (K&S) from four different models from [Küsel & Siderius, 2019]. The thin vertical lines indicate the start and the end of the change in water depth. The top plots show the results on a linear range scale and the bottom plots on a logarithmic range scale.

2.5 Test case 3: wind noise source and propagation model

Both TNO and JASCO operate wind noise source and propagation models based on the semi-empirical expressions described in [Ainslie, 2010, Chapter 8], see the T4.1 report [de Jong et al, 2018]. Test Case 3 is included here to cross-check the implementation of these models and to demonstrate the sensitivity of the calculated SPL contribution from wind to the model input parameters (wind speed and receiver depth).

2.5.1 Scenario and output specification

- **Environment:** see Test Case 1 specification (§2.3)
- **Source:** Surface dipole spectrum for a range of wind speeds at 10 m height above sea surface of 0.5, 1, 2.5, 5, 10 and 20 m/s
- **Output:**
  - Depth-averaged one-third octave band sound pressure level spectra for the six wind speeds
  - Broadband (in the 10 Hz to 20 kHz one-third octave bands) SPL as a function of receiver depth at 1 m resolution starting at 1 m below sea surface up to 49 m depth for the six wind speeds

2.5.2 Results

The model results by TNO and JASCO are shown in Figure 16.

The following is observed:

- The TNO and JASCO implementations of the wind noise model predict the same sound level at wind speeds above 1 m/s, when the effect of surface losses due to scattering and attenuation are neglected. Jasco assumes a minimum windspeed of 1 m/s, which explains the difference at a 0.5 m/s windspeed.
- JASCO has added an adapted version of the model in which the effect of wind-speed dependent surface losses, caused by scattering and attenuation, is included, see section 2.5.3 (below). The dotted lines in Figure 16 show the effect of this surface loss on the calculated SPL, which results in a maxim reduction of 6 dB compared to the results without surface loss, for the highest wind speed at frequencies around 1 kHz.

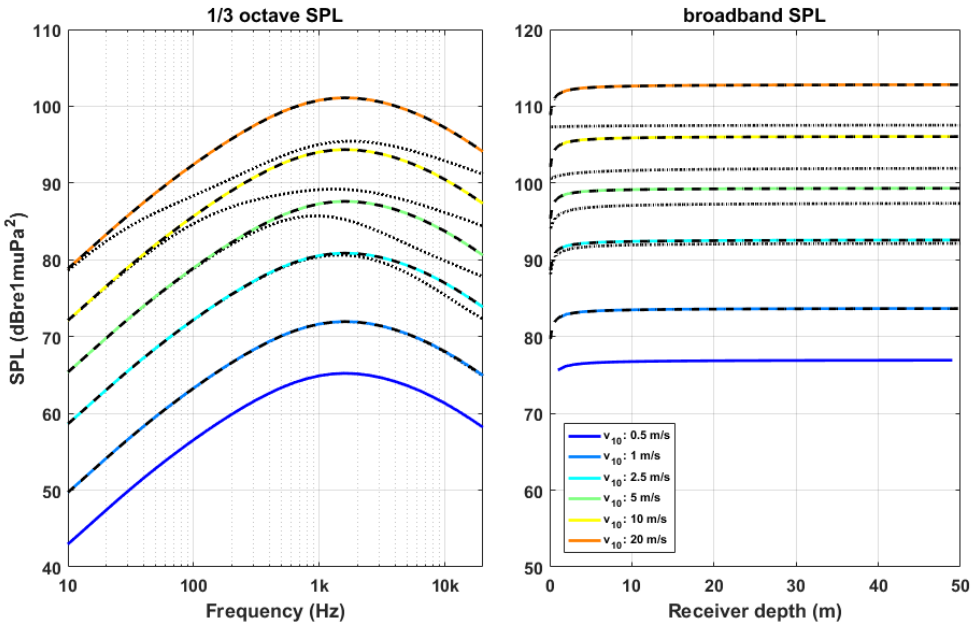

Figure 16 wind model results (left: depth-averaged one-third octave band spectrum of SPL; right: broadband SPL versus receiver depth) by TNO, without surface loss, (coloured solid lines) and JASCO, without (black dashed lines) and with surface loss (black dotted lines).

2.5.3 Surface loss in WRASP model

JASCO's Wind and Rain Ambient Sound Propagation (WRASP) model takes into account multiple reflections of surface noise via the seabed and sea surface, see section 5 of Ainslie et al. (2011). The wind noise at depth d below the water surface is calculated as the sum of direct and reflected path contributions:

$$L_{p,wind} = 2\pi K_f (n_{\mathrm{D}} + n_{\mathrm{BL}})$$

with K_f the spectral density of the areic dipole source factor of wind noise (see de Jong et al, 2018) and n_{D} and n_{BL} the direct and reflected path contributions, see Ainslie et al. (2011).

The direct path contribution is

$$n_{\mathrm{D}} = E_3(2\alpha d)$$

With $E_3(x)$ is the exponential integral of third order and α the attenuation coefficient of sea water.

The contribution of the reflected paths depends on the critical angle $\theta_c = \arccos(c_w/c_s)$, with c_w the sound speed in water and c_s the (compressional) sound speed in the sediment.

$$n_{\mathrm{BL}} = \frac{1}{\eta}\left\{\sin\theta_c - (a-b)^{-1}\left[a^{3/2}\arctan\left(a^{-1/2}\sin\theta_c\right) - b^{3/2}\arctan\left(b^{-1/2}\sin\theta_c\right)\right]\right\}$$

with $a = 2\alpha H/\eta$ (for water depth H) and $b = 1/[2(kd)^2]$ (for wavenumber k)

The seabed and sea surface reflection loss is taken into account by means of an adjustment of the form

$$\eta = \eta_{\mathrm{B}} + \eta_{\mathrm{S}}.$$

where η_{B} is the seabed reflection loss coefficient (see Eq. (8.86) of Ainslie (2010), p.378). η_{S} is calculated as a function of frequency and wind speed from Eq (8.20) by assuming the loss is proportional to grazing angle, with α_{WC} the average of the two measured values from Eq. (8.21), and subject to a maximum surface reflection loss of 15 dB for incidence at 15 degrees from the horizontal (see Ainslie, 2010, pp 365 and 368).

2.6 Discussion

Test cases 1 and 2 described in this chapter have been developed to provide benchmarks for acoustic propagation loss models for shipping noise in a shallow water environment such as the North Sea. They can be used to test the selection of appropriate models and the correct implementation of these models. Though there is no independent 'exact' solution for these benchmarks, comparison of modelling results for these test cases with the solutions provided in this chapter and other published results [Kusel & Siderius 2019] provides insight in the applicability of the selected model and in the uncertainty (or bias) associated with the specific implementation and parametrization of the model. The various model solutions provided by the JOMOPANS WP4 partners illustrate the use of these benchmark test cases. Because the wavenumber integration approach involves the least approximation, the solution from FOI's XFEM model is offered as a reference solution for this first benchmark case. In contrast with the range-independent test case 1, where the wavenumber integration models provide a trusted solution, there is no fully trusted solution for the second, range-dependent, benchmark case 2. As a compromise, the (power-) average of the solutions of the three parabolic equation models, which differ very little, is proposed as a reference solution.

The model benchmarking in WP4 involved an iterative process in which partners adapted their model parametrization to mitigate observed deviations in the results. Examples of such adaptations are the choice for the number of modes (real and evanescent or 'leaky' modes) or rays included in the modelling, the number of Padé terms in parabolic equation models (RAM) and the number of observation depths from which the depth average SPL was calculated (spatial averaging can compensate for model variability caused by using a sparse number of frequencies to compute the OTO SPL using coherent models) . Each model implementation has its own characteristic settings and running the model for the proposed test cases allows selection of the appropriated (optimal) parameter settings.

The results for test case 1 benchmark show that an agreement of the depth averaged broadband SPL <1 dB can be achieved by using the correct model configuration at ranges beyond 500 m. The benchmark results for the range-dependent scenario (test case 2) illustrate that an agreement of the broadband SPL <2 dB can be achieved at ranges beyond 500 m from the source by using the appropriate model configuration. For the testcase 2 benchmark, the different models lead to differences up to about 5 dB in the propagation loss in individual one-third octave bands and even larger in the

lowest frequency bands, close to and below the cut-on of the lowest propagating modes. However, these larger differences occur primarily at frequencies and ranges from the source that are less relevant for the broadband shipping noise calculations.

These results have been presented at the 5th Underwater Acoustics Conference and Exhibition UACE2019, Hersonissos, Crete, Greece [Binnerts et al, 2019].
The total uncertainty in shipping noise predictions includes uncertainty in the selected propagation loss model as well as uncertainties associated with the input parameters for this model (geometry and properties of water column and seabed). It also includes the uncertainties associated with the source model for the ships and its input parameters. The sensitivity of the models to these uncertain input parameters is tested in various sensitivity studies, see Chapters 3 to 6.

Test case 3 was developed to test the implementation of the available semi-empirical wind noise source and propagation model and to illustrate the sensitivity of the model output for the main input parameter (wind speed at 10 m above the water surface). Uncertainty in this model depends on the applicability of the semi-empirical model parameters and the uncertainty in the wind speed data. These uncertainties will need to be tested against North Sea noise measurements for geographical locations and time windows in which wind is the dominant contributor to the noise. Measurement data (2018) from the Love station (Norway), which is installed outside the JOMOPANS area but in a location far from shipping lanes and human activities, were included in the North Sea monitoring for this purpose.

3 Model parametrization – sensitivity studies

Reports and publications of previous underwater sound mapping efforts are often incomplete about the way in which the levels presented in sound maps are obtained, see [de Jong et al, 2018]. Also, there appears to be little consistency between the choices made in different projects and the uncertainties associated with these choices are generally not quantified. To ensure consistent and sufficiently accurate modelling of maps of the acoustical metrics, these choices need to be specified.

Important parameter choices that need to be made in the implementation of acoustic models for shipping and wind noise maps are the spectral, temporal and spatial resolution for the calculations. In practical applications, a suboptimal configuration may be required, in order to reduce the computational complexity of the models. These choices can have a large impact on the accuracy of the resulting sound maps, when they are not carefully selected. This chapter describes the results of numerical simulations that were performed to test the sensitivity of the calculation results to these parameter choices.

The objective of this chapter is to provide insight in the effect of the model parameter choices, in order to make a substantiated recommendation for future modelling efforts. The recommended model settings are aimed at providing sufficiently accurate solutions for the acoustic metric selected in Jomopans project, being: “monthly percentiles of the depth averaged SPL in one-third octave (base-10) bands”. For the sensitivity studies described in this chapter, a ~1 dB uncertainty was considered acceptable. Pending the outcome of the model validation, a larger numerical uncertainty may be found acceptable, lowering the computational complexity requirements of the models.

The modelling aspects studied in this chapter are

- the spectral resolution (section 3.1)
- map receiver spatial resolution (section 3.2)
- sound map spatial processing (section 3.3)
- temporal resolution (section 3.4)
- spatial source gridding (section 3.5)
- configuration of the propagation models (section 3.6)

The recommendations are summarised in section 3.7.

3.1 Spectral resolution

Figure 17 and Figure 18 show comparisons of the depth-average SPL for test case 2, calculated for one (geometric centre) frequency per one-third octave (i.e., 1/10 decade) band and from the sum over ten 1/100 decade sub-bands. JASCO’s MONM model was used for these calculations. Figure 17 shows the broadband SPL as a function of range and Figure 18 shows one-third octave band spectra of the SPL at 10 km and 40 km respectively.

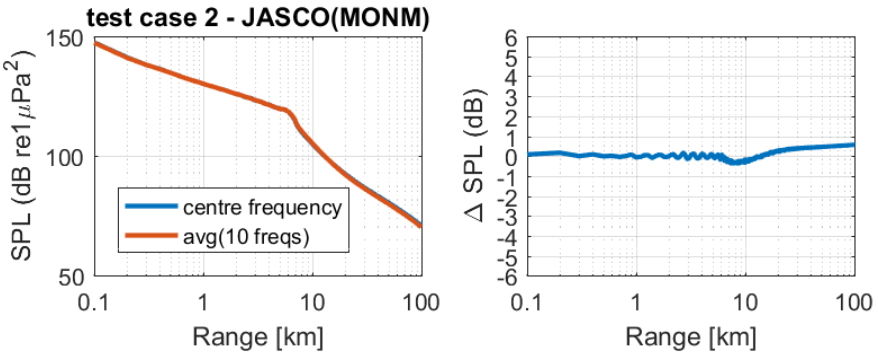

Figure 17 Left: depth-averaged broadband SPL in dB re 1 μPa² as a function of range (horizontal distance to the source) for test case 2, as calculated by JASCO’s MONM model, at the centre frequency of the one-third octave (1/10 decade) bands and as sum over ten 1/100 decade (centidecade) sub-bands. Right: difference between the single frequency and band average results.

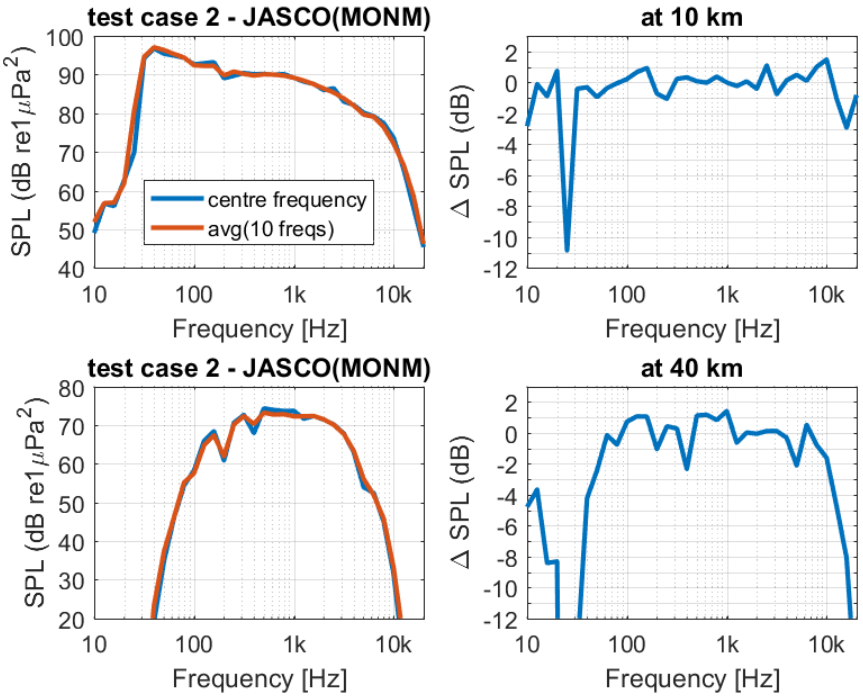

Figure 18 Left: depth-averaged broadband SPL in dB re 1 μPa^2 as a function of frequency at (upper) 10 km and (lower) 40 km from the source for test case 2, as calculated by JASCO's MONM model, at the centre frequency of the one-third octave (1/10 decade) bands and as a sum over ten 1/100 decade (centidecade) sub-bands. Right: difference between the single frequency and band average results

Figure 17 illustrates that for this modelling scenario, the effect of including more than one frequency per band in the calculation of the broadband SPL is less than 1 dB. In the individual one-third octave bands SPLs at fixed distances (10 and 40 km) the differences between the single frequency and band average results are up to 2 dB in the bands that dominate the broadband SPL (Figure 18). At the lower and higher frequency bands, where the calculated SPL values drop off steeply (and hence contribute less to the broadband SPL), the difference is substantially larger (>10 dB). Using one frequency per one-third octave band when calculating depth-averaged SPL in one-third octave bands is likely an acceptable reduction of the calculation effort, at the cost of an approximate uncertainty of 2 dB in the calculated one-third octave band SPL. It should, however, be noted that when one is interested in levels at a specific receiver depth, the error associated with using a single frequency per band is significantly larger. To mitigate this effect, it is recommended to (i) use more frequencies per band or to (ii) apply spatial averaging over range and or depth around the received cell.

For incoherent models such as incoherent mode sums, flux integrals and incoherent rays, the variability of the acoustic field is much lower, making the uncertainty associated with using a single frequency per band significantly smaller.

For the Jomopans sound maps, modelling will be carried out at the centre frequencies of one-third octave (base-10) bands.

3.2 Spatial resolution

The JOMOPANS acoustic metric specification [Merchant et al, 2018] specifies that the geospatial grid is referenced using the standardised 'C-squares' (*Concise Spatial Query And Representation System*) notation[4] [Rees, 2003].

According to Rees [2003]:

- the WMO (World Meteorological Organization) grid divides the world into 648 10×10 degree squares, each with a unique 4-digit identifier or code.
- The first digit of this code indicates the square's "global quadrant", i.e. north-east (1), south-east (3), south-west (5) or north-west (7) as indicated in Figure 20.
- The remaining three digits are derived from the minimum (smallest absolute value) bounding parallels measured in tens of degrees: digit 2 (0 through 8) for 0+ to 80+ degrees of latitude (north or south, depending on the global quadrant designated), and digits 3-4 (00 through 17) for 0+ to 170+ degrees of longitude (east or west, depending on the global quadrant).
    - The JOMOPANS area covers roughly 5°W to 14°E and 51°N to 62°N (corresponding with an area of roughly 1200 × 1200 km^2)
    - WMO square 7500 covers 10°W to 0°E and 50°N to 60°N
    - WMO square 1500 covers 0°E to 10°E and 50°N to 60°N
    - WMO square 1501 covers 10°E to 20°E and 50°N to 60°N
    - WMO square 7600 covers 10°W to 0°E and 60°N to 70°N
    - WMO square 1600 covers 0°E to 10°E and 60°N to 70°N
    - WMO square 1601 covers 10°E to 20°E and 60°N to 70°N
- C-squares extends this numbering system by recursive subdivision according to two sequences: a primary sequence at 10 × 10, 1 × 1, 0.1 × 0.1 degree squares, etc., and an "intermediate" set of subdivisions (quadrants) at 0.5 of each of these values - giving 5 × 5, 0.5 × 0.5, 0.05 × 0.05 degree squares, etc., see 0.
    - a North Sea 10 × 10 degree square is about 482 × 1153 km^2
    - a North Sea 5 × 5 degree square is about 283 × 567 km^2
    - a North Sea 1 × 1 degree square is about 63 × 112 km^2
    - a North Sea 0.5 × 0.5 degree square is about 32 × 56 km^2
    - a North Sea 0.1 × 0.1 degree square is about 6.4 × 11.1 km^2
    - a North Sea 0.05 × 0.05 degree square is about 3.2 × 5.6 km^2
    - a North Sea 0.01 × 0.01 degree square is about 0.6 × 1.1 km^2

[4] "C-squares (acronym for the concise spatial query and representation system) is a system of geocodes (actually a type of global grid) that provides a basis for simple spatial indexing of geographic features or data. It was devised by Tony Rees of CSIRO Marine and Atmospheric Research (then "CSIRO Marine Research") in 2001-2, and described in the literature in 2003.[Rees, 2003] The notation system of c-squares incorporates a compact encoding of latitude and longitude coordinates into a machine- and human-readable c-squares code, which can then be used either for spatial search or display via a suitable mapping application. The c-squares codes also provide an application- and vendor-independent, interoperable notation system for any gridded data whose units of organization correspond with steps of the c-squares hierarchy (e.g. 5-, 1-, 0.5 degree cells, etc.)." (source: https://en.wikipedia.org/wiki/C-squares)

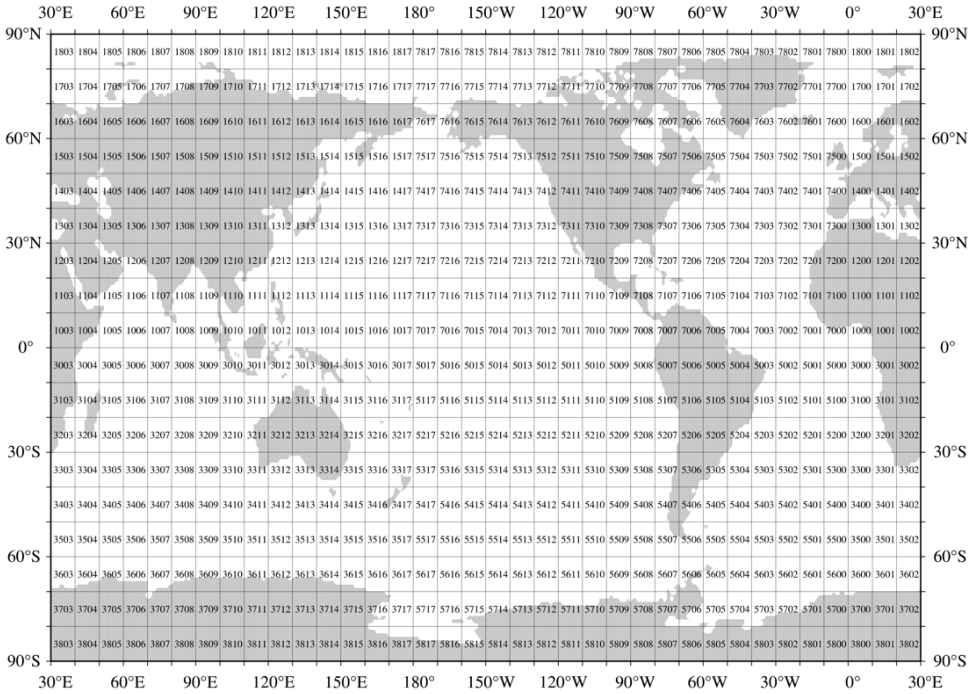

Figure 19: World Meteorological Organization squares, from [NOAA World Ocean Database 2005](#).

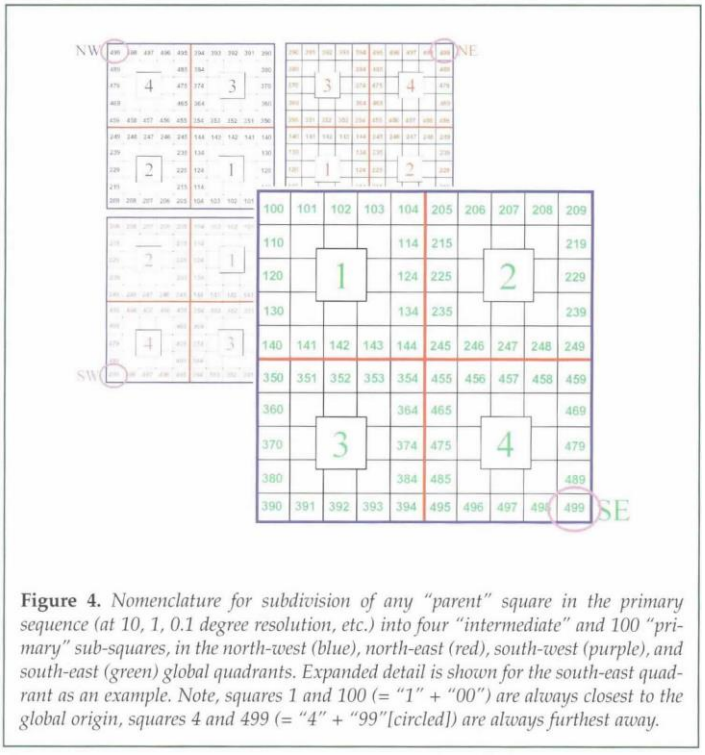

Figure 4. *Nomenclature for subdivision of any "parent" square in the primary sequence (at 10, 1, 0.1 degree resolution, etc.) into four "intermediate" and 100 "primary" sub-squares, in the north-west (blue), north-east (red), south-west (purple), and south-east (green) global quadrants. Expanded detail is shown for the south-east quadrant as an example. Note, squares 1 and 100 (= "1" + "00") are always closest to the global origin, squares 4 and 499 (= "4" + "99"[circled]) are always furthest away.*

Figure 20: C-squares nomenclature, from [Rees, 2003].

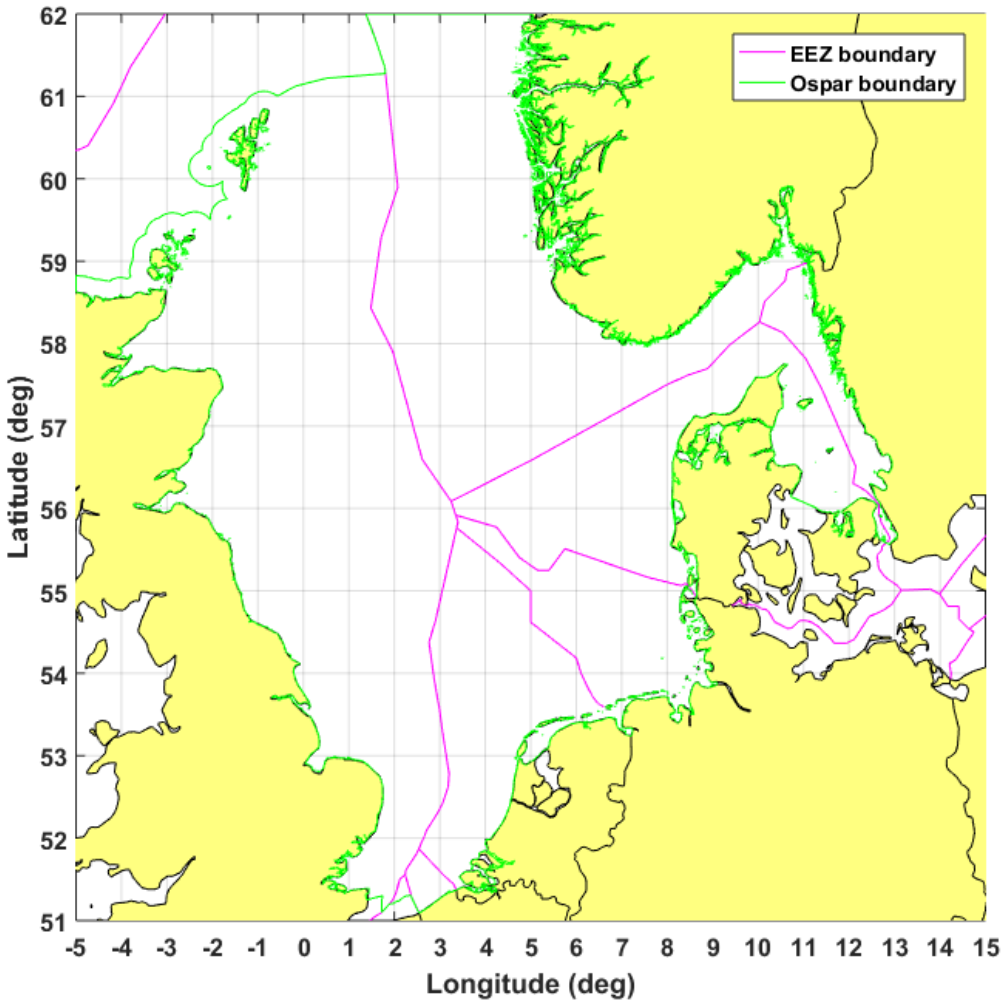

Figure 21: JOMOPANS North Sea modelling area bounded by the green contour (OSPAR boundary). The national Exclusive Economic Zone (EEZ) boundaries are shown in magenta.

For the Jomopans sound maps for the North Sea area (see Figure 21), a 'C-squares' grid with a latitude and longitude resolution of 0.05° (=3 arc minutes) has been agreed, from here on referred to as the (JOMOPANS) modelling grid.
In order to obtain more square grid cells and hence 'smoother' maps, TNO decided to apply a 0.025° longitude × 0.05° latitude grid (i.e. cells of about 3.2 × 2.8 km^2) for the North Sea maps.

Pending the computational complexity of the simulations, which depends on the final configuration of the model. It should be noted that a finer map resolution is desirable when one is interested in local effects, but that the choice is limited by computer time and memory requirements, dependent on the size of the area and the time period and resolution for which modelling results are required.

3.3 Spatial processing for sound maps

In order to reduce the computational complexity of the modelling, sound maps are generally obtained using an "$N \times 2D$ approach" for the source locations, implying that the modelling results are obtained by means of two-dimensional linear interpolation between radial transects (slices/radials) from each source. Furthermore, the modelling range (i.e. the length of the transects) has a large effect on the computational complexity.

Number of radials: For environments with a high spatial variability (e.g. strong variations in water depth or seabed properties) a large number of radials may be needed; while for more homogenous environments a smaller number can be sufficient. Uncertainties in the interpolation are expected when spatial variations occur at a scale that is smaller than the arc length between the radials (i.e. $\pi r/m$ at a distance r from the source when using m radials). Because the North Sea seabed consists primarily of sand and because the bathymetric variability is limited, the authors expect that using a limited number of radials transects is sufficient for most of the North Sea area (with the exceptions of source locations near coastal areas and strong bathymetric features, e.g. near the Skagerrak). A choice for the number

of slices will be determined by means of convergence test using the modelling scenarios for the validation sites. However, the required number radials is expected to be in between 8 and 32, and may depend on the location but also on frequency (which influences the range up to which a source may contribute). Finally, different interpolation methods may be used to obtain levels in between radials. The optimal method will also be investigated during the preparation of modelling for the model validation.

Max modelling range: Sound generated by a ship may contribute up to many kilometres, depending on frequency, environment and ambient noise produced by other sources (including wind and other ships). In order to reduce the computational complexity of the modelling, it is desirable to limit the maximum computation range where possible. The criterion proposed in the JOMOPANS project is a frequency depend threshold for the propagation loss, after which sources are expected to have a negligible effect on the underwater noise.

As part of the calculations for the model validation (T4.3), convergence test will be carried out to determine the required number of radials and maximum simulation range as a function of frequency.

3.4 Temporal resolution

The modelling of acoustic metric maps requires specifying the temporal resolution for computing the statistics of the underwater noise. Hence we need to specify the number of 'snapshots' required to get a reliable and robust calculation of the monthly percentiles. A fine temporal resolution may be needed for:

1. short distances from a shipping lane and for areas with few passing ships
2. high percentiles
3. short analysis windows
4. high propagation losses

For the JOMOPANS project:

1. the minimum range is related to the map resolution.
2. the highest percentile of interest is the 95%
3. the analysis window is one month, but validation may occur in a finer temporal window to understand the cause of model-data inaccuracies
4. propagation losses are expected to be large at low frequencies (shallow water) as well as at high frequencies (reflection losses and absorption).

In order to get a better understanding of the sensitivity of the modelling to the temporal resolution, an initial sensitivity study was carried out for a synthetic single shipping lane modelling scenario, representative for areas in the North Sea with uniform 50 m water depth in the vicinity of a shipping lane

Time analysis window: The analysis window for this initial analysis was set to 24 hours. Although the Jomopans analysis window is 1 month, for the validation it is also of interest to look at the accuracy of the models for smaller temporal windows, hence the choice for 24 hours.
Source and propagation: It was tentatively assumed for this analysis that all ships have the same source level. The simulations are based on the Aquarius 3 model results for the test case 1 environment (see section 2.3.3). Sources in the shipping lane were taken into account up to 300 km from the receiver location (indicated in Figure 22 by the black circles surrounding the receiver locations, at the coloured circles). A broadband wind noise contribution of 90 dB re 1 μPa was added at all receiver locations. Only the statistics of the broadband levels was considered.
Shipping lane: One-way direction (South to North) ship traffic along the straight green line in Figure 22; with ships moving at a constant speed of 13.5 kn (6.9 m/s). At this speed a ship sails 600 km in 24 hours. The distance in between the ships is 30 km on average, with a minimum of 15 km and a maximum of 45 km. Randomisation with a uniform distribution was applied to introduce some variability into the modelling. The mean number of ships along 600 km track length is about 20.
Receiver locations: receivers where located at 1, 2, 5, 10, 25, 50, 100, 150 & 200 km perpendicular from the shipping lane.

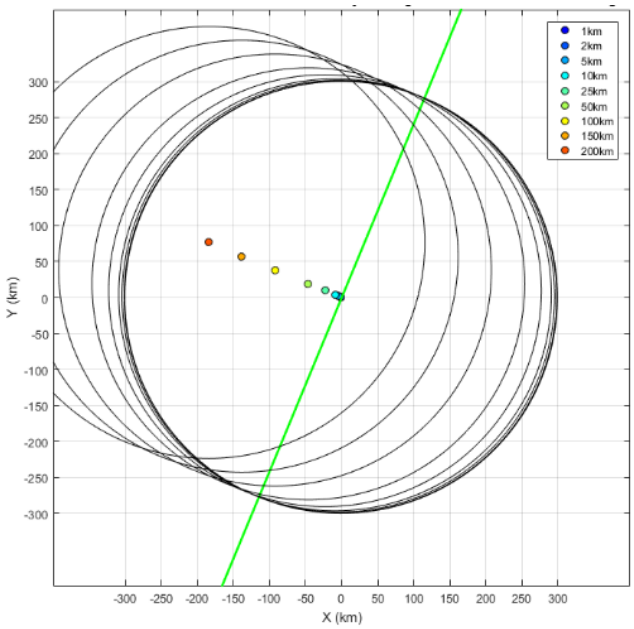

Figure 22: synthetic shipping lane modelling scenario

The depth-averaged broadband SPL was calculated for the 9 receiver locations for a period of 24 hours, in 1 minute time steps. The effect of the time step on the acoustic indicator metric was investigated by calculating the SPL percentiles for different subsets of the calculation results, corresponding with different time resolution**.** Figure 23 shows the percentiles of the modelled SPL at the 9 receiver locations for increasing time steps, indicated by the line style ('-' 1 min, '--' 5 min, '-.' 15 min, '..' 30 min).

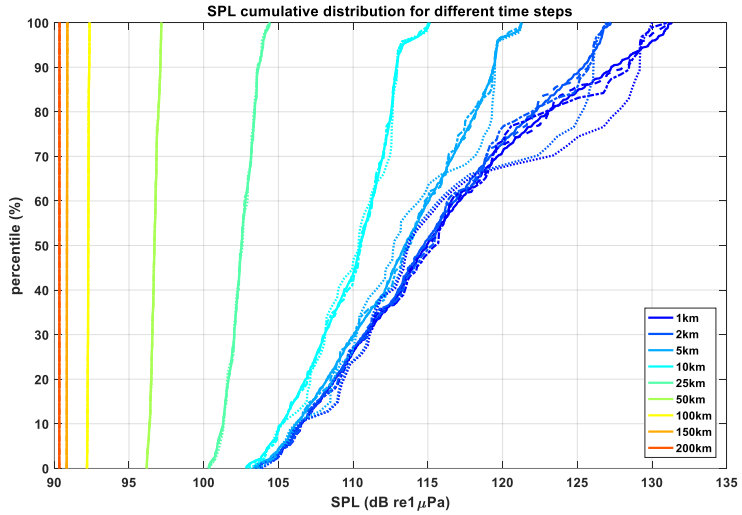

Figure 23: Modelled percentiles of the depth-averaged broadband SPL at 9 distances from the shipping lane (see legend) for different time steps indicated by the line style ('-' 1 min, '--' 5 min, '-.' 15 min, '..' 30 min).

Table 2: consequences of different time steps

Time step	Number of snapshots in 24 hours	Ship displacement along track per time step
1 min	1440	0.42 km
5 min	288	2.1 km
15 min	96	6.3 km
30 min	48	12.5 km

The results in Figure 23 show that for this scenario the difference between a 15 minute time step and a 1 minute time step is less than 1 dB at all percentiles. It is expected that there is a linear relationship between the temporal resolution that is required to limit this difference to within e.g. 1 dB and the duration of the analysis window. This ratio depends on the number of snapshots from which the

statistics are calculated, but also on details of the scenario such as the environment and ship distribution and variability. Hence this relationship will be further investigated in the modelling for the 2018 validation locations in Task T4.3. It is proposed to provide these model predictions at a resolution of 5 minutes. The influence of the temporal resolution (multiples of 5 min) can then be compared for different analysis windows. For this comparison, conclusions will be made also for individual bands. It is expected that a finer time resolution is needed at frequencies for which propagation losses are high (lowest and highest bands). Finally, it should be noted that it is planned to include the source uncertainty directly in the acoustic modelling. Because the source level variability is large (>5 dB for all bands), it is expected to have a significant effect also on the required model configuration.

For the Jomopans sound maps for the North Sea area (see Figure 21), a 'C-squares' grid with a latitude and longitude resolution of 0.05° (=3 arc minutes) has been agreed, from here on referred to as the (JOMOPANS) modelling grid. In order to obtain more square grid cells and hence 'smoother' maps, TNO decided to apply a 0.05° longitude × 0.025° latitude grid (i.e. cells of about 3.2 × 2.8 km^2) for the North Sea maps.

3.5 Spatial source gridding

To further reduce the computational complexity, propagation loss calculations can be reused when sources are aggerated on a fixed simulation grid. To test the sensitivity of the acoustic indicator to source gridding (aggregation/binning), the modelling scenario for testing the effect of the temporal resolution is adapted by projecting the ships from the shipping lane on a source grid relative to the receiver grid, as depicted in Figure 24. Note that the model results are for the specified receiver locations along the transect perpendicular to the shipping lane.

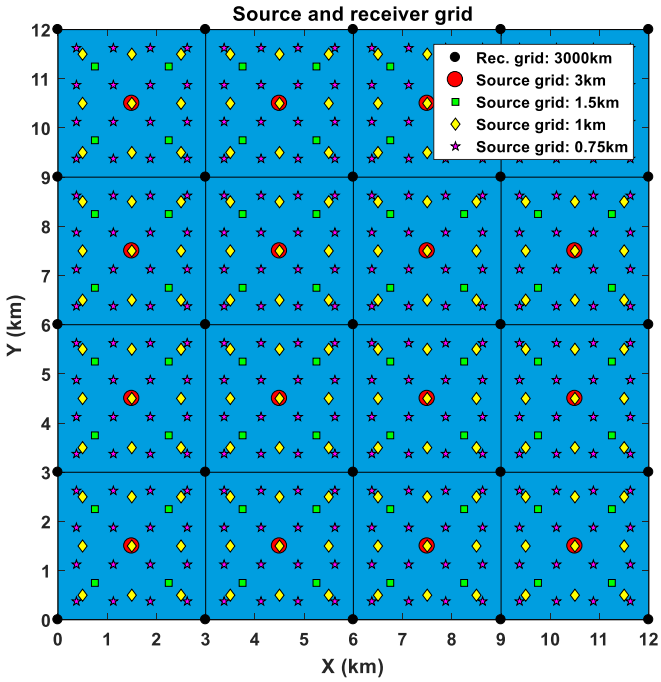

Figure 24: illustration of source gridding with respect to receiver grid.

Figure 25 shows the calculated SPL percentiles (for 5 minute temporal resolution) for various source grid resolutions, indicated by the line style ('-' no source gridding, '--' 3 km, '-.' 1.5 km, '..' 1 km), for which the locations are depicted in Figure 24.

The results show that source gridding increases the model uncertainty at short ranges from the shipping lane for higher percentiles. The error introduced by the source gridding is independent on the analysis period because sources are systematically relocated to the same fixed source grid resulting. For the 3 km source grid resolution a maximum error of 3 dB is observed for the highest percentiles at short ranges. For the 1.5 km source grid the error is generally smaller than 1 dB for all percentiles.

To minimize the computational complexity, a coarse source grid is desirable as the computational efforts for the propagation modelling increase with the number of source grid points. Figure 25 suggest that the effect of source gridding can be significant at shorter ranges, for this generic scenario. This will be further investigated in the modelling for the 2018 validation locations in Task T4.3, for a more

realistic ship distribution based on AIS data. If the validation results show that the error due to source gridding is considered unacceptable, two options are foreseen to reduce this error:

1) Refinement of the source grid resolution at the cost of a lower computational efficiency
2) Shifting of the source grid to the real source location by means of interpolation (assuming that the environment relative to the source can be shifted, but correcting the range)

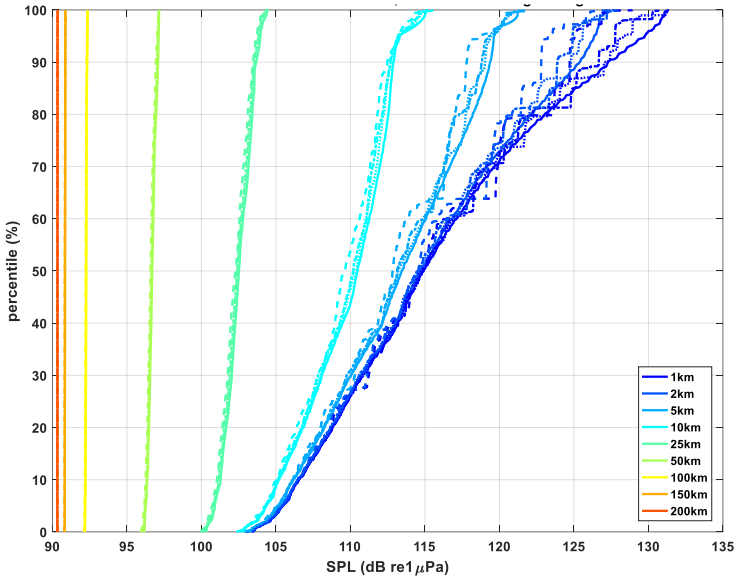

Figure 25: Percentile plot of depth averaged broadband SPL for various source gridding resolutions at the selected receiver positions (not gridded). The line style indicates the source gridding resolution ('-' no source gridding, '--' 3 km, '-.' 1.5 km, '..' 1 km)

3.6 Configuration of propagation models

In the benchmark studies described in chapter 2 the models were configured to provide optimal accuracy, in order to obtain a trusted solution against which models can be tested and their accuracy can be quantified. This model configuration can be referred to as a 'high fidelity' (HiFi) configuration. For practical ('operational') modelling purposes, however, a HiFi configuration may be too computationally intensive. The large area and long period noise modelling requirements for the JOMOPANS project will limit other relevant modelling parameters such as the ones discussed earlier in this chapter. The models will be used in their operational mode for the validation and mapping (TNO only).

	Aquarius 3 (TNO)	**High fidelity**	**Operational**
1	**Discretisation of mode stripping integral**	400 angles	100 angles
2	**Maximum number of modes**	200	25
3	**Receiver depth resolution**	Water depth / 10	Water depth / 10
4	**Receiver range resolution and profile**	100 m	Logarithmic profile[5]
5	**Numerical range resolution**	10 m	100 m
6	**Number of discrete modes modelled**	5	5
	RAM (Quiet Oceans)	**High fidelity**	**Operational**
1	**Number of Padé terms**	8	4
2	**Range numerical grid discretisation**	10 m	Wavelength
3	**Depth numerical grid discretisation**	Wavelength /10	Wavelength /10
4	**Receiver depth discretisation**	Wavelength /10	1 m
5	**Receiver range discretisation**	10 m	Wavelength
	Bellhop (Quiet Oceans)	**High fidelity**	**Operational**
1	**N Rays**	300,000	100,000
2	**Beam type**	Coherent gaussian	Incoherent gaussian
3	**Beam opening angle**	89	89
4	**Receiver depth discretisation**	0.5 m	1 m
5	**Receiver range discretisation**	10 m	Wavelength

Here the 'receiver depth resolution' determines the number of receiver depth positions required to get a reliable and robust calculation of the depth-averaged SPL. Coherent models need more receiver depths than incoherent models. In particular when combined with calculations for one frequency per one-third octave band and not applying range averaging, one would need a number of points per wavelength across the water depth in order to obtain a smooth solution with range.

Figure 26 shows the test case 1 (top) and test case 2 (bottom) spectral modelling results for Aquarius 3 and Quonops (RAM + Bellhop) models at 10 and 50 km range for the high fidelity (HiFi) and operational (LoFi) settings. The results show that introduced bias is generally smaller than 1 dB for all frequencies.

[5] A minimum receiver range step of 100 m and a maximum range step of 2 km is used to avoid unnecessary fine sampling in the near field (where modelling is in general considered inaccurate) and to avoid to sparse sampling in the near field to avoid bathymetric blockages or large effect of the changing bathymetry on the sound propagation. For a 100 km simulation range the following receiver range profile is used (described using Matlab syntax): [logspace(100,15e3,37) 17e3:2e3:100e3].

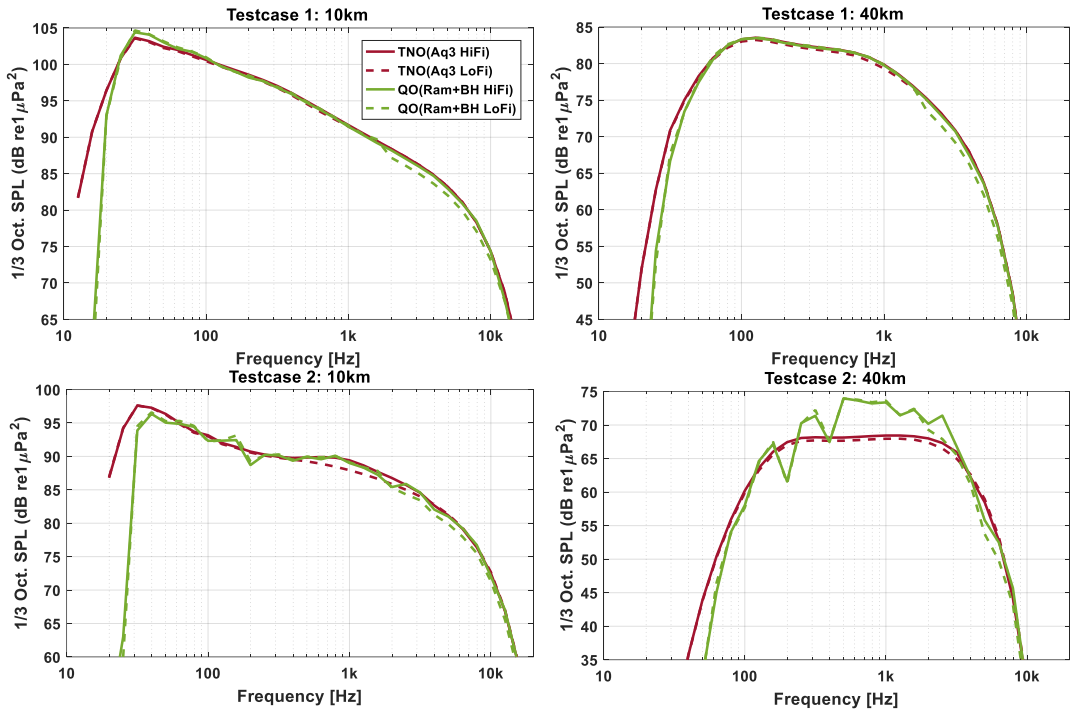

Figure 26 Test case 1 (upper graphs) and testcase 2 (lower graphs) spectral modelling results for Aquarius 3 and Quonops (RAM+Bellhop) models at 10 and 40 km range.

4 Sensitivity scenarios

In this chapter, sensitivity studies are described that systematically address the various parameter dependencies and modelling errors and uncertainties associated with modelling underwater sound maps.

The objective of these sensitivity scenarios is to provide insight in the uncertainty in the maps associated with the environmental input to the models:

- Seabed loss as a function of sediment grain size (section 4.1)
- Surface loss as a function of wind speed (section 4.2)
- Propagation loss as a function of sound speed profile (section 4.3)

and with the ship and wind source models and input data (section 5)

4.1 Seabed loss

4.1.1 Description of methods

Two different approaches for deriving seabed acoustic parameters for the North Sea sound maps have been identified in [de Jong et al, 2018]:

1) from the Folk 7 and 5 data available from Emodnet geology portal
2) from maps of median grainsize data (https://doi.org/10.1594/WDCC/coastMap_Substrate_MGS).

Examples of maps of these two sediment classifications are shown in Figure 27.

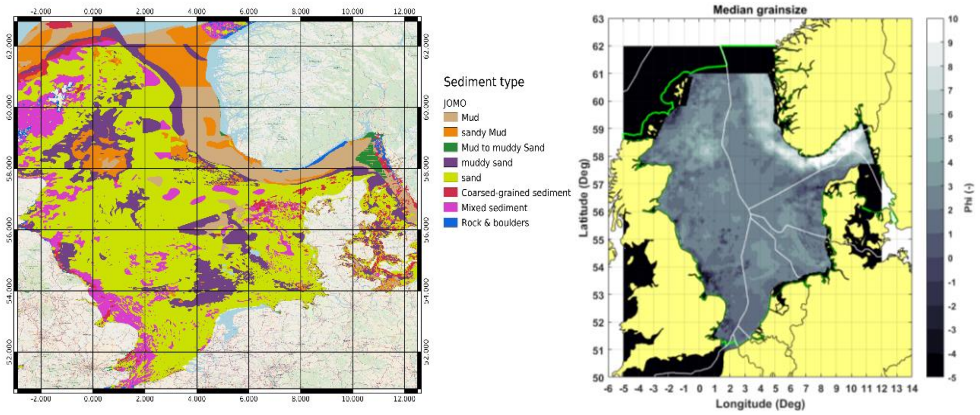

Figure 27 Left: Map of the Folk type sediment data from the Emodnet geology portal. Right: Grainsize parameter map from https://doi.org/10.1594/WDCC/coastMap_Substrate_MGS.

Mapping seabed sediment properties is subject to many uncertainties [van Heteren & Van Lancker, 2015; Bockelmann et al, 2018]. The conversion of Folk class or grain size distributions to geo-acoustical parameters adds additional uncertainty. The study described in this chapter is aimed at quantifying the sensitivity of the ship noise modelling to the uncertain sediment parameters.

TNO has proposed to derive the geo-acoustic parameters from the median grainsize map. The area distribution of the median grain sizes in the Jomopans area (Figure 28) shows that a large fraction of the North Sea sediment is 'sandy', with grain size parameter $M(\phi)$ between 1 and 3.

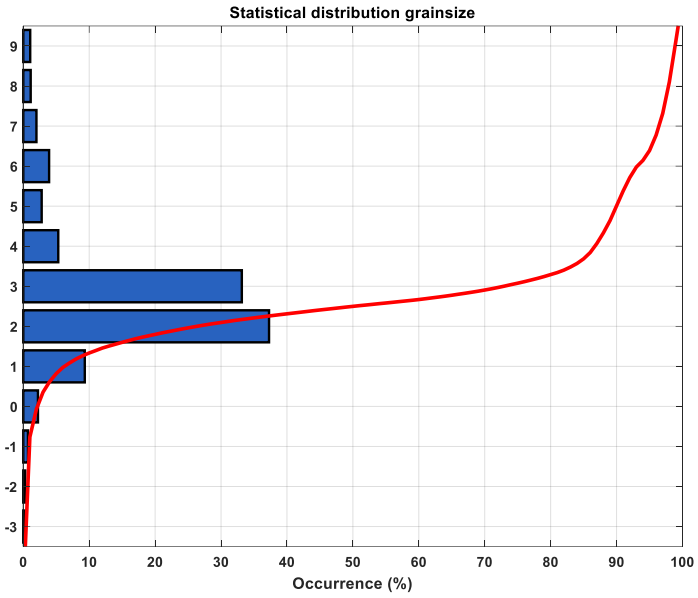

Figure 28 Distribution of median grain sizes (expressed by the grain size parameter $M(\phi)$) in the Jomopans area.

Quiet Oceans (QO) has proposed the following conversion table to relate the Folk types to geo-acoustical properties of the sediment (here limited to the dominant classes found in the Jomopans area).

Table 4.1 Correspondence between Folk types and geo-acoustical properties used in the modelling of QO.

Folk 7 type		Density	Compressional Speed	Attenuation
		kg/m^3	m/s	dB/λ
11	Mud	1146	1501.11	0.089
12	Sandy Mud	1149	1508.59	0.211
13	Muddy Sand	1339	1650.24	0.943
2	Sand	1530	1708.00	0.910
4	Mixed sediment	2030	1855.00	0.890

There is no direct link between Folk type and median grain size, but based on Table 4.16 in [Ainslie, 2010] and subjective judgement, the Folk 7 types can be roughly connected with median grain sizes in the range between the minimum and maximum values given in Table 4.2. Table 4.2 also gives the corresponding ranges of density, compressional sound speeds and attenuation coefficients, applicable for the mid-frequency range (1-10 kHz), from Table 4.18 in [Ainslie, 2010].

Table 4.2 Correspondence between Folk types and geo-acoustical properties from Table 4.18 in [Ainslie, 2010].

	Folk 7 type	$M(\phi)$		Density kg/m^3		Compressional Speed m/s		Attenuation dB/λ	
		min	max	min	max	min	max	min	max
11	Mud	7	9	1353	1474	1481.6	1521.0	0.08	0.13
12	Sandy Mud	6	7	1474	1555	1521.0	1552.8	0.13	0.21
13	Muddy Sand	3	6	1555	1879	1552.8	1697.1	0.21	0.96
2	Sand	1	3	1879	2162	1697.1	1833.9	0.87	0.96
4	Mixed sediment	-1	1	2162	2492	1833.9	2005.5	0.87	0.91

Note that the values proposed in Table 4.1 are not all within the ranges of values proposed in Table 4.2. In particular, the densities in Table 4.2 are consistently higher. Comparison of table 4.18 (MF geo-acoustic parameters, 1-10 kHz) and table 4.17 (HF geo-acoustic parameters, 10-100 kHz) confirms that the MF densities are consistently higher than the HF densities. This is because the HF sound penetrates only the first few centimetres of sediment, where the density is lower, and the MF sound penetrates the first few metres, where the density is higher.

4.1.2 Scenario description

Without further evidence it is unclear which geo-acoustic parameter values provide the best description of the North Sea sediment. In order to investigate the sensitivity of the model results to the specific choice for the geo-acoustic parameters, a set of simulations is carried out for the test case 1 scenario for a majority (80% of North Sea, Figure 28) of the grain sizes, varying from 1 to 5 ϕ (for which the corresponding geo-acoustical properties are shown in Table 4.3). The quantity compared for this range of geo-acoustic properties is the depth-average SPL as a function of range and frequency.

For the uncertainty analysis it would also be of interest to evaluate possible effects of modelling sediment layering and (frequency -dependent) dispersion and shear properties of the sediment and of layering, in particular at low frequencies. However, the proposed models for large scale sound mapping do not include these effects. Hence, these effects could not be directly quantified in the scope of this sensitivity study.

Table 4.3 geo-acoustical properties from Table 4.18 in [Ainslie, 2010] for a range of grain sizes $M(\phi)$,for a sound speed of 1500 m/s and a 1000 kg/m3 density of water.

$M(\phi)$	Density kg/m^3	Compressional Speed m/s	Attenuation dB/λ
7	1474	1521.0	0.13
6	1555	1552.8	0.21
5	1650	1592.9	0.71
4	1758	1640.9	1.13
3	1879	1697.1	0.96
2	2014	1761.4	0.88
1	2162	1833.9	0.87
0	2314	1916.7	0.87
-1	2492	2005.5	0.91

4.1.3 Results

Figure 29 shows the broadband SPL (left) and the difference (right) with respect to the solution corresponding to $M = 3\ \phi$. These results show that for the test case 1 scenario, the selection of geo-acoustic properties for the 'muddy sand' to 'sand' sediment that is found over large areas of the North Sea can lead to a maximum difference in the broadband (10 Hz – 20 kHz) SPL predictions of 12 dB.

Analysis of the spectral levels in one-third octave bands (Figure 30) shows that the effect of geo-acoustic properties on the broadband SPL increases significantly towards the lower end of the frequency spectrum. In the 125 Hz bands the maximum difference is about 10 dB, in the 63 Hz band it is 16 dB;

It is important to note that this is a simplified analysis for a constant water depth (50 m), where larger differences are expected for shallower water. Also, the seabed is assumed to be homogenous (semi-infinite) and it is assumed that the values given in Table 4.3 are valid for all frequencies. In reality heterogenous seabed properties or possible nonlinear frequency dependence of the geo-acoustical properties, due to the increasing depth to which the sound penetrates into the sediment towards lower frequencies, will have a significant effect on the model predictions.

In task T4.3, the models will be validated against measurements at North Sea 2018 monitoring locations. Observed differences between model predictions and measurements may lead to the conclusion that different parameter values than the values given in Table 4.3 give a better description of the seabed properties in the North Sea. In such a case, an update of the selected geo-acoustical input might prove beneficial. For the JOMOPANS project, such a recalibration of geo-acoustic parameters should however only be done for a subset of the locations to avoid over calibration of the models to specific sites, potentially resulting in an underestimating of the uncertainty associated with the large scale maps.

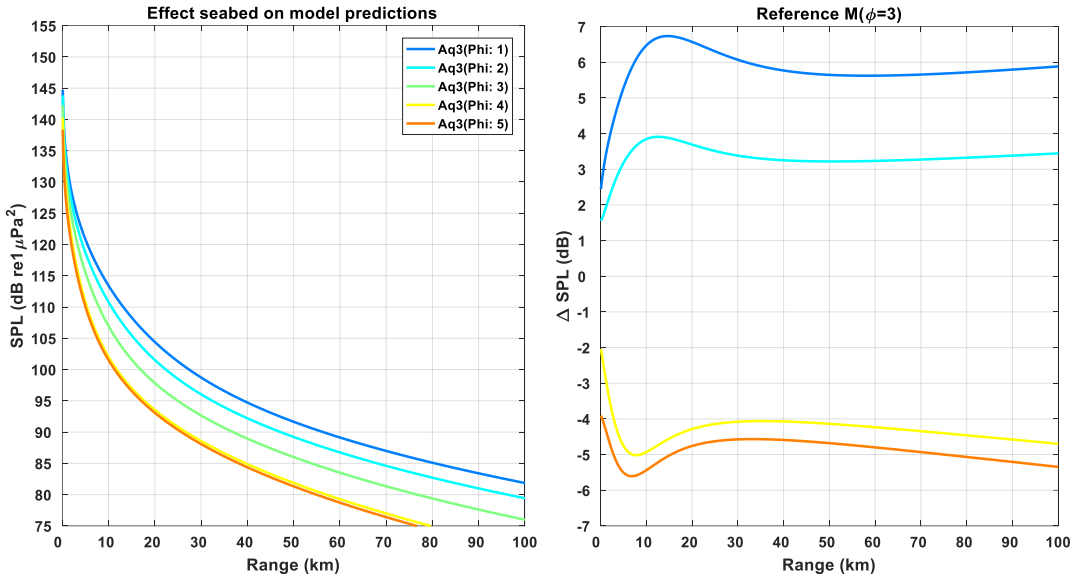

Figure 29 Broadband SPL as a function of range as calculated by TNO's Aquarius 3 model for the test case 1 scenario (§2.3) and the sediment properties from Table 4.3. The righthand figure shows the difference of the results for the different grain sizes relative to the results for the 3 ϕ grain size

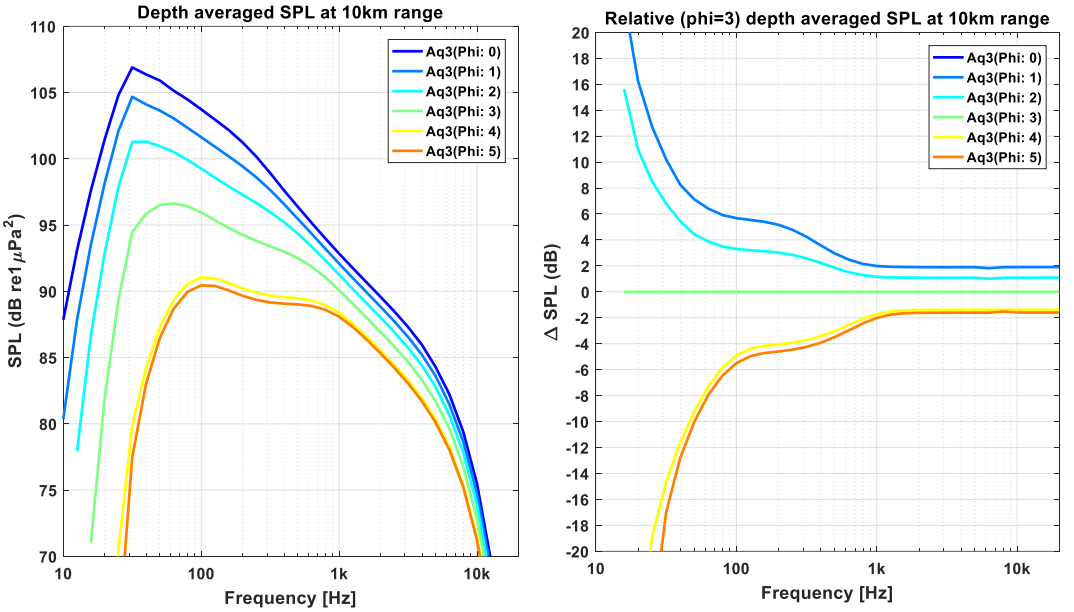

Figure 30 Broadband SPL at 10 km distance from the source as a function of frequency (in one-third octave bands) as calculated by TNO's Aquarius 3 model for the test case 1 scenario (§2.3) and the sediment properties from Table 4.3. The righthand figure shows the difference of the results for the different grain sizes relative to the results for the 3 ϕ grain size

4.2 Surface loss

The objective of this section is to evaluate the influence of surface losses due to surface roughness (for example caused by wind-driven surface waves) on the calculated SPL percentiles of shipping noise in the North Sea.

Ocean waves can be classified in several ways. The most intuitive and commonly used classification is based on the wave period or the associated wavelength. A graphical representation is provided in Figure 31 (Holthuijsen, 2007), where an idealized wave energy spectrum shows the full range of ocean wave components. We here concentrate on wind-generated waves that affect the sound propagation and contribute to the ocean sounds. A statistical analysis of the North Sea wind data for March 2018 shows that half of the time, wind speeds at 10 m height are larger than 10 knots.[6]

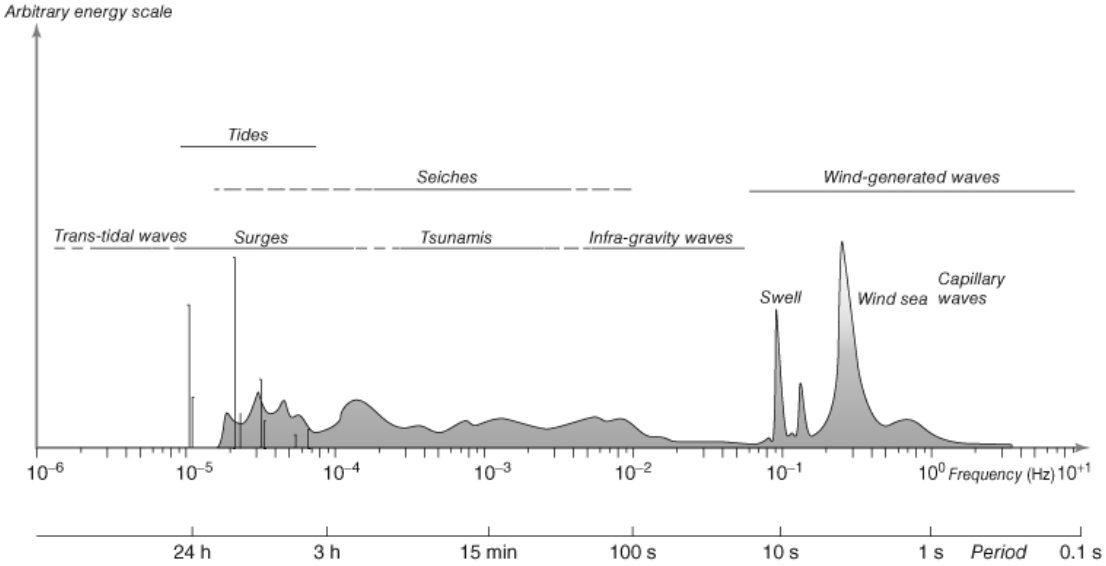

Figure 31 Frequency and period of ocean waves. (Reproduced from Holthuijsen, 2007. © Cambridge University Press, 2007.)

4.2.1 Description of surface loss model

There is a number of approaches of diverse complexity to model the effect of the surface roughness generated by the wind on underwater sound propagation. As a first approach, it is suggested by QO to use the Kirchhoff model for a randomly rough surface (see e.g. [Jensen et al, 2011]). It gives a model for the reflection loss (RL) in dB per surface bounce, as a function of the grazing angle and the wind speed (or surface roughness).

The Kirchhoff model is implemented using the following expression that describes a randomly rough surface [Jensen et al, 2011]

$$R_{\mathrm{coh}} = -\mathrm{e}^{-0.5\Gamma^2}$$

$$\Gamma = 2kh\sin\theta$$

With

- k is wavenumber;
- h is rms surface roughness;
- θ is grazing angle, radians;
- R_{coh} is sound pressure reflection coefficient.

The conversion from 'equivalent' wind speed w to surface roughness h is done using the following formula [Ainslie, 2010 p.167]:

$$h = \sqrt{D_{\mathrm{PM}} w^2}$$

With:

- w wind speed
- h is rms surface roughness.
- $D_{\mathrm{PM}} = 2.85 \times 10^{-5}$ m^{-2}s^4

[6] 1 knot = 1852/3600 m/s

The Reflection Loss becomes in dB per surface bounce

$$\mathrm{RL} = 3.10^{-4}\left(\frac{h}{1\ \mathrm{m}}\right)^2\left(\frac{f}{1\ \mathrm{Hz}}\right)^2\left(\frac{\theta}{1\ \mathrm{rad}}\right)^2\ \mathrm{dB}$$

Examples are displayed in Figure 32:

- Left: for a 1 m wave height[7] h at 10 Hz, 100 Hz, 1 kHz and 10 kHz,
- Right: at 1 kHz, for h =0 (flat) to h =1.5 m wave height.

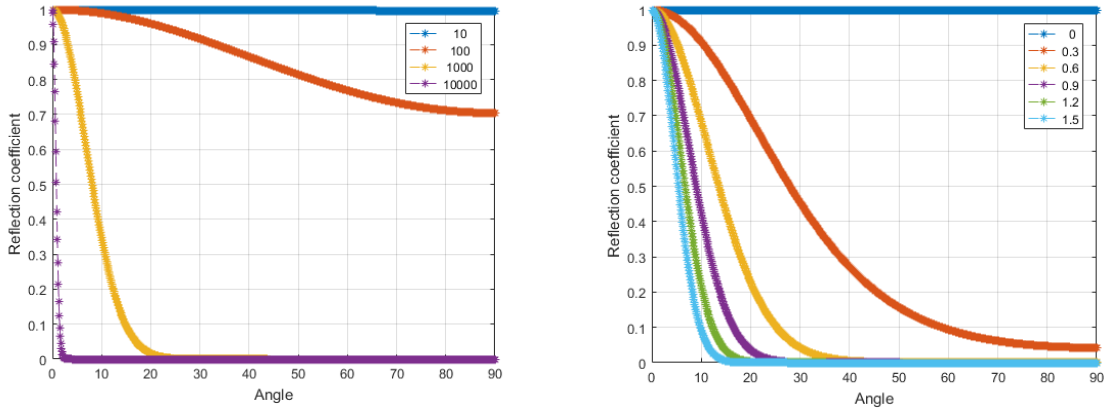

Figure 32 Surface reflection loss as a function of grazing angle as given by the Kirchhoff model. Left: at 10 Hz, 100 Hz, 1 kHz and 10 kHz for h=1 m; Right: h=30 cm, 60 cm, 90 cm, 1.2 m and 1.5 m at 1 kHz

It is recognized that this is a simplified approach, that, in particular, does not consider the generation of bubbles when wind picks up [Weston, 1989; Norton & Novarini, 2001; Ainslie, 2005]. The Kirchhoff model therefore tends to underestimate the surface loss at higher wind speeds. It also underestimates for low wind speed (even without bubbles) at low angles, see Kuo (1988).

4.2.2 Scenario description

The scenario modelled is similar to scenario 1 in which the water depth is 50 m, the sound speed profile is iso-velocity, the sea bottom sediment is equivalent to sand and the sound source is at 5 m depth. An increase in wind speed is modelled via an increase of the rms wave height, from a perfectly flat surface (as per scenario 1) at zero wind speed up to a rms wave height of 4 m.

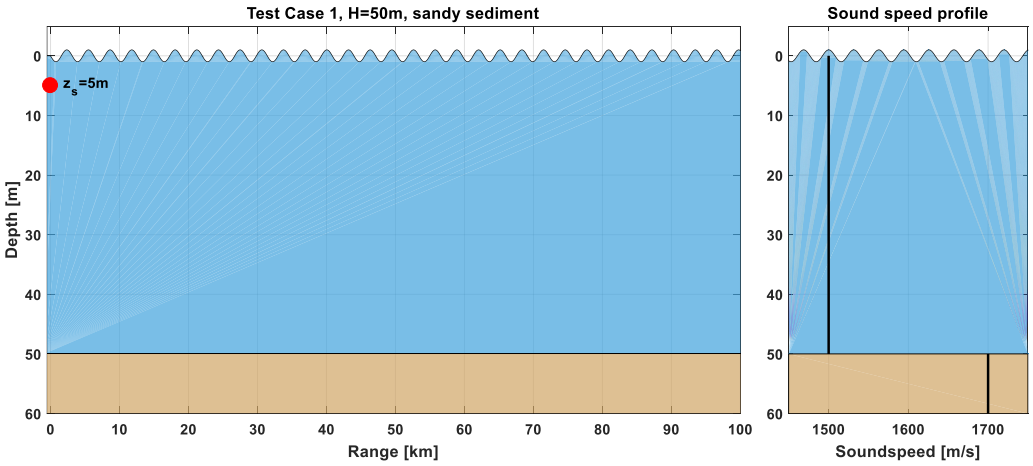

Figure 33 Schematic representation of surface loss benchmark scenario (based on Test Case 1).

[7] The rms surface roughness is the square root of the variance of the sea surface elevation above its mean value. This is about one fourth of the 'significant wave height', which is often used as descriptor of 'wave height' (see e.g. Ainslie, 2010, section 4.3.2.1).

Table 4: Parameters used for assessing the effect of the surface roughness to the sound propagation.

Ref	Water depth	Hrms	Equivalent wind speed at 10 m height[8]	SSP	Seabed sound speed	Seabed density	Seabed attenuation
01	50 m	0 m	0 m/s	1500 m/s	1700.0 m/s	2000 kg/m^3	0.5 dB/λ
02		0.5 m	9.6 m/s				
03		1 m	13.6 m/s				
04		2 m	19.3 m/s				
05		3 m	23.6 m/s				
06		4 m	27.3 m/s				

4.2.3 Results

The results show that the surface roughness decreases the depth-averaged sound pressure levels rapidly at relative short ranges of a few kilometres. Although it is acknowledged that the Kirchhoff model under-estimates the effect of wind-generated waves, the model already highlights about 5 dB reduction for h=1 m (sea-state 3) and about 10 dB reduction for h =2 m (sea-state 4).

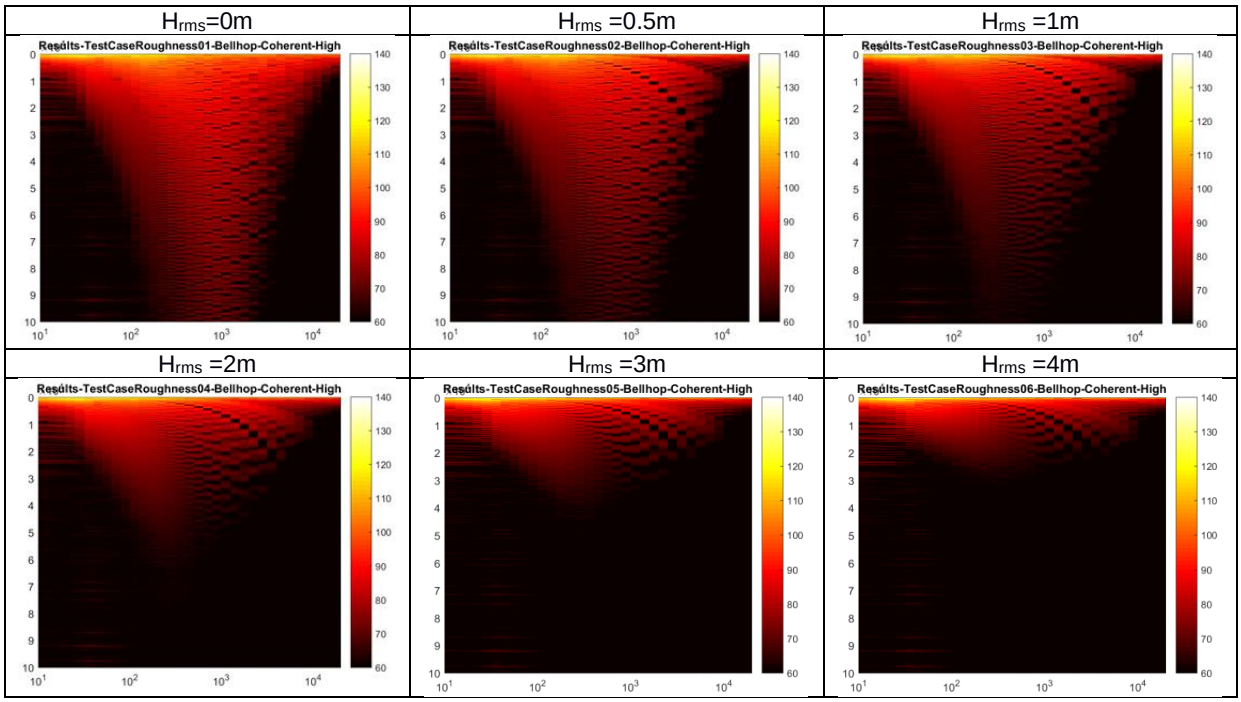

Figure 34 Depth-averaged SPL in dB re 1 μPa2 as a function of frequency (one-third octave bands) and range (km), as calculated by Bellhop HiFi (Quiet-Oceans) for the flat surface (left), and regularly increasing rms surface height at 50 cm, 1 m and 1.5 m.

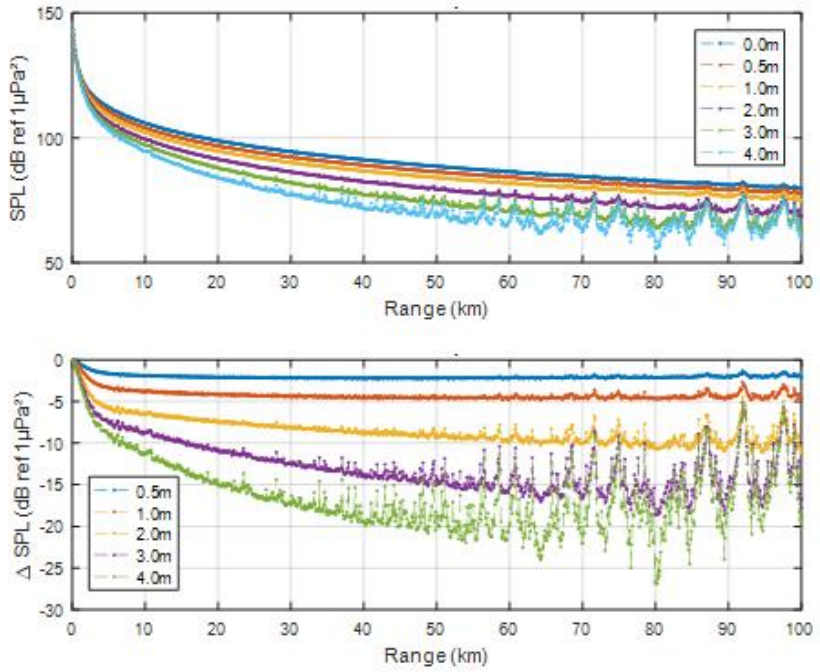

Figure 35 Depth-averaged broadband SPL in dB re 1 μPa^2 as a function of range (km), as calculated by Bellhop HiFi (Quiet-Oceans) for various h ranging from a flat surface to 2 m. The figure on the bottom show the difference from the iso-velocity case taken as reference.

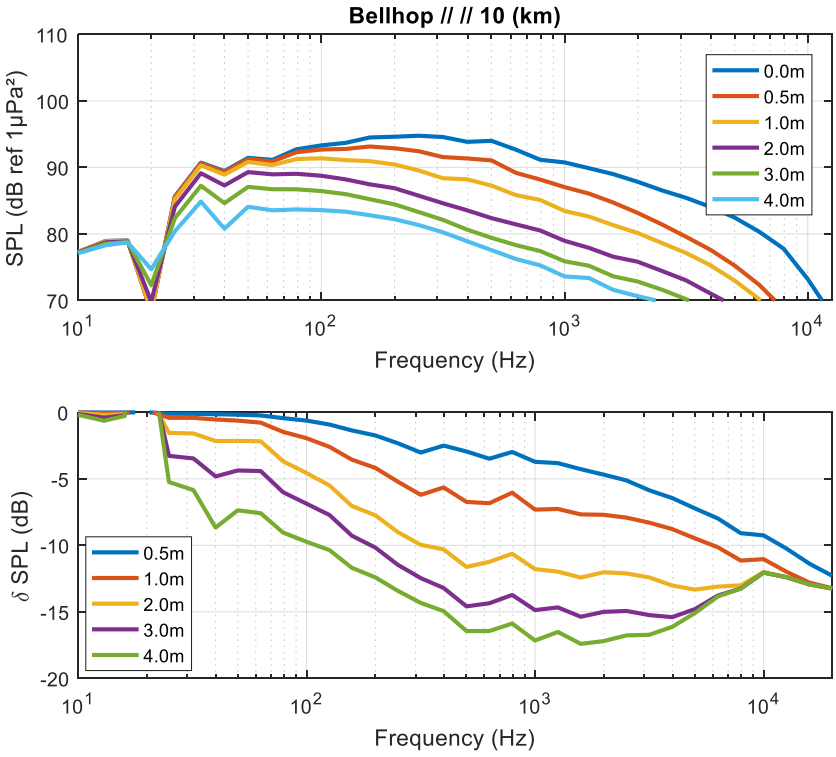

Figure 36 Depth-averaged broadband SPL in dB re 1 μPa^2 at 10 km range as a function of frequency, as calculated by Bellhop HiFi (Quiet-Oceans) for various h ranging from a flat surface to 2 m. The figure on the bottom show the difference from the flat surface case (scenario 1) taken as reference.

4.3 Sound speed profile

This section discusses the relevance of taking the sound speed into consideration in the modelling of the underwater noise for the North Sea (JOMOPANS area). This is of particular importance since some acoustic models assume exclusively iso-velocity profiles.

Oceanographic data envisioned as input to produce noise maps describe temperature and salinity as a function of time, latitude, longitude and depth. The Hydrographic Society (Pike and Beiboer, 1993) has produced a good summary of the main algorithms for converting these to sound speed in the ocean, including information of the domains of validity of the main equations and on depth to pressure conversions.

The international standard algorithm, often known as the UNESCO algorithm [Fofonoff and Millard, 1983] uses pressure as a variable rather than depth because it is based on measurements made in small laboratory pressurised chambers. Useful guidance and suitable equations for converting pressure into depth and depth into pressure can be found in [Leroy and Parthiot, 1998], see also p.128 of [Ainslie, 2010]. An equation for the calculation of sound speed in seawater as a function of temperature, salinity, depth, and latitude in all oceans and open seas, which agrees to better than $\pm 0.2\ \mathrm{m}/s$ with two reference complex equations is proposed by [Leroy et al, 2008].

To assess the sensitivity of the acoustic prediction for the vertical sound speed distribution, modelling is performed with range-independent sound speed profiles representative of the winter and summer seasons. Sound source depth and characteristics, surface and bottom properties are kept identical to the test case 1. The presence of a thermocline modifies the geometry of the propagation and therefore the interaction with the bottom. To address this, a “shallow” water and a “deep” water case have been defined.

The results of the summer and winter profile modelling are compared to the results of a propagation in an iso-velocity configuration and differences are quantified.

4.3.1 Scenario description

The following modelling scenarios have been defined to address the relevance for taking into account the vertical distribution of the sound speed. Based on the analysis of one year of oceanographic data across the North Sea taken from the Copernicus Marine Environment Monitoring Service (CMEMS[9]), two representative scenarios have been defined by QO, for summer and for winter respectively (Table 4.5). The sound speed profile (SSP) data in this table are computed with the UNESO formula, using temperature, salinity and pressure data from CMEMS.

The modelling scenarios are derived from test case 1, in which the following parameters have been modified:

- Bathymetry remains flat (range independent) in all scenarios, one scenario has a 50 m depth bathymetry (as per test case 1), and a second scenario has a 200 m depth bathymetry in order to address the deepest part of the North Sea;
- Sound speed profiles considered are iso-velocity (as per test case 1), winter profile and summer profile, as defined in Table 4.5. The sound speed profiles are cropped to the effective water depth.

The geo-acoustical properties of the seabed are related to the water properties near the seabed. More reliable acoustic modelling is expected when the seabed sound speed and density are computed from a fixed ratio with the equivalent water properties. For this sensitivity study, the compressional speed of the bottom is set fixed as in the test case 1, independent of the sea water sound speed at the interface. The seabed attenuation is assumed to be independent of depth. The geo-acoustical properties are shown in Table 4.6.

[9] http://marine.copernicus.eu/

Table 4.5: Left: Table with SSP values used for the sensitivity study. Linear interpolation and extrapolation are used to obtain values at intermediate depth values and at depths < 0.5m. The data source is CMEMS, layer GLOBAL_ANALYSIS_FORECAST_PHY_001_024, obtained at N 60.043433, E 3.585500 at dates (ISO 8601) 2018-01-15 (winter SSP) and 2017-08-07 (summer SSP). Right: plot of tabulated SSP values. The data are available at daily intervals.

Depth m	Summer SSP m/s	Winter SSP m/s	Shallow profile	Deep profile
0.49	1502.94	1483.88	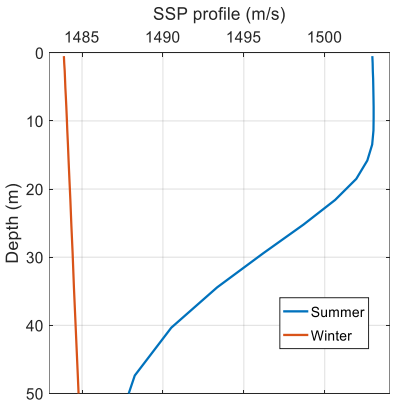	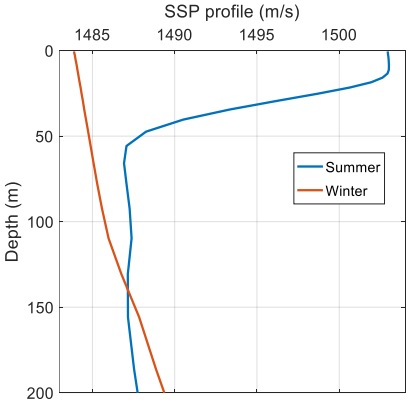
1.54	1502.96	1483.90		
2.65	1502.97	1483.93		
3.82	1502.99	1483.95		
5.08	1503.00	1483.97		
6.44	1503.01	1484.00		
7.93	1503.02	1484.03		
9.57	1503.02	1484.06		
11.40	1503.01	1484.09		
13.47	1502.93	1484.13		
15.81	1502.63	1484.17		
18.50	1501.95	1484.22		
21.60	1500.64	1484.28		
25.21	1498.69	1484.34		
29.44	1496.19	1484.42		
34.43	1493.35	1484.50		
40.34	1490.52	1484.61		
47.37	1488.26	1484.74		
55.76	1487.07	1484.89		
65.81	1486.92	1485.07		
77.85	1487.07	1485.29		
92.33	1487.26	1485.58		
109.73	1487.38	1485.98		
130.67	1487.15	1486.76		
155.85	1487.16	1487.84		
186.13	1487.53	1488.86		
222.48	1488.10	1490.19		
266.04	1488.41	1489.86		

Table 4.6: Summary of the scenario to address the relevance of sound speed vertical distribution for noise mapping in the North Sea.

Water depth	Sound Speed Profile	Seabed sound speed	Seabed density	Seabed attenuation
50 m	1500 m/s	1700.0 m/s	2000 kg/m^3	0.5 dB/λ
50 m	Summer profile	1700.0 m/s	2000 kg/m^3	0.5 dB/λ
50 m	Winter profile	1700.0 m/s	2000 kg/m^3	0.5 dB/λ
200 m	1500 m/s	1700.0 m/s	2000 kg/m^3	0.5 dB/λ
200 m	Summer profile	1700.0 m/s	2000 kg/m^3	0.5 dB/λ
200 m	Winter profile	1700.0 m/s	2000 kg/m^3	0.5 dB/λ

4.3.2 Model used

The acoustic model used to run the SSP scenarios is Quiet-Oceans' parabolic equation code in high-fidelity mode (RAM-Surf HiFi).

4.3.3 Results

The results of the modelling of both shallow and deep-water scenarios are analysed by using the following metrics:

- The depth averaged broadband SPL as a function of range from 0 to 100 km, as done for the test case 1;
- The depth averaged SPL as a function of frequency and range;
- The SPL as a function of range from 0 to 100 km at 15 m depth.

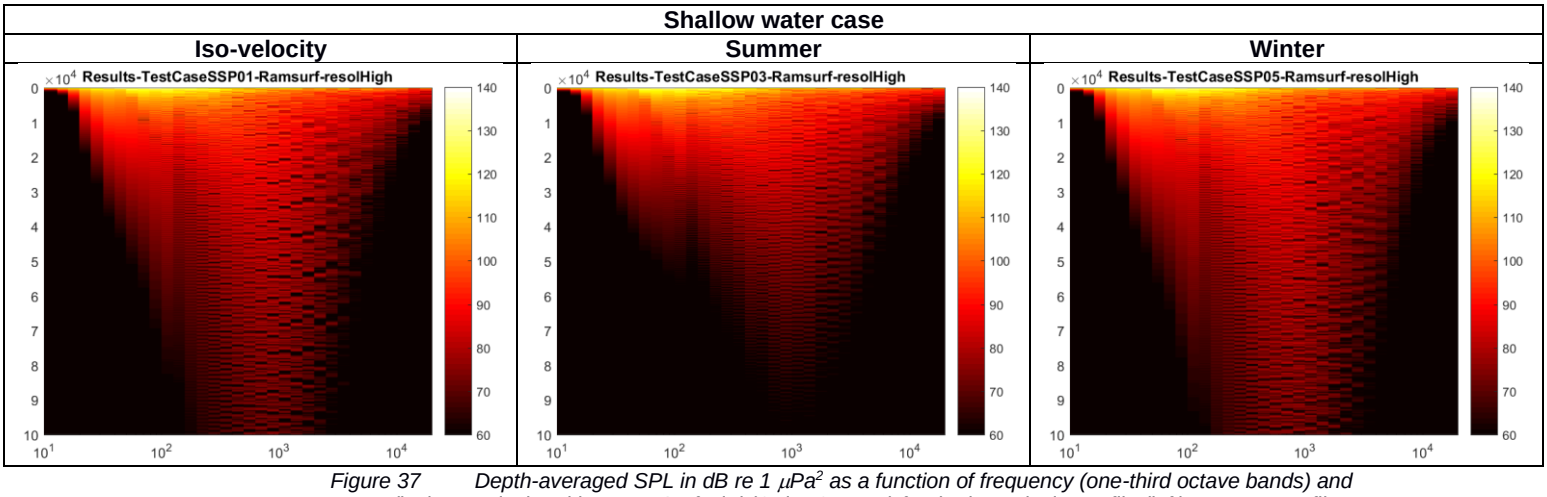

Figure 37 Depth-averaged SPL in dB re 1 μPa^2 as a function of frequency (one-third octave bands) and range (km), as calculated by RAM-Surf HiFi (Quiet-Oceans) for the iso-velocity profile (left), summer profile (centre) and winter profile (right).

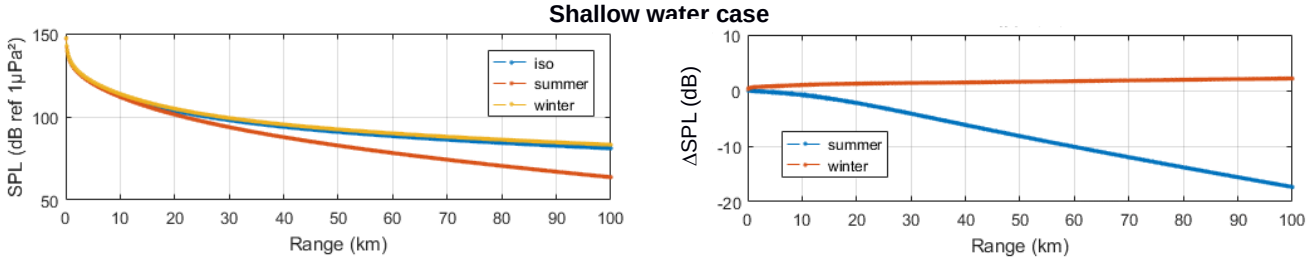

Figure 38 Depth-averaged broadband SPL in dB re 1 $\mu Pa2$ as a function of range (km), as calculated by RAM-Surf HiFi (Quiet-Oceans) for the shallow water case (50m of water depth). The figure on the right show the difference from the iso-velocity case taken as reference.

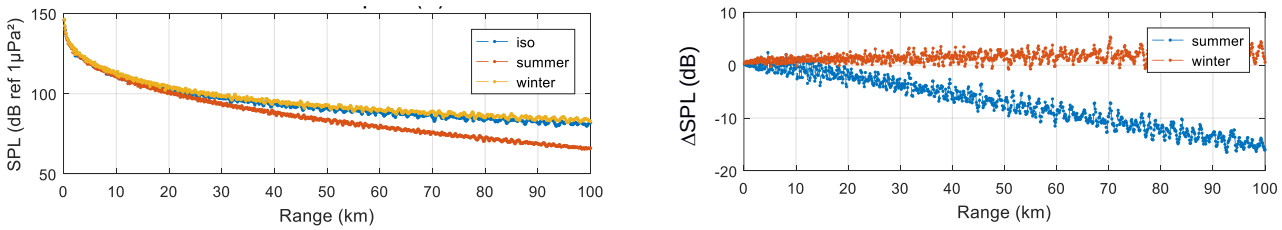

Figure 39 Broadband SPL at 15m depth in dB re 1 $\mu Pa2$ as a function of range (km), as calculated by RAM-Surf HiFi (Quiet-Oceans) for the shallow water case (50m of water depth). The figure on the right show the difference from the iso-velocity case taken as reference.

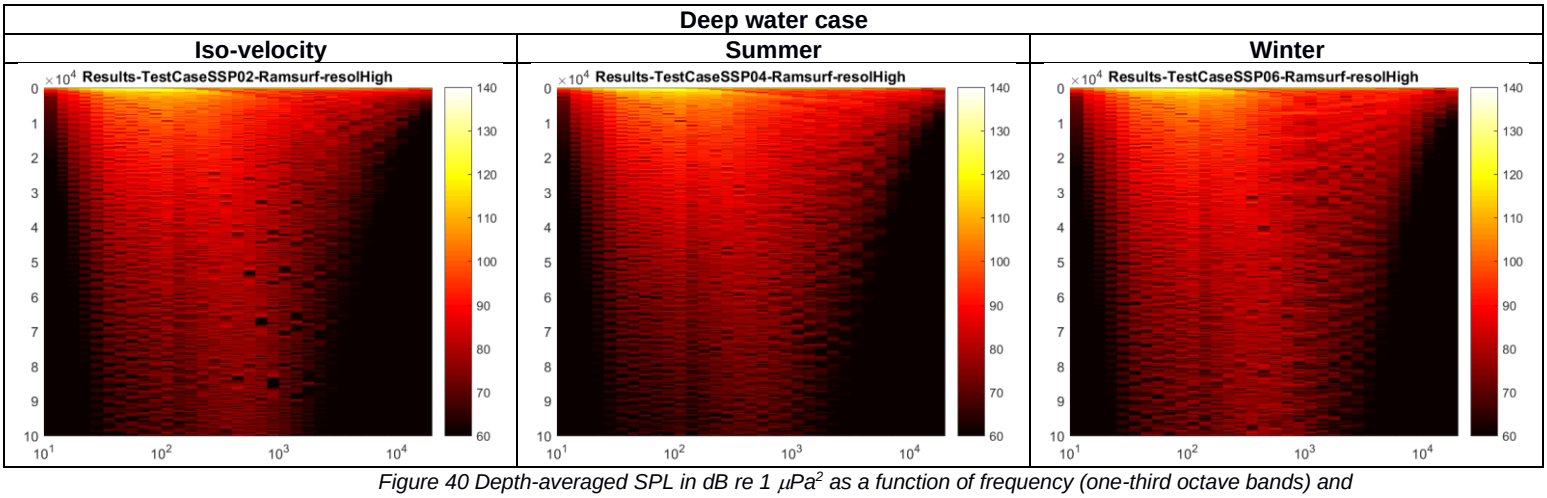

Figure 40 Depth-averaged SPL in dB re 1 μPa^2 as a function of frequency (one-third octave bands) and range (km), as calculated by RAM-Surf HiFi (Quiet-Oceans) for the iso-velocity profile (left), summer profile (centre) and winter profile (right).

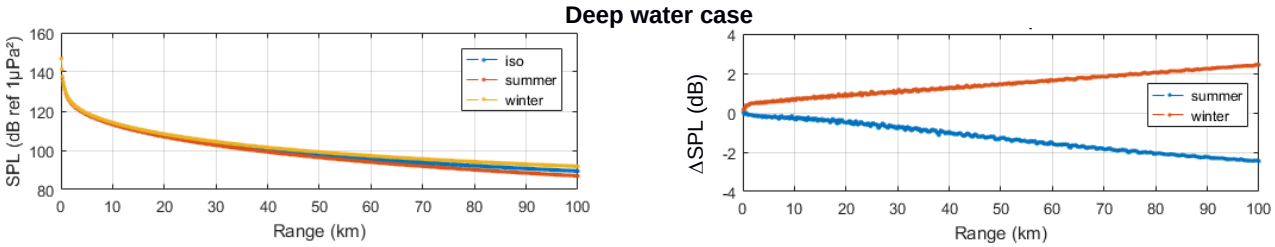

Figure 41 Depth-averaged broadband SPL in dB re 1 μPa^2 as a function of range (km), as calculated by RAM-Surf HiFi (Quiet-Oceans) for the deep-water case (200m of water depth). The figure on the right show the difference from the iso-velocity case taken as reference

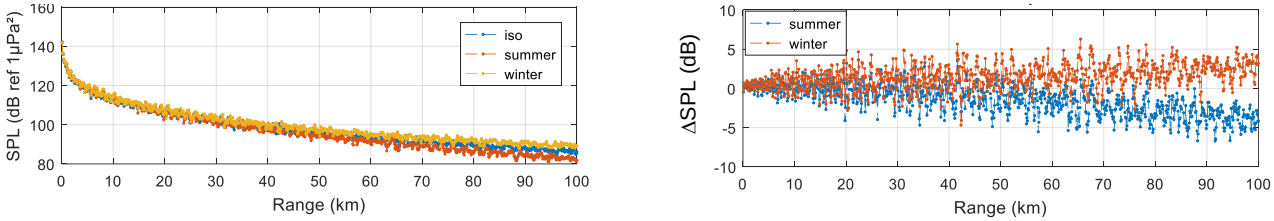

Figure 42 Broadband SPL at 15m depth in dB re 1 $\mu Pa2$ as a function of range (km), as calculated by RAM-Surf HiFi (Quiet-Oceans) for the deep-water case (200m of water depth). The figure on the right show the difference from the iso-velocity case taken as reference

4.3.4 Conclusions

The modelling results show seasonal deviations of the broadband levels, depth-averaged and at 15m depth, of about 3 dB at 10km, 10 dB at 50 km and 20 dB at 100 km in the shallow water case. The deep water case shows less differences of about 1 dB, 3 dB and 5 dB respectively. The presence of the thermocline in summer tend to bend the acoustic rays toward the bottom. Deviations are therefore increasing with range, which can be explained by the increasing and cumulative effects of the interaction of the sound with the bottom. These interactions increase the losses induced by the bottom at each reflection. In the deep-water case, the bottom is deeper, and therefore the sound has less interaction. The fact that the sound source is close to the surface is likely to attenuate the effect of the thermocline which would have been larger if the sound source would have been placed deeper.

These scenario results suggest that the assumption of an iso-velocity profile instead of a sound speed profile a may increase the uncertainty on the long range propagation loss. In task T4.3, QO will investigate the effect of the SSP on the monthly SPL percentiles, using the Quonops models, in the validation scenarios against measurements at North Sea 2018 monitoring locations.

5 Ship source level model and statistics

There are no generally accepted models that can calculate the source level of individual ships from the available from ship traffic information such as AIS. Two alternative semi-empirical ship source level models are presented in the JOMOPANS T4.1 report (de Jong et al, 2018):

1. Wales & Heitmeyer (2002), see §5.1
2. RANDI 3.1 (Ross, 1978, Breeding et al, 1996), see §5.2

JASCO has evaluated these models against a large database of ship noise measurements that has been collected by JASCO's PortListen® noise measurement system in the Haro strait as part of the Vancouver Fraser Port Authority's 'Enhancing Cetacean Habitat and Observation' (ECHO) program, see §5.3 [MacGillivray et al, 2019].
The aim of this evaluation was to select an appropriate statistical model for ship source level spectra (in one-third octave bands) to be used for calculating shipping noise maps for the JOMOPANS North Sea area, on the basis of information provided from AIS. Sections 5.5 to 5.8 describe steps towards an updated source level model.

5.1 Wales & Heitmeyer (2002)

The model proposed by Wales and Heitmeyer (2002) for the source spectral density level (Ainslie et al, 2020) is described by the equation.

$$L_{\mathrm{WH02}}(f) = \langle L_{S,f}(f) \rangle = 230.0 \text{ dB} - 10\log_{10}\left(\left(\frac{f}{1 \text{ Hz}}\right)^{3.594}\right) \text{dB} + 10\log_{10}\left[\left(1 + \left(\frac{f}{340 \text{ Hz}}\right)^2\right)^{0.917}\right] \text{dB}, \quad (5\text{-}1)$$

The source levels observed by Wales & Heitmeyer (2002) are normally distributed, characterized by a mean value and a standard deviation. The associated standard deviation is approximately (Ainslie et al, 2018)

$$\sigma_{\mathrm{WH02}}(f) = \begin{cases} 5.3 \text{ dB} & f < 150 \text{ Hz} \\ 5.3 \text{ dB} - 0.0088 \text{ dB} \left(\frac{f - 150 \text{ Hz}}{1 \text{ Hz}}\right) & 150 \text{ Hz} \le f < 400 \text{ Hz} \\ 3.1 \text{ dB} & f \ge 400 \text{ Hz} \end{cases} \quad (5\text{-}2)$$

The T4.1 report recommends using the value $\langle L_{S,f}(30 \text{ Hz}) \rangle$ when extrapolating to frequencies below 30 Hz, and to continue to use the above equations when extrapolating to frequencies above 16 kHz.

$$L_S(f) = \begin{cases} L_{\mathrm{WH02}}(30 \text{ Hz}) & f < 30 \text{ Hz} \\ L_{\mathrm{WH02}}(f) & f \ge 30 \text{ Hz} \end{cases} \quad (5\text{-}3)$$

For a normal distribution of source levels, the level of the mean source factor is (Ainslie et al, 2018; Sertlek et al, 2019):

$$L_{<S>}(f) = L_{\mathrm{WH02}} + \frac{\ln 10}{20}\left(\frac{\sigma_{\mathrm{WH02}}}{\text{dB}}\right)^2 \text{ dB}. \quad (5\text{-}4)$$

5.2 RANDI 3.1 (Ross, 1978, Breeding et al, 1996)

The RANDI 3.1 model spectral density equation is customarily written in the form:

$$L_S(f, V, L) = L_{S0}(f) + 60\log_{10}(V/V_0) \text{ dB} + 20\log_{10}(l/l_0) \text{ dB} + df \cdot dl + 3.0 \text{ dB}, \quad (5\text{-}5)$$

where $V_0 = 12$ kn and $l_0 = 300$ ft are the reference speed and the reference length,[10] and:

$$L_{S0}(f) = \begin{cases} -10\log_{10}\left(10^{-1.06\log_{10}(f/f_0) - 14.34} + 10^{3.32\log_{10}(f/f_0) - 21.425}\right) \text{dB} & \text{for } f < 500 \text{ Hz} \\ 173.2 \text{ dB} - 18\log_{10}(f/f_0) \text{ dB} & \text{for } f \ge 500 \text{ Hz}, \end{cases} \quad (5\text{-}6)$$

where $f_0 = 1$ Hz and $dl = (l/1 \text{ ft})^{1.15}/3643.0$ and

$$df = \begin{cases} 8.1 \text{ dB} & \text{for } f < 28.4 \text{ Hz} \\ 22.3 \text{ dB} - 9.77\log_{10}(f/f_0) \text{ dB} & \text{for } 28.4 \text{ Hz} < f \le 191.6 \text{ Hz} \end{cases} \quad (5\text{-}7)$$

This semi-empirical model was developed from ship noise measurements in shallow water without correction for the actual propagation loss in the environment, and therefore represent a radiated noise level (as defined in ISO 17208-1) and not a source level in the sense of ISO 18405.

We assume that the RANDI 3.1 model spectrum represents the mean value of normal distribution and that the associated standard deviation can be assessed from the statistics of model-data comparisons.

[10] 1 knot = 1852/3600 m/s
1 ft = 0.3048 m

5.3 ECHO Source Level data (MacGillivray & Li, 2018)

A total of 1862 ship source level measurements from the ECHO voluntary slowdown trial in Haro Strait (from 6 Jul to 27 Oct 2017) were included in this analysis. These measurements represented a wide range of operating speeds, as vessels were requested to voluntarily reduce their transit speed in the international shipping lane to 11 knots during a two-month period. The measurements also sampled a wide range of vessel sizes and types. Thus, these measurements provided an excellent dataset for validating speed and length dependencies assumed in source level models, such as RANDI 3.1.

The ship source levels have been obtained as the sum of the measured sound pressure level and a numerically calculated propagation loss, using the parabolic equation model RAM, in one-third octave bands to 5 kHz and an image reflectivity model at higher frequencies.
For this dataset, the monopole source depth (z_s) is calculated from the draft (as reported over AIS) according to the following method:

1. Assume z_s = 0.5×draft.
2. Assume the source depth has a Gaussian distribution, with the distribution parameter proportional to the propeller diameter (D_{prop}): $\sigma = D_{\mathrm{prop}}/4$
3. The propeller diameter is not reported over AIS and therefore estimated from the draft as follows: $D_{\mathrm{prop}} = (\mathrm{draft} - z_s)/0.85 = z_s/0.85$
4. The source distribution is limited to the depth interval [1 m, 24 m].

The PortListen system assigns vessels to one of 16 vessel classes according to their AIS SHIPTYPE ID or their registration sub-type ID. The vessel sub-type of each vessel is recorded in an AIS registry for each vessels MMSI identification number. PortListen automatically extracts the registration sub-type ID from Marine Traffic website, when available. If it cannot locate the sub-class description, it assigns the vessel to a default type corresponding to its AIS Vessel Type ID[11], see Table 5.1.

Table 5.1: Port Listen vessel class cross-references with AIS type ID and Marine Traffic sub-type ID.

Port-Listen Vessel Class	**AIS SHIPTYPE ID**	**Marine Traffic sub-type ID**
Fishing Vessel	30	2, 3, 5-8,11
Tug	31,32,52	12-23, 76, 77, 109
Naval Vessel	35	51-63, 128
Recreational Vessel	36,37,	64, 65
Government/Research	51,53,55	4, 9, 10, 80, 83, 96, 107
Cruise (= Passenger > 100 m)	60-68	158,159
Passenger (≤100 m)	60-68	158,159
Bulk Carriers + Bulkers + Open Hatch Cargo Ships Name: **Bulkers**	70, 75-79	175-178, 182, 186,189, 198-201, 203, 215, 210, 212, 213 185,
Container Ships + Reefers Name: **Container Ship**	71-74	179, 197, 181, 187
Vehicle Carrier		180, 184, 190-192, 214
Crude Oil Tankers + Chemical Products Carriers + Tankers Name: **Tanker**	80-84,85-89	219, 224, 225, 188, 218, 216, 217, 220-223, 226, 228-234
Other	34,50,54, 56-59,90-99	26, 38, 40, 50, 66-75, 78, 79, 81, 82, 84-95, 97-106, 108, 110-127, 129-157, 164-174, 183, 193-196, 202, 204-209, 211, 227

As can be observed in Table 5.1, the AIS broadcasted 'ship type' alone is not sufficient to identify the PortListen Class ID. In particular, the same AIS ship type 70-79 ('Cargo') is used for both 'bulkers' and 'container ships', although the latter in general have a higher transit speed. The identification of

[11] In some cases, the vessel name is used to override the default system. The PortListen system maintains its own list of vessels for this purpose. This is useful, for example, to categorize certain vessels that do not have an appropriate AIS sub-type. An example is PortListen type Whale Watch, which often has an AIS default type as Passenger Vessel.

container ships on the basis of the hazardous cargo code (AIS ID 71-74 corresponds with 'Hazard A-D') proposed in Table 5.1 was previously investigated in [Brooker et al, 2015], taking a sample from Marine Traffic (www.marinetraffic.com) of 100 bulk carriers and 100 container ships in European waters. It was found that any "cargo" ship with a hazardous cargo code can be assumed to be a container ship. Not all container ships are categorised with a hazardous cargo type, but in the sample of 100 container ships about 66 are identified by the hazardous cargo type.

5.4 RANDI 3.1 model versus the ECHO data set

JASCO applied the Wales & Heitmeyer and RANDI 3.1 models to calculate the source level of the individual vessels in the data set and compared these with the measured source levels.
For this initial comparison it was tentatively assumed that the RANDI 3.1 model output can be compared with the source levels (SL) in the ECHO data set (with the vessel draft-dependent source depth distribution), although the RANDI 3.1 documentation (Breeding et al, 1996) suggests that the RANDI 3.1 model predicts a 'radiated noise level' (RNL, independent of the assumed source depth). SL and RNL are both expressed in decibels with reference to 1 μPa·m, and their numerical values are similar. The consequences of this comparison of incompatible quantities will be temporarily ignored, and then reconsidered in the model update (section 5.7).

Figure 43 show the statistics of the difference between modelled broadband RNL and measured broadband SL for 12 vessel classes (i.e. classes 2-6, 8-12 and 16 from Table 5.1, with an extra class called 'cruise' for passenger vessels longer than 100 m). This illustrates that there are significant deviations between models and measurements. Figure 44 shows the speed dependence of the measured and modelled (RANDI 3.1) source levels for the different categories. This suggests that the speed dependence of the RANDI 3.1 model approximately agrees with the speed dependence in the measurements, and that the model-data deviation is approximately independent of ship speed, but dependent on vessel class. The Wales & Heitmeyer model does not describe the speed dependence that is observed rather consistently in the broadband source level data. Hence, the use of a RANDI 3.1-style ship source model is considered more appropriate for AIS-based sound mapping.

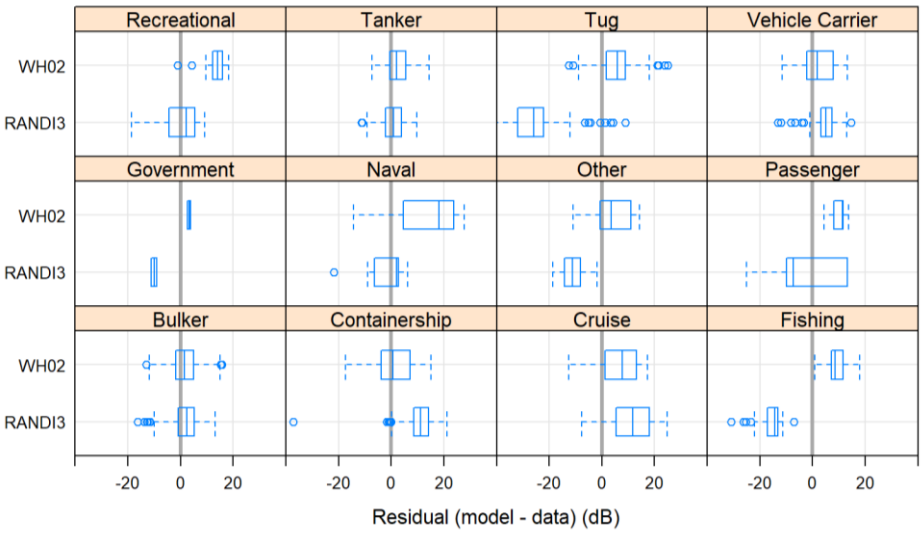

Figure 43 Box and whisker plots of broadband (20 Hz - 20 kHz one-third octave bands) model-data residuals for RANDI 3.1 and Wales and Heitmeyer (2002) vessel source level models (by vessel class)

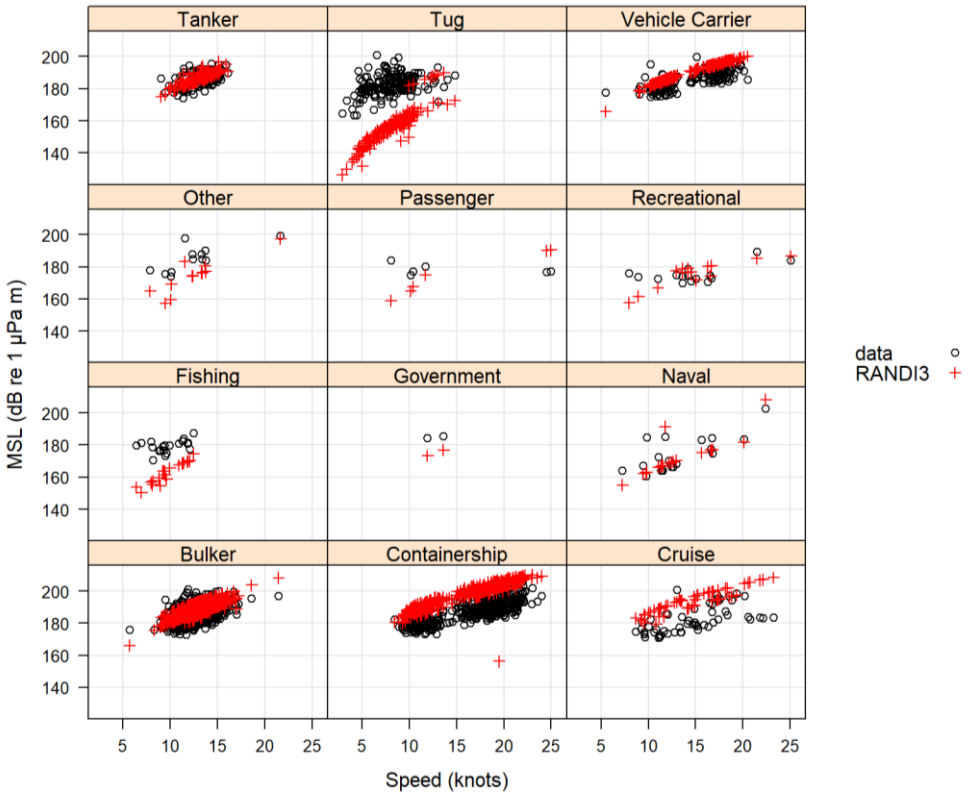

Figure 44 Scatter plots of broadband (20 Hz - 20 kHz one-third octave bands) source level (MSL) versus speed (by vessel class) as measured (o) and calculated (+) by the RANDI 3.1 model, using the default parameters.

5.5 Ship source model update RANDI 3.1a

To reduce the ship class dependent deviation between measured and modelled source levels, the RANDI 3.1 model was adapted, by replacing the generic reference speed $V_0 = 12$ kn by a reference speed V_{vc} per vessel class (vc). This new reference speed is obtained from the mean model-data residuals $\overline{\Delta}_{0,\mathrm{vc}}$ for broadband source level per vessel class for model predictions with the default reference speed, according to the following formula:

$$V_{vc} = V_0 10^{\overline{\Delta}_{0,vc}/(60\ dB)} \tag{5-8}$$

The resulting reference speeds per vessel class and the corresponding statistic parameters (mean and standard deviation) of the residuals between the updated model (with the class-dependent reference speed) model are given in Table 5.2, column ‘RANDI 3.1a’.

Table 5.2: Model parameters and model data differences per vessel class for the updates of the RANDI 3.1 proposed in this Chapter (see text). n is the number of measurements per vessel class in the ECHO dataset, z_s is the source depth in metres, V_{vc} is the reference speed per vessel class in knots, $\overline{\Delta}_{vc}$ is the mean value of the updated model-data residual (broadband source level difference in decibels) per vessel class and σ_{vc} is the standard deviation of the updated model-data residuals (in decibels) per vessel class.

		RANDI 3.1a				**RANDI 3.1b**			**RANDI 3.1c**		
		$z_s = 0.5\ D$				z_s=6 m			z_s=6 m		
Vessel class	n	z_s	V_{vc},	$\overline{\Delta}_{\mathrm{vc}}$	σ_{vc}	V_{vc}	$\overline{\Delta}_{\mathrm{vc}}$	σ_{vc}	V_{vc}	$\overline{\Delta}_{\mathrm{vc}}$	σ_{vc}
Fishing	21	2.2	6.8	-0.2	5.9	7.5	-0.2	6.1	7.5	-2.8	6.6
Tug	173	3.8	4.4	0.2	7.6	4.9	0.1	7.3	4.9	-3.0	4.1
Naval	19	1.7	12.1	-0.3	6.9	14.2	-0.1	5.5	14.2	-2.6	6.1
Recreational	15	1.5	12.8	-0.3	7.6	14.0	-0.2	7.8	14.0	-2.6	5.4
Government	2	4.2	8.5	0.4	1.6	9.2	0.4	2.3	9.2	-2.0	15.2
Cruise	54	1.7	19.6	0.3	8.2	20.2	0.6	6.7	20.2	-2.6	4.2
Passenger	6	2.3	10.7	0.4	14.9	11.7	0.4	15.2	11.7	-1.5	4.9
Bulker	850	4.8	13.6	0.4	4.6	14.1	0.3	4.2	14.1	-2.8	4.7
Container ship	440	5.6	19.4	0.4	4.3	19.3	0.4	4.1	19.3	-2.8	4.1
Vehicle Carrier	141	2.5	15.3	0.2	4.2	16.4	0.1	4.2	16.4	-2.2	7.3
Tanker	129	2.3	12.9	0.4	4.2	13.1	0.4	4.2	13.1	-3.0	4.2
Other	12	4.3	8.1	0.6	4.4	8.8	1.1	5.0	8.8	-2.7	7.8
All	1862	m	kn	dB	dB	kn	dB	dB	kn	dB	dB

5.6 Ship source model update RANDI 3.1b

Source depth is an important parameter in association with the source level of surface ships. However, the RANDI 3.1 model description (Breeding et al, 1996) is not clear about source depth. The RANDI 3.1 manual [Breeding et al, 1994] suggests that the model assumes a fixed source depth ('*Ship source depth … will usually be 6 meters, the average propellor* [sic] *depth of a merchant ship*').

The ECHO source depths are based on the static drafts of the vessels at the time of measurement (assuming a monopole source with Gaussian amplitude distribution). To correct the comparison of the ECHO data set to the RANDI 3.1 source level model, an adjustment of the ECHO source levels to a standard depth of 6 m has been made, according to the procedure described in Appendix A.

For the JOMOPANS noise mapping, the selection of a fixed reference source depth for all vessels has the advantage that it offers the possibility to decrease the complexity of the propagation loss model calculations.

The result of fitting a reference speed per vessel class to the ECHO source levels converted to a standard depth of 6 m are given in Table 5.2, column 'RANDI 3.1b'. The selection of a fixed 6 m source depth implies a significant (up to a factor of 4) increase in source depth for most ship classes. Consequently, the fitted reference speeds increase as well (up to 17%). The quality of the broadband SL model-data fit does not change significantly. The mean residuals per vessel class remain smaller than 0.6 dB after the source depth conversion and the standard deviations change at maximum 1.5 dB.

5.7 Ship source model update RANDI 3.1c

Figure 45 shows the residuals between model calculations and measurements of the ECHO vessel source levels, in one-third octave frequency bands. Figure 46 shows the mean residuals per vessel class and Figure 47 shows the one-third octave spectrum of the mean residual for all vessel classes. This suggests that there is a clear bias in the one-third octave residuals, independent of vessel class.

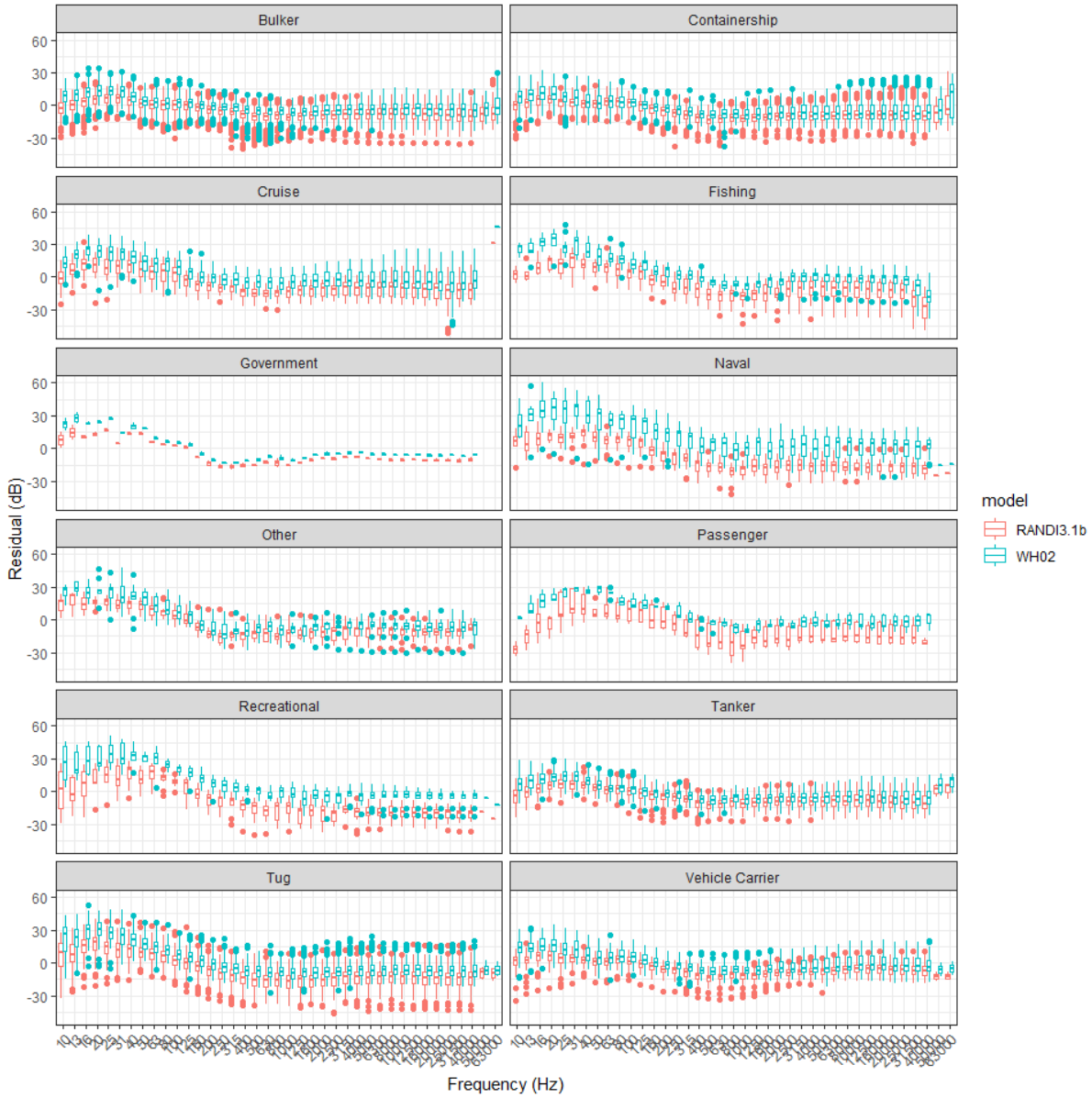

Figure 45 Box and whisker plots of the one-third octave residuals between modelled (Wales & Heitmeyer, WH02, and RANDI 3.1, update b), and measured source levels for the 12 vessel classes in the ECHO data set.

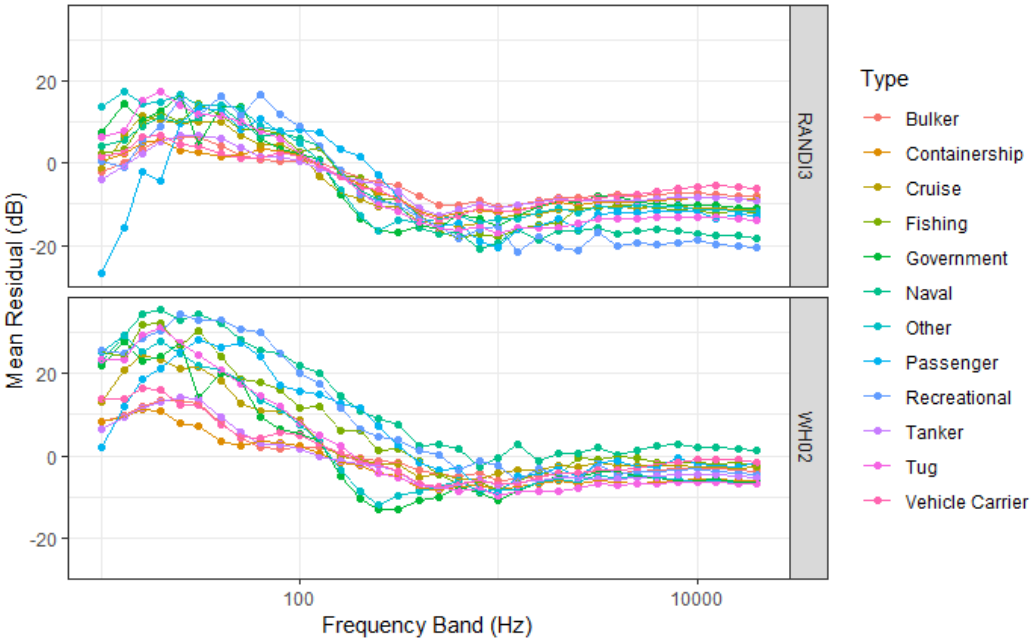

Figure 46 Mean one-third octave residuals between modelled (Wales & Heitmeyer, WH02, and RANDI 3.1, update b), and measured source levels for the 12 vessel classes in the ECHO data set.

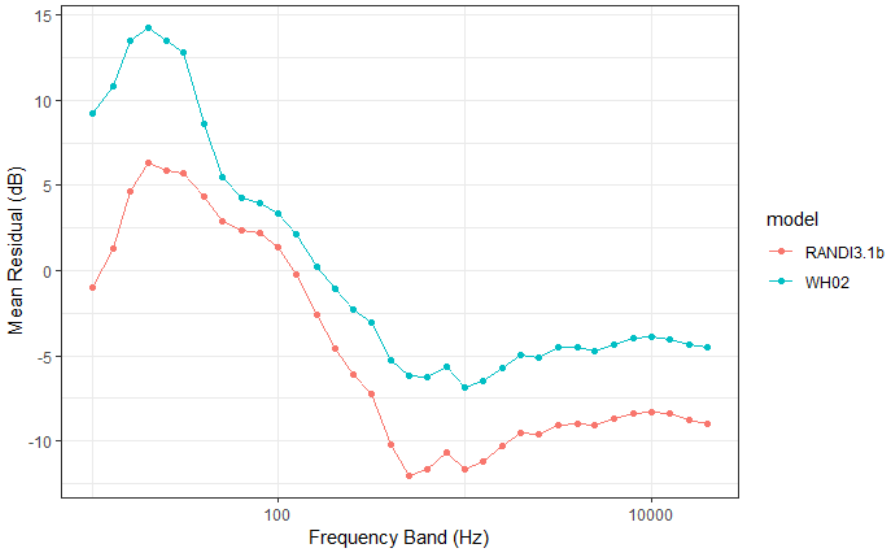

Figure 47 Mean one-third octave residuals between modelled (Wales & Heitmeyer, WH02, and RANDI 3.1, update b), and measured source levels, averaged over the 12 vessel classes in the ECHO data set.

Because the RANDI 3.1 model is based on a baseline spectrum, independent of vessel class, size and speed, this bias can be reduced by updating the baseline spectrum with a correction for the observed bias (mean residual) in one-third octaves. Instead of providing a table with the updated source level baseline spectrum, a formula similar to the formula for the original RANDI 3.1 baseline spectrum is fitted to the data:

$$L_{S0,\mathrm{new}}(f) = -10\log_{10}\left(10^{-A\log_{10}(f/f_0)-B} + 10^{C\log_{10}(f/f_0)-D}\right)\ \mathrm{dB} \qquad (5\text{-}9)$$

For the 'optimized' baseline model it was no longer necessary to use a different slope above 500 Hz (unlike the original RANDI 3.1 baseline spectrum), because the formula (5-9) fit well for all frequencies. Table 5.3 provides the coefficients for the optimized model (RANDI 3.1, update c) and Figure 48 shows the resulting 'optimized' baseline spectrum.

Because this optimized spectrum is fitted to the ship SL data from the ECHO data set, the RANDI 3.1c model is a SL model, instead of the original RANDI 3.1 which was fitted to (unpublished) RNL data.

Table 5.3: Optimized baseline spectrum coefficients for the RANDI 3.1c updated model (Eq 5-9), obtained by fitting coefficients of the RANDI 3.1 baseline model to ECHO residuals.

Coefficient	Original (RANDI 3.1)	Optimized
A	1.060	0.000
B	14.340	15.342
C	3.320	1.959
D	21.425	18.836

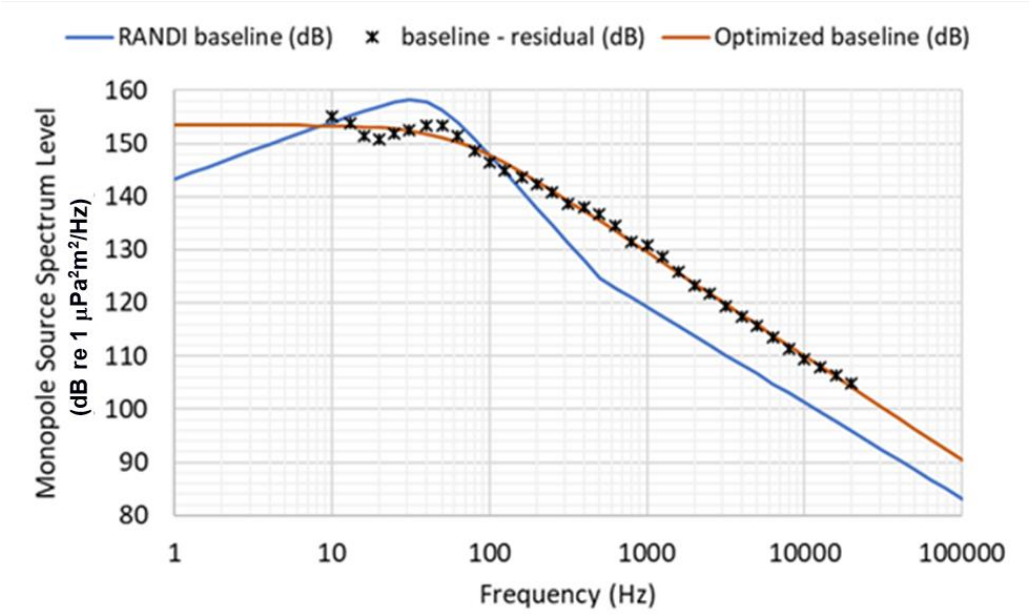

Figure 48 Optimized baseline source level spectrum for the RANDI 3.1c updated model, obtained by fitting coefficients of the RANDI 3.1 baseline model to ECHO residuals.

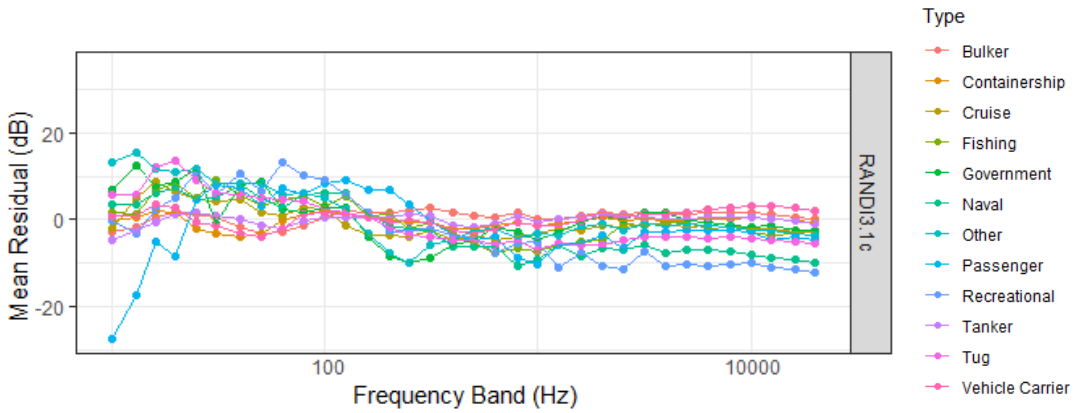

Figure 49 demonstrates that the 'optimized' baseline spectrum reduces the bias in the mean model-data residuals. A further reduction of bias might perhaps be achieved by a new fit of the reference speeds per ship class for the model with the updated baseline spectrum, but such an iterative model update was not undertaken in the framework of his study. Note that the optimization on the mean model-data residuals in one-third octave bands results in a -2 dB to -3 dB mean broadband model-data residual per vessel class, see Table 5.2.

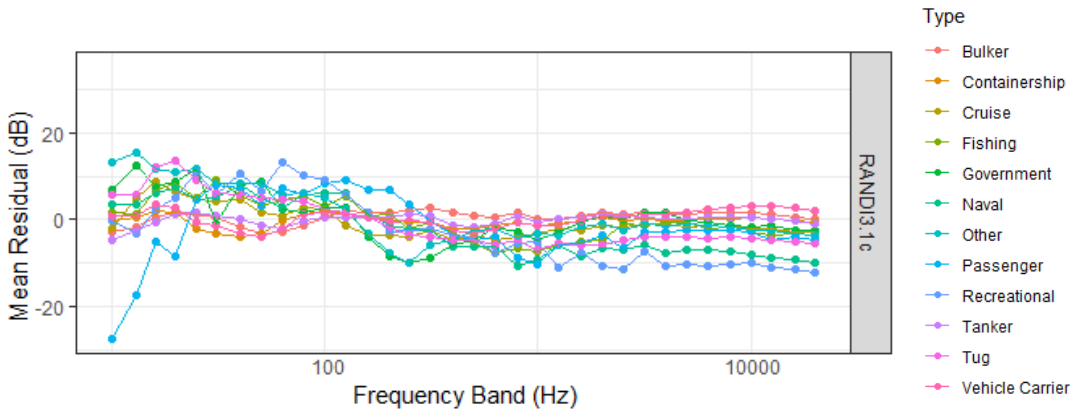

Figure 49 Mean one-third octave band residuals between modelled (RANDI 3.1, update c, with optimized baseline spectrum), and measured source levels, averaged for the 12 vessel classes in the ECHO data set.

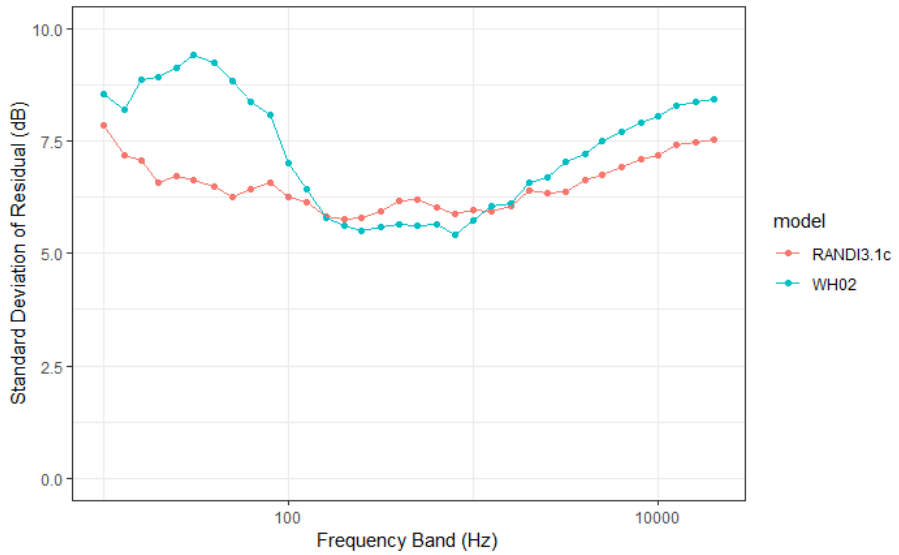

Figure 50 Standard deviation of one-third octave band residuals between modelled (Wales & Heitmeyer, WH02, and RANDI 3.1, update c, with optimized baseline spectrum), and measured source levels, averaged over the 12 vessel classes in the ECHO data set. Note that the standard deviation values are identical between updates b and c of the RANDI 3.1 model because the optimized baseline only affects the mean residual in each band.

Figure 50 shows the frequency-dependent standard deviation of the model-data residuals in the optimized model (RANDI3.1, update c). The maximum absolute value of the average residual (averaged over all vessel classes) over the frequency range is 2 dB, the root-mean-square residual is 1 dB and the root-mean-square value of the average standard deviation is 6.5 dB.

5.8 Updated RANDI 3.1c model compared with SHEBA dataset

The updated RANDI 3.1c model was also applied to ship source level recordings from the SHEBA (Sustainable shipping and environment of the Baltic sea region) research project [Karasalo et al, 2017]. The SHEBA data set does not contain detailed information of the vessel class. Hence, the vessel class was derived from the AIS 'SHIPTYPE ID' parameter (see Table 5.1), with 2 exceptions:

i. Passenger vessels (AIS SHIPTYPE ID 60-69) are classified as 'cruise vessel' when they are longer than 100 m;
ii. Cargo vessels (AIS SHIPTYPE ID 70 and 75-79) are classified as 'container vessel' when their speed (at CPA) is higher than 16 knots.

A comparison of the residuals between modelled and measured source levels per vessel class in Figure 51 and Figure 52 demonstrates that the updated RANDI 3.1c model provides a much better agreement with the data than the original RANDI 3.1 model. The residual at frequencies below about 200 Hz appears to be much larger than for the ECHO data set, but the standard deviation is much larger as well below 100 Hz, see Figure 53.

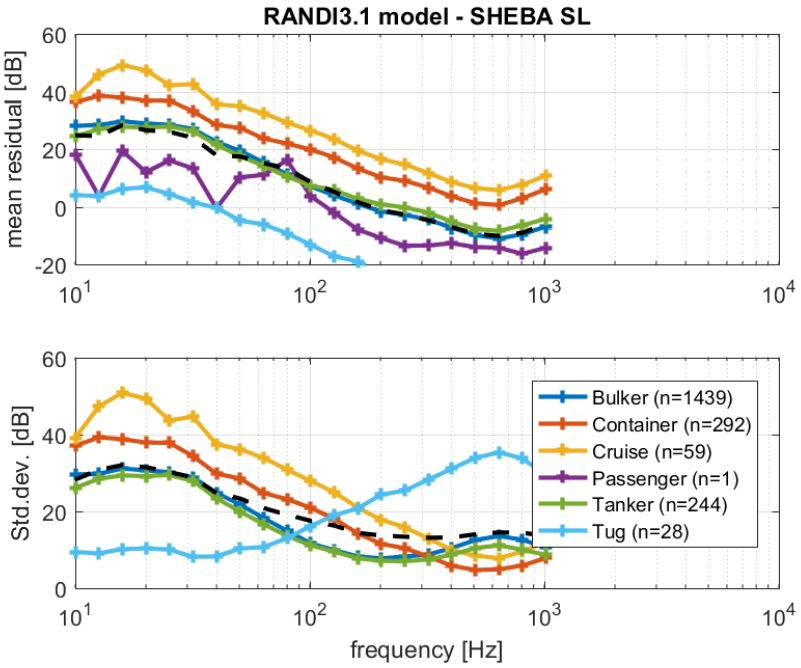

Figure 51 One-third octave band spectra of the mean value (upper graph) and the associated standard deviation of the residual between modelled (RANDI 3.1, original), and measured source levels, for the 6 vessel classes in the SHEBA data set. The black dashed lines give the average value over the classes.

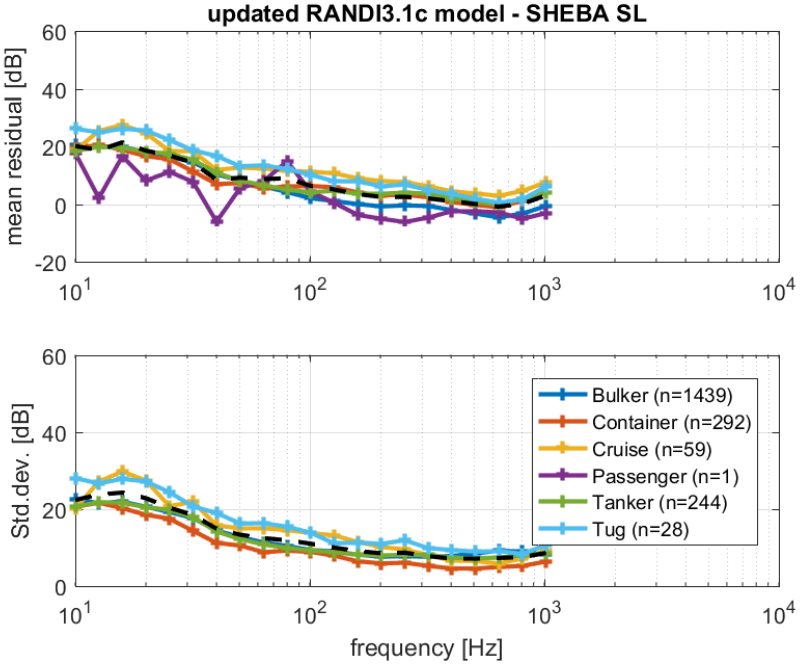

Figure 52 One-third octave band spectra of the mean value (upper graph) and the associated standard deviation of the residual between modelled (RANDI 3.1, update c, with optimized baseline spectrum), and measured source levels, for the 6 vessel classes in the SHEBA data set. The black dashed lines give the average value over the classes.

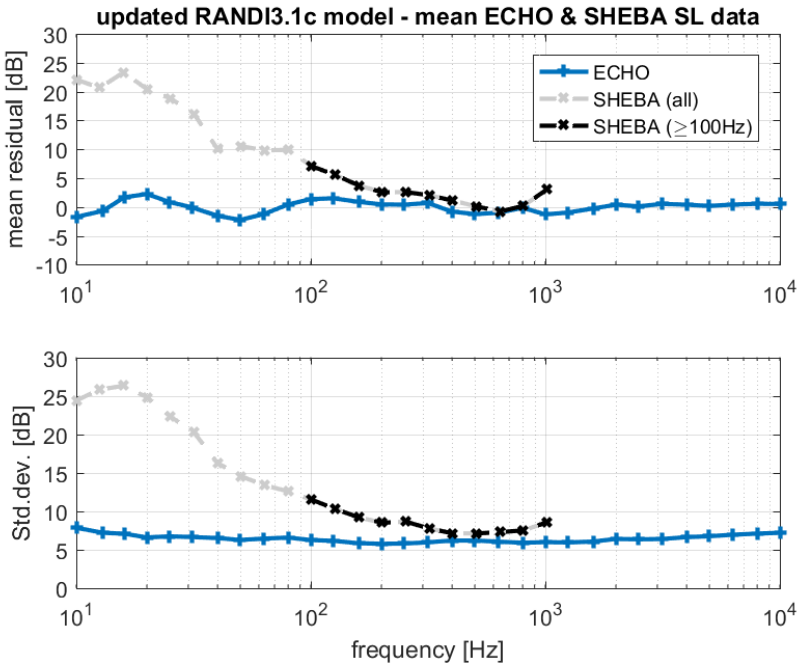

Figure 53 One-third octave band spectra of the mean value (upper graph) and the associated standard deviation of the residual between modelled (RANDI 3.1, update c, with optimized baseline spectrum), and the measured source levels, averaged over all vessel classes in the ECHO and SHEBA data sets. The SHEBA data below 100 Hz are shaded because they are considered to be unreliable (see the text).

An investigation of the reason for the large difference between the source levels (below 200 Hz) in the ECHO and SHEBA data sets is beyond the scope of the JOMOPANS project. However, the paper describing the SHEBA data [Karasalo et al 2017] suggests that "*The poor model–prediction agreement observed for low frequencies is likely due to the lack of reliable hydrophone calibration data.*". Moreover, the ECHO measurements have been carried out in deeper water (170 m water depth) than the SHEBA measurements (~40 m depth), so that the latter have a greater uncertainty associated with the propagation correction at lower frequencies.

Figure 54 illustrates the difference between the (mean) source levels per ship class measured by the ECHO and SHEBA projects.

Table 4 shows that the ships in the SHEBA data set are generally smaller and travelled at a slower speed than in the ECHO data set. To correct for these differences in the comparisons between the data sets, the measured (mean) source levels per ship class were corrected for the speed and length dependence ($60\log_{10}(V/V_0)$ dB $+ 20\log_{10}(l/l_0)$ dB $+ df \cdot dl + 3.0$ dB) from the RANDI3.1c model. The resulting mean baseline spectra are shown in Figure 55.

This shows that the RANDI3.1c model matches closely with the ECHO data for most vessel classes at frequencies above 500 Hz. The baseline spectrum for the cruise vessels appears to be about 3 dB higher than that of the other classes, which suggests that the reference speed for this class ($V_{vc} = 20.2$ kn) may be overestimated. This is not unlikely, since the number of cruise vessels in the data set is rather low ($n = 23$). A reference speed of 18 kn would result in a ($60\log_{10}(20.2/18)$ dB $\approx$) 3 dB lower baseline spectrum, matching with the rest above 500 Hz.

The baseline spectrum for the larger merchant vessels (container, bulker, tanker) show a peak in the 20 to 80 Hz range, that is not included in the RANDI3.1c model (underestimated by up to 5 dB in individual one-third octave bands). The baseline spectra of other vessel classes (cruise vessels and tugs) drop of towards lower frequencies (below 250 Hz) and are therefore overestimated by the RANDI3.1c model.

In the following phase of WP4, an attempt will be made to develop a next update of the source level model that accounts for these deviations.

Although the comparison with the (independent) SHEBA data set provides only a limited validation, for frequencies greater than about 200 Hz, we considered the updated RANDI 3.1c model to be the best currently available model for generating AIS-based ship noise maps.

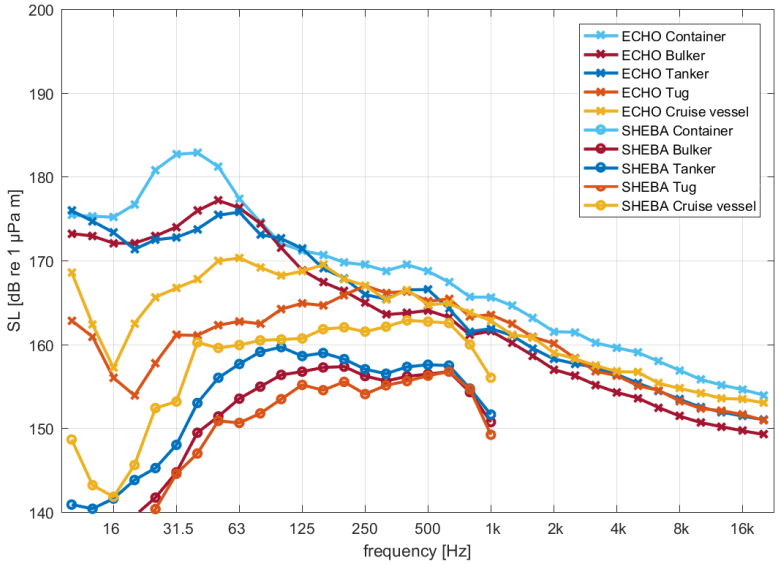

Figure 54 One-third octave band spectra of the mean value of the source level measured for five vessel classes in the ECHO (MacGillivray & Li, 2018) and SHEBA (Karasalo et al 2017) data sets.

Table 4 Comparison of the number of ships measured (n), their average speed through the water (STW) in knots and their average length in metres, for the ECHO (MacGillivray & Li, 2018) and SHEBA (Karasalo et al 2017) data sets.

	ECHO			SHEBA		
	n	STW	avg length	n	STW	avg length
Bulker	360	13.5	200	1731	12	113
Container ship	195	18.8	295	n/a		
Cruise ship	23	16.4	290	61	21	191
Tanker	53	13.5	180	244	12	118
Tug	67	8.1	50	30	7	28
Vehicle Carrier	65	17.0	200	n/a		

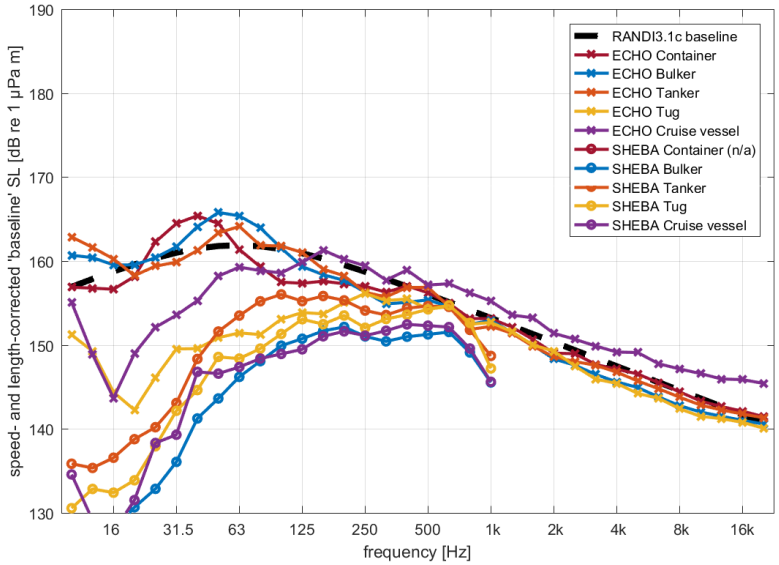

Figure 55 One-third octave band spectra of the mean value of the source level measured for five vessel classes in the ECHO (MacGillivray & Li, 2018) and SHEBA (Karasalo et al 2017) data sets, scaled to an equivalent baseline spectrum $L_{S0,new}(f)$, by correcting the measured mean spectra with the speed and length dependence from the RANDI3.1c model. The dashed black line presents the corresponding RANDI3.1c baseline spectrum.

6 Statistical modelling

The Jomopans project (Merchant, Farcas, & Powell, 2018) specifies the acoustic metric which will be used in the field measurements and acoustic modelling of continuous noise in the North Sea as follows:

- **Physical quantity**: sound pressure level (SPL), measured in decibels relative to 1 micropascal (dB re 1 μPa).
- **Temporal unit**: percentiles of the SPL distribution, based on individual SPL measurements of 1 second (snapshot duration). The period over which the percentiles will be computed is one month. Suggested percentiles are 5th, 10th, 25th, 50th, 75th, 90th, and 95th.
- **Frequency**: one-third octave bands, with centre frequencies between 10 Hz and 20 kHz, defined using the base-ten convention (ANSI 2009; IEC 2014).
- **Space**: Depth-averaged value of the metric either at the centroid of each grid cell, or as a spatial average of the levels within the grid cell. Geospatial grid referenced using the standardised C-square notation (Rees, 2003).

The North Sea ship noise maps that are to be produced in Jomopans WP4 will present an acoustic indicator that is based on these metrics. Hence, the acoustic modelling in WP4 must be aimed at calculating the suggested percentiles of the probability density function (PDF) of SPL at a selected receiver grid.

A one-month period consists of about 2.5 million subsequent non-overlapping 1-second snapshots. Direct numerical calculation of the SPL for all snapshots is unfeasible in practice because of the large computing efforts it requires, especially for a receiver grid covering the complete North Sea area for Jomopans. Moreover, the numerical model calculations are subject to several uncertainties associated with the selected modelling approach and with the available input data.

A probabilistic modelling approach, such as proposed by Gervaise et al [2015] can reduce the computing efforts as well as help to include modelling uncertainties in the noise maps.

This Chapter describes a proposal for the implementation of a probabilistic modelling approach for Jomopans.

6.1 Acoustic modelling for ambient noise maps (ships and wind)

Jomopans WP4 starts with the modelling for maps of noise of ships and wind:

- At each time step t_n, each ship (i) at location $\underline{x}_{S,i}(t_n)$ generates underwater radiated noise, resulting in a sound pressure level $L_{p,i}(\underline{x}_R, f, t_n)$ at receiver location $\underline{x}_R$ and frequency f.
- At each time step t_n and map location $\underline{x}_R$, the wind generates wind noise resulting in a sound pressure level $L_{p,w}(\underline{x}_R, f, t_n)$.

For the JOMOPANS GES-tool (WP7) it is proposed to generate maps of monthly percentiles (an appropriate selection of from the 5th, 10th, 25th, 50th, 75th, 90th and 95th percentiles) of 1 s snapshots for the one-third octave (base-10) bands from 10 Hz to 20 kHz (and/or weighted sums over these bands) of:

a) the total depth averaged SPL of ships and wind at receiver location $\underline{x}_R$ at time t_n, i.e. the incoherent sum of the contributions of $N_S(t_n)$ ship sources, at different source positions, and of wind noise:

$$L_{p,\mathrm{tot}}(\underline{x}_R, f, t_n) = 10\ \mathrm{dB} \log_{10}\left\{10^{L_{p,w}(\underline{x}_R,f,t_n)/10\ \mathrm{dB}} + \sum_{i=1}^{N_S(t_n)} 10^{L_{p,i}(\underline{x}_R,f,t_n)/10\ \mathrm{dB}}\right\} \quad (6.1)$$

b) the depth averaged SPL of wind noise at receiver location $\underline{x}_R$ at time t_n:

$$L_{p,w}(\underline{x}_R, f, t_n) \quad (6.2)$$

c) the level difference ('excess level') between the total depth averaged SPL of ships and wind and the depth averaged SPL of wind noise alone, at receiver location $\underline{x}_R$ at time t_n:

$$\Delta L(\underline{x}_R, f, t_n) = L_{p,\mathrm{tot}}(\underline{x}_R, f, t_n) - L_{p,w}(\underline{x}_R, f, t_n) \quad (6.3)$$

d) the depth averaged SPL of contributions of selected vessel classes (TYPE) at receiver location $\underline{x}_R$ at time t_n to the total noise:

$$\Delta L_{p,\mathrm{TYPE}}(\underline{x}_R, f, t_n) = 10\ \mathrm{dB} \log_{10}\left\{\sum_{i=1}^{N_{\mathrm{TYPE}}(t_n)} 10^{L_{p,\mathrm{TYPE_i}}(\underline{x}_R,f,t_n)/10\ \mathrm{dB}}\right\} - L_{p,tot}(\underline{x}_R, f, t_n) \quad (6.4)$$

To obtain these monthly percentiles, time series (t_n) of ship and wind noise levels are modelled, on a specified receiver grid ($\underline{x}_R$). The uncertainty in the modelling is explicitly taken into account according to the method described hereafter.

6.1.1 Ship noise:

The sound pressure level $L_{p,i}(\underline{x}_R, f, t_n)$ contribution of each ship is calculated from the difference of the source level $L_{S,i}(f)$ of that ship and the propagation loss $N_{\mathrm{PL},i}(\underline{x}_R, \underline{x}_{S,i}(t_n), f)$ between ship location $\underline{x}_{S,i}(t_n)$ and receiver location $\underline{x}_R$:

$$L_{p,i}(\underline{x}_R, f, t_n) = L_{S,i}(f, t_n) - N_{\mathrm{PL},i}(\underline{x}_R, \underline{x}_{S,i}(t_n), f) \quad (6.5)$$

- Ship locations $\underline{x}_{S,i}(t_n)$ as a function of time are obtained from AIS, an applied either 'exact' or approximated by the nearest source grid position. Uncertainty in ship location contributes to the uncertainty in propagation loss.
- A source level model (updated RANDI3.1c, see section 5.7) provides the mean value $\langle L_{S,i}(f, t_n)\rangle$ and standard deviation $\sigma_{L_S}(f)$ of an assumed normal distribution of source level estimations for ship i at time t_n, based on the AIS parameters vessel type TYPE_i, vessel length L_i and vessel speed $V_i(t_n)$. Note that the uncertainty in the source level estimation of an individual vessel i, applies only ones and that $L_{S,i}$ for each vessel only varies over time through the relation between $L_{S,i}$ and $V_i(t_n)$, not through a time dependent random process.
- A propagation loss model provides the mean value $\langle N_{\mathrm{PL},i}(\underline{x}_R, \underline{x}_{S,i}(t_n), f)\rangle$ and standard deviation $\sigma_{N_{\mathrm{PL},i}}(\underline{x}_R, \underline{x}_{S,i}(t_n), f)$ of an assumed normal distribution of propagation loss estimations between source position $\underline{x}_{S,i}(t_n)$ and receiver position $\underline{x}_{S,i}(t_n)$.
- It is assumed that the final version of the propagation model is validated (and, if necessary calibrated, i.e. bias removed) in such a manner that these uncertainties can be quantified in terms of a statistical distribution. For the time being, we assume that this is a normal distribution.
- Using a fixed source grid $\underline{x}_S$ allows calculating $\langle N_{\mathrm{PL},i}(\underline{x}_R, \underline{x}_S, f)\rangle$ only once and then looking up values $N_{\mathrm{PL},i}(\underline{x}_R, \underline{x}_{S,i}(t_n), f)$ per time step. For fixed grids, the propagation loss N_{PL} may vary over time due to time-variations in the environmental parameters (temperature, wind, etc). We assume that these variations are included in the standard deviation. It still needs to be decided how to quantify the uncertainty $\sigma_{N_{\mathrm{PL},i}}(\underline{x}_R, \underline{x}_{S,i}(t_n), f)$.
- For now, it is proposed to ignore the uncertainty in the propagation loss model. A first check might be to investigate the consequences of a generic overall $\sigma_{L_{p,w}}$ (e.g. of 5 dB) on the monthly percentiles.

6.1.2 Wind noise:

- A wind noise model provides the mean value $\langle L_{p,w}(\underline{x}_R, f, t_n)\rangle$ and standard deviation $\sigma_{L_{p,w}}(f)$ of an assumed normal distribution of wind noise SPL at receiver position $\underline{x}_R$ an time t_n, due to wind speed $V_w(\underline{x}_R, t_n)$. It still needs to be decided how to quantify $\sigma_{L_{p,w}}(f)$.
    - The ERA5 (HRES) modelled wind databases provides one 12 min average of wind speed per hour. In addition, the ECMWF provides mean and spread (standard deviation), computed across a 10 member ensemble (EDA). The EDA has lower resolution than the HRES, with 3 hourly data on a 62 km grid.
- For now, it is proposed to ignore the uncertainty in the wind model. A first check might be to investigate the consequences of a generic overall $\sigma_{L_{p,w}}$ (e.g. of 5 dB) on the monthly percentiles.

6.2 Uncertainty in the percentiles

The monthly percentiles describe the fraction of the time during which $L_{p,\mathrm{tot}}$, $L_{p,w}$ and ΔL and $\Delta L_{p,\mathrm{TYPE}}$ are below the corresponding 'percentile' level. This can be calculated exactly if the calculated SPL time series are exact. However, since the source level and propagation loss calculations are uncertain, the SPL time series and hence also the percentiles are uncertain.

6.3 Uncertainty in SPL (or level difference) time series

Due to the energetic summation over the contributions of multiple sources, the uncertainty in $L_{p,\mathrm{tot}}$, $\Delta L_{p,\mathrm{TYPE}}$ and ΔL cannot be derived analytically from the normal distributions of $L_{p,w}$, $L_{S,i}$ and $N_{\mathrm{PL},i}$.

6.4 'Monte Carlo' approach

The uncertainties can be quantified by means of 'Monte Carlo' simulation, using a set of M random realisations of the individual source contributions and propagation losses per time step. This provides M estimations of the time series of $L_{p,\mathrm{tot}}$, $L_{p,w}$ and ΔL and $L_{p,\mathrm{TYPE}}$, from which the uncertainty (e.g. mean and standard deviation) of the calculated time percentiles can be determined. It still needs to be investigated how many estimations M are required for a stable result.

Each realisation m is calculated from values of $L_{p,w}$, $L_{S,i}$ and $N_{\mathrm{PL},i}$ drawn from the corresponding normal distributions, characterized by mean and standard deviation:

- Wind SPL: $\{L_{p,w}(\underline{x}_R, f, t_n)\}_m$, based on $\langle L_{p,w}(\underline{x}_R, f, t_n)\rangle$ and $\sigma_{L_{p,w}}(f)$, drawn for the first time step and then adjusted for the $V_w(\underline{x}_R, t_n)$
- Ship source level: $\{L_{S,i}(f, t_n)\}_m$, based on $\langle L_{S,i}(f, t_n)\rangle$ and $\sigma_{L_S}(f)$, drawn for the first time step for each vessel and then adjusted for the $V_i(t_n)$
- Propagation loss: $\{N_{\mathrm{PL},i}(\underline{x}_R, \underline{x}_{S,i}(t_n), f)\}_m$, based on $\langle N_{\mathrm{PL},i}(\underline{x}_R, \underline{x}_{S,i}(t_n), f)\rangle$ and $\sigma_{N_{\mathrm{PL},i}}(\underline{x}_R, \underline{x}_{S,i}(t_n), f)$, redrawn for each time step

For each time series realization m, the temporal percentiles $\{L_{p_{\mathrm{tot},q\%}}(\underline{x}_R, f)\}_m$ can be calculated from the time distribution $\{L_{p,\mathrm{tot}}(\underline{x}_R, f, t_n)\}_m$, using e.g. the Matlab command 'prctile'.

From the m realisations of each percentile we than calculate the mean $\langle L_{p_{\mathrm{tot},q\%}}(\underline{x}_R, f)\rangle$ and the standard deviation $\sigma_{L_{p_{\mathrm{tot},q\%}}}(\underline{x}_R, f)$, to get an assessment of the uncertainty in the percentiles.

To avoid having to store the complete time series for each realisation, the time percentiles and their uncertainty can possibly also be quantified from the mean and standard deviation over the realisation per time step, by calculating the time percentiles of $\langle L_{p,\mathrm{tot}}(\underline{x}_R, f, t_n)\rangle$ and of $\langle L_{p,\mathrm{tot}}(\underline{x}_R, f, t_n)\rangle \pm \sigma_{L_{p,\mathrm{tot}}}(\underline{x}_R, f, t_n)$. Both methods will be compared.

6.5 Gervaise et al [2015] approach

Gervaise et al [2015] have proposed a probabilistic shipping sound exposure level (SEL) modelling method, which obtains the PDF of SEL using the sonar equation and statistical relations linking the PDFs of ship traffic density, source levels, and transmission losses to their products and sums. Note that the SEL metric in their paper is related to the metric specified by Jomopans, because SEL and SPL represent integration and averaging respectively of the squared sound pressure over a given time window. However, the time windows (snapshot durations) are selected differently (1 s for Jomopans versus 30 minutes for Gervaise et al [2015]).

Recalling that the probability distribution of the sum of two independent random variables is the convolution of their individual distributions, Gervaise et al [2015] propose a numerical solution of the resulting PDFs via cumulative convolution ($\otimes$) of the individual PDFs:

$$\mathrm{PDF}\left(\frac{p_{\mathrm{tot}}^2}{p_{\mathrm{ref}}^2}\right) = \mathrm{PDF}\left(\sum_{i=1}^{N}\frac{p_i^2}{p_{\mathrm{ref}}^2}\right) = \otimes_{\mathrm{i=1}}^{\mathrm{N}}\mathrm{PDF}\left(\frac{p_i^2}{p_{\mathrm{ref}}^2}\right) \tag{6.6}$$

in which the subsequent convolution steps are:

$$(\mathrm{PDF}_n \otimes \mathrm{PDF}_{n-1})(\chi) = \int_{-\infty}^{\infty}\mathrm{PDF}_n(\xi)\cdot\mathrm{PDF}_{n-1}(\chi-\xi)\mathrm{d}\xi \tag{6.7}$$

Finally, Gervaise et al [2015] suggest in their eq.(7) that the probability density function of the total sound pressure level in a receiver cell is:

$$\mathrm{PDF}(L_{p_{\mathrm{tot}}}) = \frac{\ln 10}{10\ \mathrm{dB}}\left(\frac{p_{\mathrm{tot}}^2}{p_{\mathrm{ref}}^2}\right)\ \mathrm{PDF}\left(\frac{p_{\mathrm{tot}}^2}{p_{\mathrm{ref}}^2}\right) \tag{6.8}$$

However, Gervaise et al [2015] do not detail how the probability functions and the cumulative convolution are implemented in their numerical modelling. Hence, we prefer the 'Monte Carlo' approach proposed above.

6.6 Source level statistics

The input for the shipping noise calculations is obtained from AIS. From the AIS messages received from the majority of the ships in the area we use the following parameters (all subject to uncertainties):

- ship type
- ship length

- geospatial (LAT/LON) location, at a specified time grid
- speed over ground, at a specified time grid

A source level model (chapter 5) provides, for each ship, the acoustic source level spectrum and associated uncertainty (standard deviation). In Jomopans, recent data sets of source level measurements from JASCO, TNO and FOI have been used to derive an updated semi-empirical source level model and to quantify the associated source level PDF. This model is a new version of the RANDI3.1 model, which estimates source level as a function of ship length and speed and ship type.

For efficient acoustic modelling, the sources will be projected on a regular spatial source grid. For each grid cell, the acoustic source is then assumed to be located at the geometric centre, while the receiver grid is defined at the corners of each cell. Uncertainty in ship type, length and speed will contribute to uncertainty in the source level. It is here assumed that this uncertainty can be quantified in terms of a probability density functions (PDF_{L_S}.) which is normally distributed.

6.6.1 Propagation loss statistics

A suitable propagation model is applied to calculate the (mean) propagation loss between the centre position x_S of each source grid cell and each receiver grid position x_R.

This propagation loss calculation is uncertain due to uncertainties in

- the propagation model (numerical accuracy, approximations, etc.)
- the environmental input data (bathymetry, sediment properties, surface properties, sound speed profile, etc.)
- the difference between the source grid position and the actual (GPS) position of the ship

It is here assumed that the final version of the propagation model will be validated and calibrated (i.e. bias removed) in such a manner that these uncertainties can be quantified in terms of a normally distributed $\mathrm{PDF}_{N_{\mathrm{PL}}}$.

Hence, the $\mathrm{PDF}_{N_{\mathrm{PL}}}$ will account for the uncertainty in both the model and environmental input parameters and the statistical variations in the AIS data per grid cell. Assuming that both effects lead to a normal distribution, their variances (σ^2) can be linearly added.

- In the Jomopans T4.2 benchmark scenarios (Chapter 2) it has been shown that the differences between different propagation models for a well-defined benchmark scenario can be smaller than 2 to 5 dB at distances from the sources larger than about 500 m and at frequencies above 50 Hz, depending on the water depth. Towards lower frequencies and shorter distances there are increasingly larger deviations, with a clear bias between models, and it is not yet clear which model is correct.
- The sensitivity of the PL calculations to simplifications in the modelling (e.g. ignoring effects of tidal variations, or of sound speed profile) and to uncertainty in the environmental input parameters is studied in generic benchmark scenarios (chapter 4). The uncertainty in the environmental parameters from external databases is not always clear.
- The variations in the PL calculations associated with the statistics of the source location depends on the size of the source grid cells and the statistics of the source locations in the grid cell. The uncertainty decreases with increasing distance between the receiver and source locations.

6.7 Acoustic metric statistics

The acoustic metrics to be calculated in Jomopans are the 5th, 10th, 25th, 50th, 75th, 90th, and 95th percentiles of the distribution of individual SPL spectra (1 second averages) over one month. If the individual SPL spectra would be exact, these percentiles would provide an indication of the fraction of the time during which a certain SPL is exceeded in that month.

Variations and uncertainty in source levels and propagation losses lead to variations in the individual SPL snapshots. The monthly percentiles for the acoustic metric can then be calculated for each of the snapshot percentiles, e.g. the monthly statistics of the median values (50th percentile) of the snapshots. If the individual snapshots have a wide distribution due to modelling uncertainties, it will be difficult to reliably assess the monthly percentiles of the SPL. Whether this is the case will be clearer after application of the proposed analysis to actual data for the T4.3 validation scenarios.

7 Conclusions and way ahead

This report described the developments in T4.2 of the JOMOPANS project, in which verification benchmarks and sensitivity studies have been carried out to support the selection of the appropriate models, model parameters and input parameters for the future production of North Sea underwater sound maps.

7.1 Model verification:

Test cases 1 and 2 described in chapter 2 have been developed to provide benchmarks for acoustic propagation loss models for shipping noise in a shallow water environment such as the North Sea. They can be used to test the selection of appropriate models and the correct implementation of these models. Comparison of modelling results for these test cases with the solutions provided in this chapter provides insight in the applicability of the selected model and in the uncertainty (or bias) associated with the specific implementation and parametrization of the model. The various model solutions provided by the JOMOPANS WP4 partners illustrate the use of these benchmark test cases.

Test case 3 was developed to test the implementation of the available semi-empirical wind noise source and propagation model and to illustrate the sensitivity of the model output for the main input parameter (wind speed at 10 m above the water surface).

7.2 Model sensitivity studies

When presenting modelled sound maps, it is important to be able to provide insight in the uncertainty in the presented metrics. Chapter 6 describes an approach to deal with the cumulation of uncertainties in models, model parameters and input data.

Chapter 3 describes the results of studies into the effect of the model parameter choices on the uncertainty and provides preliminary recommendations for model parameter choices, aimed at providing sufficiently accurate solutions for the acoustic metric selected in Jomopans project at acceptable computational effort. These choices will be reconsidered after the first comparison of modelling results with measured data from the 2018 validation sites.
The model parameters studied in this chapter are

- the spectral resolution (section 3.1)
- receiver spatial resolution (section 3.2)
- spatial processing (section 3.3)
- temporal resolution (section 3.4)
- spatial source gridding (section 3.5)

Chapter 4 describes studies of the sensitivity of the modelling associated with uncertainties in the modelling associated with the conversion available information of seabed properties to appropriate geo-acoustic parameters. It also describes studies of the consequences of ignoring effects of wind-driven sea surface waves and seasonal sound speed profiles for the uncertainty in the modelled propagation loss.

Chapter 5 describes the available models for calculating the source level of ships on the basis of the parameters that can be extracted from AIS (automatic identification of ships) data. It proposes the development of an updated semi-empirical model, making use of the extensive database of measured ship source levels that has become available thanks to the ECHO (enhancing cetacean habitat and observation) program of the of the Vancouver Fraser Port Authority [MacGillivray et al, 2019].

7.3 Way forward

The model verification and sensitivity studies described in this report provide a useful starting point for experimental validation of the model predictions (T4.3) as well as for the development of the capability to generate sound maps (T4.4).

The total uncertainty in the modelled nose metrics results from the cumulation of uncertainties in models, model parameters and input data. The total modelling is too complex to provide a generic quantitative uncertainty analysis. However, the model validation scenarios against measurements at the North Sea 2018 monitoring locations, combined with the statistical approach described in Chapter 6 will provide quantitative insight in the model uncertainty at a number of North Sea locations.

The model validation approach (T4.3) is as follows:

1. WP4 provides 1st iteration model predictions to WP6 for comparison with the data for the 8 sites at which one month of acoustic data has been obtained (WP5)
2. WP6 carries out the model-data comparison and provide feedback to WP4
3. WP4 investigates and implement possibilities to optimize the selection of models, model parameters and input data, with the aim to reduce observed model-data bias, where applicable
4. WP4 provides 2nd iteration optimized) model predictions to WP6 for comparison with the data for the 2018 sites
5. WP6 and WP4 jointly quantify the remaining uncertainty in the model predictions

Based on the findings of the model verification and sensitivity studies in this report, the authors expect that the following model components may need to be optimized to reduce bias and uncertainty in the model predictions:

- conversion of sediment properties to geo-acoustic parameters, including frequency dependence to account for dispersion and layering in the sediment
- include sea surface losses in the propagation models (both for ships and wind)
- provide one further update of the ship source level model
- further investigate the need for including sound-speed profile effects on the predictions

WP4 will then use the optimized modelling to produce North Sea sound maps for 2019 (T4.4), to be used in the GES (good environmental state) tool (WP7). WP6 will carry out model-data comparisons for the 2019 measurement sites and quantify the uncertainty of the sound maps.

8 Acknowledgement

The authors thank Elizabeth Küsel for making available the data underlying figures 5-7 in [Küsel & Siderius, 2019], used in sections 2.3.4 and 2.4.2 of this report.

9 References

Ainslie, 2005	Ainslie, M. A. (2005). Effect of wind-generated bubbles on fixed range acoustic attenuation in shallow water at 1–4 kHz. *The Journal of the Acoustical Society of America*, *118*(6), 3513-3523
Ainslie, 2010	Ainslie, M.A. (2010). *Principles of Sonar Performance Modeling*. Springer
Ainslie, 2010a	Ainslie, M. A. (2010) "Editorial: Validation of sonar performance assessment tools, in validation of sonar performance assessment tools (workshop held in memory of David E. Weston, 7-9 April 2010)," *Proc. Inst. Acoust*., Part 2, vol. 32, pp.1–8.
Ainslie et al, 2011	Ainslie, M. A., Harrison, C. H., & Zampolli, M. (2011). An Analytical Solution for Signal, Background and Signal to background Ratio for a Low Frequency Active Sonar in a Pekeris Waveguide Satisfying Lambert's Rule.
Ainslie et al, 2016	Ainslie , M.A., Halvorsen, M.B., Dekeling, R.P.A., Laws, R.M., Duncan, A.J., Frankel, A.S., Heaney, K.D., Küsel, E.T., MacGillivray, A.O., Prior, M.K, Sertlek, H.Ö. and Zeddies, D.Z. (2016) "Verification of airgun sound field models for environmental impact assessment," *Proc. Meetings Acoust*., vol. 27, no. 1, pp. 1–13
Ainslie et al, 2018	Ainslie, M.A., Miksis-Olds, J.L., Martin, B., Heaney, K., de Jong, C.A.F., von Benda-Beckmann, A.M., and Lyons, A.P. (2018). "ADEON Underwater Soundscape and Modeling Metadata Standard". Version 1.0. Technical report by JASCO Applied Sciences for ADEON Prime Contract No. M16PC00003. https://doi.org/10.6084/m9.figshare.6792359.v2
Ainslie et al, 2019	Ainslie, M. A., Laws, R. M. and Sertlek H. Ö. (2019). International Airgun Modeling Workshop: Validation of Source Signature and Sound Propagation Models—Dublin (Ireland), July 16, 2016—Problem Description. IEEE Journal of Oceanic Engineering. Digital Object Identifier 10.1109/JOE.2019.2916956
Ainslie et al 2020	Ainslie, M.A., C.A.F. de Jong, S.B. Martin, J.L. Miksis-Olds, J.D. Warren, K.D. Heaney, C.A. Hillis, and A.O. MacGillivray. 2020. ADEON Project Dictionary: Terminology Standard. Document 02075, Version 1.0. Technical report by JASCO Applied Sciences for ADEON, see https://doi.org/10.6084/m9.figshare.12436199.v2
Binnerts et al, 2019	Binnerts, B, de Jong, CAF, Karasalo, I, Östberg, M, Folegot, T, Clorenneq, D, Ainslie, MA, Warner, G, Wang, L (2019) Model benchmarking results for ship noise in shallow water. Proceedings of the 5th Underwater Acoustics Conference and Exhibition UACE2019, Hersonissos, Crete, Greece
Bockelmann et al, 2018	Bockelmann, F.-D., Puls, W., Kleeberg, U., Müller, D. and Emeis, K.-C. (2018), "Mapping mud content and median grain-size of North Sea sediments – A geostatistical approach", *Marine Geology* 397, 60–71
Brooker et al, 2015a	Brooker, A. and Humphrey, V. (2015). "Noise model for radiated noise/source level (intermediate)", report FP7-314394-SONIC Deliverable 2.3 (SOTON-DEL-D2.3-V4.0)
Brooker et al, 2015b	Brooker, A., Humphrey, V., Mumm, H., Jansen, E. and de Jong, C. (2015). "Development of improved noise models for radiated noise/source level using database (Final)", report FP7-314394-SONIC Deliverable 2.4 (SONIC-SOTON-DEL-D2.4-V1.0)
Carey, 2009	Carey, W. (2009) "Lloyd's mirror—image interference effects", Acoustics Today, April 2009, 14-20
Colin et al, 2015	Colin, M., Ainslie, M. Binnerts, B, de Jong, C., Sertlek, Ö, Karasalo, I., Östberg, M., Folegot, T. and Clorennec, D. (2015), "Definition and results of test cases for shipping sound maps", *Proc. IEEE OCEANS 2015* – Genova, https://ieeexplore.ieee.org/document/7271461/
de Jong et al, 2018	de Jong, CAF, Binnerts, B, Östberg, M, Folegot, T, Ainslie, MA (2018) *Jomopans model and data inventory*. Report of the EU INTERREG Joint Monitoring Programme for Ambient Noise North Sea (JOMOPANS).
Farcas et al, 2016	Farcas, A., Thompson, P.M. and Merchant, N.D. (2016), "Underwater noise modelling for environmental impact assessment*", Environmental Impact Assessment Review* 57, 114–122
Fofonoff and Millard, 1983	Fofonoff, N.P. and Millard Jr., R.C. (1983) "Algorithms for computation of fundamental properties of seawater", Unesco technical papers in marine science 44

Gervaise et al, 2015	Gervaise, C., Aulanier, F., Simar, Y. and Roy, N. (2015), “Mapping probability of shipping sound exposure level”, *J. Acoust. Soc. Am.* 137(6), EL429-435
Harrison, 2003	Harrison, C.H. (2003), “Closed-form expressions for ocean reverberation and signal excess with mode stripping and Lambert’s law”, J. Acoust. Soc. Am. 114 (5), 2744–2756
Jansen & de Jong, 2017	Jansen, E. and de Jong, C. (2017). “Experimental Assessment of Underwater Acoustic Source Levels of Different Ship Types”, *IEEE Journal of Oceanic Engineering* 42(2), 439-448
Jensen et al, 2011	Jensen, F.B., Kuperman, W.A., Porter, M.B. and Schmidt, H. (2011), “Computational Ocean Acoustics”, 2nd ed., Springer, New York
Jones et al, 2009	Jones, A.D., Sendt, J. Duncan, A.J., Clarke, P.A. and Maggi, A. (2009), “Modelling the acoustic reflection loss at the rough ocean surface”, Proceedings of ACOUSTICS 2009, Adelaide Australia
Karasalo et al, 2017	Karasalo, I., Östberg, M., Sigray, P., Jalkanen, J.-P., Johansson, L., Liefvendahl, M. and Bensow, R. (2017), “Estimates of source spectra of ships from long term recordings in the Baltic sea”, *Frontiers in Marine Science* · June 2017
Kuo, 1988	Kuo, E. Y. (1988). Sea surface scattering and propagation loss: review, update, and new predictions. *IEEE Journal of Oceanic Engineering*, *13*(4), 229-234
Küsel & Siderius, 2019	Küsel, E.T. and Siderius, M., (2019), “Comparison of Propagation Models for the Characterization of Sound Pressure Fields”, *IEEE Journal of Oceanic Engineering* (DOI: 10.1109/JOE.2018.2884107)
Leroy & Parthiot, 1998	Leroy, C.C. and Parthiot, F. (1998), “Depth-pressure relationship in the oceans and seas”, J. Acoust. Soc. Am. 103(3) pp 1346-1352
Leroy et al, 2008	Leroy, C.C., Robinson, S.P. and Goldsmith, M.J. (2008), “A new equation for the accurate calculation of sound speed in all oceans”, J. Acoust. Soc. Am. 124(5) pp. 2774–2782
MacGillivray et al, 2019	MacGillivray, A.O., Li, Z., Hannay, D.E., Trounce, K.B. and Robinson, O.M. (2019), “Slowing deep-sea commercial vessels reduces underwater radiated noise”, J. Acoust. Soc. Am. 146 (1), pp 340–351
Merchant et al, 2018	Merchant, N., Farcas, A. and Powell, C. (2018) “Acoustic metric specification”, Report of the EU INTERREG Joint Monitoring Programme for Ambient Noise North Sea (JOMOPANS).
Norton & Novarini, 2001	Norton, G. V., & Novarini, J. C. (2001). On the relative role of sea-surface roughness and bubble plumes in shallow-water propagation in the low-kilohertz region. *The Journal of the Acoustical Society of America*, *110*(6), 2946-2955.
Perkins & Thorsos, 2007	Perkins, J. S. and Thorsos, E. I., (2007), “Overview of the reverberation modeling workshops,” *J. Acoust. Soc. Amer.*, 122(5), pp. 3074–3074.
Rees, 2003	Rees, T. (2003) *"C-Squares", a New Spatial Indexing System and its Applicability to the Description of Oceanographic Datasets*, Oceanography 16(1), pp.11-19
Robinson & Wang, 2020	Robinson, S. and Wang, L. (2020), “Standard for Terminology”, Report of the EU INTERREG Joint Monitoring Programme for Ambient Noise North Sea (JOMOPANS).
Sertlek & Ainslie, 2014	Sertlek, H.Ö. and Ainslie, M.A. (2014), “A depth-dependent formula for shallow water propagation”, *J. Acoust. Soc. Am.* 136 (2), pp. 573–582
Sertlek, 2016	Sertlek, H.Ö. (2016) “Aria of the Dutch North Sea - Propagation, source and sound mapping simulations for the Dutch North Sea”, PhD Thesis, Leiden University
Sertlek et al, 2018	Sertlek, H.Ö., Ainslie, M.A. and Heaney, K.D. (2018), “Analytical and Numerical Propagation Loss Predictions for Gradually Range-Dependent Isospeed Waveguides”, *IEEE Journal of Oceanic Engineering*
van Heteren & Van Lancker, 2015	van Heteren, S. and Van Lancker, V. (2015), “Collaborative Seabed-Habitat Mapping: Uncertainty in Sediment Data as an Obstacle in Harmonization”, Chapter 8 of “Collaborative Knowledge in Scientific Research Networks”, ed. Diviaccio et al, IGI Global, Hershey PA, USA

Wales & Heitmeyer, 2002	Wales, S.C. and Heitmeyer, R.M. (2002) “An ensemble source spectra model for merchant ship-radiated noise”, *J. Acoust. Soc. Am.* 111(3), 1211–1231
Weston, 1989	Weston, D. E. (1989). On the losses due to storm bubbles in oceanic sound transmission. *The Journal of the Acoustical Society of America*, *86*(4), 1546-1553
Zampolli et al, 2010	Zampolli, M., Ainslie, M.A. and Schippers, P. (2010). “Scenarios for benchmarking range-dependent active sonar performance models”. *Proc. Institute of Acoustics*, *32* (Pt 2), pp.53-63

Annex A Effect of source depth on ship RNL and SL

The draft international standard ISO DIS 17208-2 summarizes the theory for conversion between deep water Radiated Noise Level (L_{RN}) and Source Level (L_s):

$$L_s = L_{\mathrm{RN}} + \Delta_L \tag{A.1}$$

A simple approximation, valid when $kd_s \ll 1$) is:

$$\Delta_L \approx 20log_{10}\left(\frac{1}{2\,sin(kd_s\,sin\,\alpha)}\right)\,dB = -10log_{10}\left(4sin^2\,(kd_s\,sin\alpha)\right)\,\mathrm{dB} \tag{A.2}$$

This may be approximated by:

$$\Delta_L \approx \begin{cases} -10\log_{10}(4sin^2\,(kd_s\,sin\alpha))\;dB & kd_s\sin\alpha \leq 3\pi/4 \\ -10\log_{10}(2)\;dB & kd_s\,\sin\alpha > 3\pi/4 \end{cases} \tag{A.3}$$

Here $k = 2\pi/c$ is the acoustic wavenumber, d_s the source depth and α the vertical observation angle, see eq.(A.4).

Annex A.1 JASCO'S ECHO ship source level dataset

The hydrophone depth (d_h) is 248 m and measurements are carried out following the ANSI-ASA S12.64:2009 (Part 1) Grade C method. This requires hydrophone angles $\alpha = 20° \pm 5°$, hence ships are assumed to be passing the hydrophone at a closest distance (D_{cpa}):

$$D_{CPA} = d_h/\tan(\alpha) \tag{A.4}$$

α	15°	20°	25°
D_{CPA}	926 m	681 m	532 m

Eq. (A.2), for a single (mean) source depth leads to the spectrum of $L_{\mathrm{RN}} - L_s = -\Delta_L$ shown in Figure A.1.

JASCO uses a Gaussian source depth distribution, with mean value d_s and standard deviation $\sigma_s = d_s/0.85/4$, limited to interval [1 m, 24 m]. Taking 1000 realisations from this distribution and power averaging over the calculation results leads to the spectra shown in Figure A.2.

Hence, hydrophone angle variations lead to ± 2 dB uncertainty in the reported source level for the ideal deep water scenario. Uncertainty of applying propagation loss modelling needs another assessment.

Mean source depth variations (i.e. variations in kd_s) lead to frequency-dependent uncertainty, which seems to be also limited to ± 2 dB for approximately $kd_s > 2$. For $c = 1500\frac{\mathrm{m}}{\mathrm{s}}$, $kd_s = 2$ is equivalent to $f_s \approx (477\ \mathrm{m}\cdot\mathrm{Hz})/d_s$. Source depth has no significant (> 2 dB) effect above f_s

d_s	1.5 m	2.5 m	5 m	10 m
f_s	318 Hz	191 Hz	95 Hz	48 Hz

The 'smoothing' from this Gaussian distribution seems to be approximated well (≤ 1 dB) by eq.(A.3), see Figure A.3

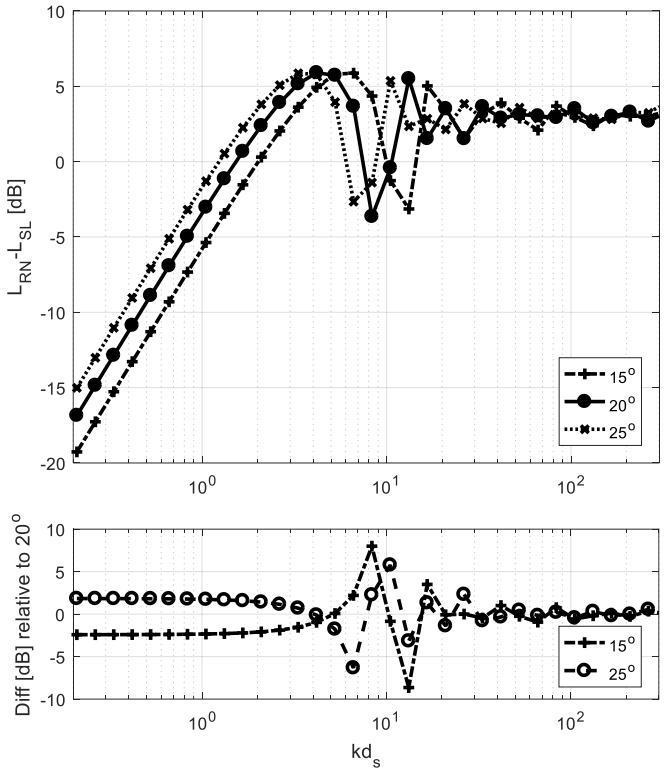

Figure A.1: correction $-\Delta_L = L_{\mathrm{RN}} - L_s$, power averaged over 11 logarithmically spaced frequency lines per one-third octave band, for three observation angles, according to eq.(A.2).

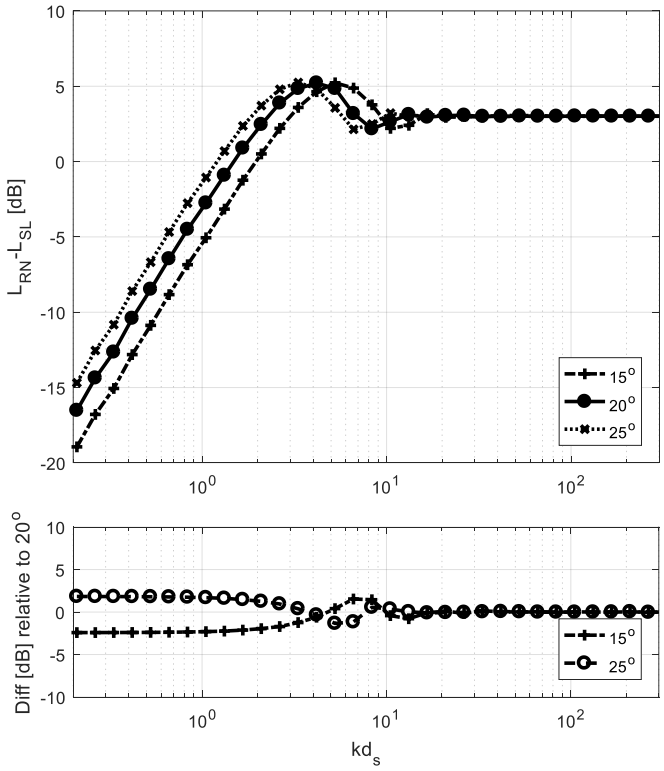

Figure A.2: correction $-\Delta_L = L_{\mathrm{RN}} - L_s$, power averaged over 11 logarithmically spaced frequency lines per one-third octave band and over a Gaussian source depth distribution, for three observation angles, according to eq.(A.2).

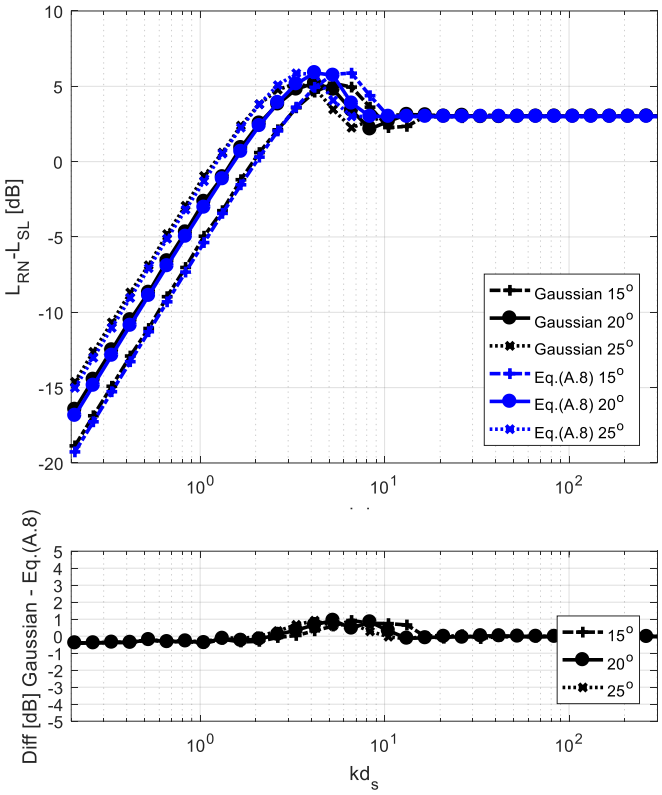

Figure A.3: correction $-\Delta_L = L_{RN} - L_s$, from figure A.2, compared with approximations according to eq.(A.3).

Annex A.2 Source depth conversion

A conversion of SL reported for one (mean) source depth $d_{s,1}$ to another source depth $d_{s,2}$ can be done by applying the correction

$$L_s(d_{s,2}) \approx L_s(d_{s,1}) + \Delta_L(d_{s,2}) - \Delta_L(d_{s,1}) \quad \text{(A.5)}$$

Where Δ_L can be calculated from eq.(A.3).

Annex A.3 EXAMPLE

As an example, the RANDI 3.1 SL model for a tug, length 100 feet (30 m) at its reference speed, for the default RANDI 3.1 source depth of 6m, is converted to the SL of the same tug, at the ECHO mean source depth of 2.27 m, assuming that it was measured at a hydrophone angle $\alpha = 20°$.

In the lowest frequency bands the difference is approximately $-20\log_{10}\left(\frac{d_{s,2}}{d_{s,1}}\right)\text{dB} \approx 8\text{ dB}$

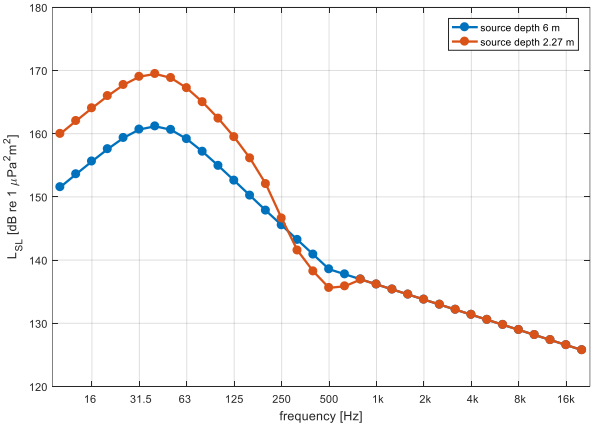

Figure A.4: RANDI 3.1a source level for a tug with a source depth of 6 m, and the source level after conversion to a source depth of 2.27 m (using eq.A.5)

Annex B Vessel types

Table B-1: AIS Vessel Type ID and Vessel Types

AIS TYPE ID	TYPE NAME	AIS TYPE SUMMARY	TYPE DESCRIPTION
10-19	Reserved	Unspecified	
20-28	Wing In Grnd	Wing in Grnd	Wing In Ground Effect Vessel
29	SAR Aircraft	Search and Rescue	
30	Fishing	Fishing	Fishing Vessel Trawler Fishery Protection/Research Fish Carrier Fish Factory Factory Trawler Fish Storage Barge Fishery Research Vessel Fishery Patrol Vessel Fishery Support Vessel
31	Tug	Tug	Towing Vessel Tug/Tender Tug/Supply Vessel Tug/Fire Fighting Vessel Tug Tug/Pilot Ship Anchor Handling Salvage Tug Towing/Pushing Tug/Ice Breaker Tractor Tug Tug/Support Articulated Pusher Tug
32	Tug	Tug	
33	Dredger	Special Craft	Suction Hopper Dredger Dredger Drill Ship Grab Hopper Dredger Grab Dredger Sand Suction Dredger Hopper Dredger Cutter Suction Dredger Cutter Suction Hopper Dredger Suction Dredger Bucket Dredger Trailing Suction Hopper Dredge Trailing Suction Dredger Inland Dredger Drilling Jack Up Bucket Ladder Dredger Drill Barge Bucket Hopper Dredger Bucket Dredger Pontoon Bucket Wheel Suction Dredger Dredging Pontoon Backhoe Dredger Suction Dredger Pontoon Water Jet Dredging Pontoon Grab Dredger Pontoon Kelp Dredger
34	Dive Vessel	Special Craft	Diving Support Vessel
35	Military Ops	Special Craft	Naval/Naval Auxiliary Vessel Naval Auxiliary Tug Logistics Naval Vessel Mine Hunter Minesweeper

			Combat Vessel Command Vessel Naval Salvage Vessel Torpedo Recovery Vessel Naval Research Vessel Naval Patrol Vessel Troopship Radar Vessel
36	Sailing Vessel	Sailing Vessel	Sailing Vessel
37	Pleasure Craft	Pleasure Craft	Yacht Museum Ship Exhibition Ship Floating Hotel/Restaurant Theatre Vessel
38	Reserved	Unspecified	
39	Reserved	Unspecified	
40-49	High-Speed Craft	High-Speed Craft	Hydrofoil Hovercraft
50	Pilot Vessel	Special Craft	
51	SAR	Search and Rescue	Salvage/Rescue Vessel Offshore Safety Vessel Standby Safety Vessel
52	Tug	Tug	Icebreaker Inland Tug Pusher Tug
53	Port Tender	Special Craft	Tender Crew Boat Pilot Ship Supply Tender
54	Anti-Pollution	Special Craft	Pollution Control Vessel
55	Law Enforce	Special Craft	Patrol Vessel
56	Local Vessel	Special Craft	
57	Local Vessel	Special Craft	
58	Medical Trans	Special Craft	Hospital Ship
59	Special Craft	Special Craft	Multi Purpose Offshore Vessel Barge Carrier Heavy Lift Vessel Special Vessel Maintenance Vessel Pipe Layer Waste Disposal Vessel Supply Vessel Training Ship Floating Storage/Production Radio Ship Research/Survey Vessel Repair Ship Support Vessel Fire Fighting Tractor Tug Landing Craft Floating Crane Fire Fighting/Supply Vessel Whaler Multi-Purpose Vessel Tank-Cleaning Vessel Mining Vessel Fire Fighting Vessel Paddle Ship Anchor Handling Vessel Nuclear Fuel Carrier Sludge Carrier Whale Factory Utility Vessel Work Vessel Platform Mission Ship

			Buoy-Laying Vessel Well Stimulation Vessel Motor Hopper Cable Layer Anchor Handling/Fire Fighting Crane Ship Inland Supply Vessel Offshore Supply Ship Trenching Support Vessel Offshore Construction Jack Up Pile Driving Vessel Replenishment Vessel Construction Support Vessel Pipelay Crane Vessel Crane Barge Work Pontoon Production Testing Vessel Floating Sheerleg Mooring Vessel Diving Support Platform Support Jack Up Sealer Trans Shipment Vessel Floating Linkspan Crane Jack Up Pumping Platform Air Cushion Vessel Power Station Vessel Supply Jack Up Radar Platform Jacket Launching Pontoon Pipe Layer Platform Pipe Burying Vessel Air Cushion Patrol Vessel Air Cushion Work Vessel Pearl Shells Carrier Steam Supply Pontoon Incinerator Jack Up Barge Desalination Pontoon Grain Elevating Pontoon
60-69	Passenger	Passenger	Passengers Ship Inland Passengers Ship Inland Ferry Floating Hotel Ferry Ro-Ro/Passenger Ship Accommodation Ship Accommodation Barge Accommodation Jack Up Accommodation Vessel Passengers Landing Craft Houseboat Accommodation Platform Air Cushion Passenger Ship Air Cushion Ro-Ro/Passenger Sh
70	Cargo	Cargo	Passenger/Cargo Ship Livestock Carrier Bulk Carrier Ore Carrier General Cargo Wood Chips Carrier Container Ship Ro-Ro Cargo Reefer Heavy Load Carrier Barge

			Ro-Ro/Container Carrier Inland Cargo Cement Carrier Reefer/Containership Vegetable/Animal Oil Tanker Obo Carrier Vehicles Carrier Inland Ro-Ro Cargo Ship Rail/Vehicles Carrier Pallet Carrier Cargo Barge Hopper Barge Deck Cargo Ship Cargo/Containership Aggregates Carrier Limestone Carrier Ore/Oil Carrier Self Discharging Bulk Carrier Deck Cargo Pontoon Bulk Carrier With Vehicle Deck Pipe Carrier Cement Barge Stone Carrier Bulk Storage Barge Aggregates Barge Timber Carrier Bulker Trans Shipment Barge Powder Carrier Cabu Carrier Vehicle Carrier Cargo
71	Cargo – Hazard A (Major)	Cargo	
72	Cargo – Hazard B	Cargo	
73	Cargo – Hazard C (Minor)	Cargo	
74	Cargo – Hazard D (Recognizable)	Cargo	
75-79	Cargo	Cargo	
80	Tanker	Tanker	Tanker Asphalt/Bitumen Tanker Chemical Tanker Crude Oil Tanker Inland Tanker Fruit Juice Tanker Bunkering Tanker Wine Tanker Oil Products Tanker Oil/Chemical Tanker Water Tanker Tank Barge Edible Oil Tanker Lpg/Chemical Tanker Shuttle Tanker CO_2 Tanker
81	Tanker – Hazard A (Major)	Tanker	
82	Tanker – Hazard B	Tanker	
83	Tanker – Hazard C (Minor)	Tanker	
84	Tanker – Hazard D (Recognizable)	Tanker	LNG Tanker LPG Tanker Gas Carrier
85-89	Tanker	Tanker	
90-99	Other	Other	

Table B-2: Marine Traffic Vessel Sub-Type description

ID	Sub-Type	ID	Sub-Type	ID	Sub-Type
1	Wing In Ground Effect Vessel	**80**	Pilot Ship	**159**	Inland Passengers Ship
2	Fishing Vessel	**81**	Supply Tender	**160**	Inland Ferry
3	Trawler	**82**	Pollution Control Vessel	**161**	Floating Hotel
4	Fishery Protection/Research	**83**	Patrol Vessel	**162**	Ferry
5	Fish Carrier	**84**	Hospital Ship	**163**	Ro-Ro/Passenger Ship
6	Fish Factory	**85**	Multi Purpose Offshore Vessel	**164**	Accommodation Ship
7	Factory Trawler	**86**	Barge Carrier	**165**	Accommodation Barge
8	Fish Storage Barge	**87**	Heavy Lift Vessel	**166**	Accommodation Jack Up
9	Fishery Research Vessel	**88**	Special Vessel	**167**	Accommodation Vessel
10	Fishery Patrol Vessel	**89**	Maintenance Vessel	**168**	Passengers Landing Craft
11	Fishery Support Vessel	**90**	Pipe Layer	**169**	Houseboat
12	Towing Vessel	**91**	Waste Disposal Vessel	**170**	Accommodation Platform
13	Tug/Tender	**92**	Supply Vessel	**171**	Air Cushion Passenger Ship
14	Tug/Supply Vessel	**93**	Training Ship	**172**	Air Cushion Ro-Ro/Passenger Ship
15	Tug/Fire Fighting Vessel	**94**	Floating Storage/Production	**173**	Passenger/Cargo Ship
16	Tug	**95**	Radio Ship	**174**	Livestock Carrier
17	Tug/Pilot Ship	**96**	Research/Survey Vessel	**175**	Bulk Carrier
18	Anchor Handling Salvage Tug	**97**	Repair Ship	**176**	Ore Carrier
19	Towing/Pushing	**98**	Support Vessel	**177**	General Cargo
20	Tug/Ice Breaker	**99**	Fire Fighting Tractor Tug	**178**	Wood Chips Carrier
21	Tractor Tug	**100**	Landing Craft	**179**	Container Ship
22	Tug/Support	**101**	Floating Crane	**180**	Ro-Ro Cargo
23	Articulated Pusher Tug	**102**	Fire Fighting/Supply Vessel	**181**	Reefer
24	Suction Hopper Dredger	**103**	Whaler	**182**	Heavy Load Carrier
25	Dredger	**104**	Multi-Purpose Vessel	**183**	Barge
26	Drill Ship	**105**	Tank-Cleaning Vessel	**184**	Ro-Ro/Container Carrier
27	Grab Hopper Dredger	**106**	Mining Vessel	**185**	Inland Cargo
28	Grab Dredger	**107**	Fire Fighting Vessel	**186**	Cement Carrier
29	Sand Suction Dredger	**108**	Paddle Ship	**187**	Reefer/Containership
30	Hopper Dredger	**109**	Anchor Handling Vessel	**188**	Vegetable/Animal Oil Tanker
31	Cutter Suction Dredger	**110**	Nuclear Fuel Carrier	**189**	Obo Carrier
32	Cutter Suction Hopper Dredger	**111**	Sludge Carrier	**190**	Vehicles Carrier
33	Suction Dredger	**112**	Whale Factory	**191**	Inland Ro-Ro Cargo Ship
34	Bucket Dredger	**113**	Utility Vessel	**192**	Rail/Vehicles Carrier
35	Trailing Suction Hopper Dredge	**114**	Work Vessel	**193**	Pallet Carrier

36	Trailing Suction Dredger	**115**	Platform	**194**	Cargo Barge
37	Inland Dredger	**116**	Mission Ship	**195**	Hopper Barge
38	Drilling Jack Up	**117**	Buoy-Laying Vessel	**196**	Deck Cargo Ship
39	Bucket Ladder Dredger	**118**	Well Stimulation Vessel	**197**	Cargo/Containership
40	Drill Barge	**119**	Motor Hopper	**198**	Aggregates Carrier
41	Bucket Hopper Dredger	**120**	Cable Layer	**199**	Limestone Carrier
42	Bucket Dredger Pontoon	**121**	Anchor Handling/Fire Fighting	**200**	Ore/Oil Carrier
43	Bucket Wheel Suction Dredger	**122**	Crane Ship	**201**	Self Discharging Bulk Carrier
44	Dredging Pontoon	**123**	Inland Supply Vessel	**202**	Deck Cargo Pontoon
45	Backhoe Dredger	**124**	Offshore Supply Ship	**203**	Bulk Carrier With Vehicle Deck
46	Suction Dredger Pontoon	**125**	Trenching Support Vessel	**204**	Pipe Carrier
47	Water Jet Dredging Pontoon	**126**	Offshore Construction Jack Up	**205**	Cement Barge
48	Grab Dredger Pontoon	**127**	Pile Driving Vessel	**206**	Stone Carrier
49	Kelp Dredger	**128**	Replenishment Vessel	**207**	Bulk Storage Barge
50	Diving Support Vessel	**129**	Construction Support Vessel	**208**	Aggregates Barge
51	Naval/Naval Auxiliary Vessel	**130**	Pipelay Crane Vessel	**209**	Timber Carrier
52	Naval Auxiliary Tug	**131**	Crane Barge	**210**	Bulker
53	Logistics Naval Vessel	**132**	Work Pontoon	**211**	Trans Shipment Barge
54	Mine Hunter	**133**	Production Testing Vessel	**212**	Powder Carrier
55	Minesweeper	**134**	Floating Sheerleg	**213**	Cabu Carrier
56	Combat Vessel	**135**	Mooring Vessel	**214**	Vehicle Carrier
57	Command Vessel	**136**	Diving Support Platform	**215**	Cargo
58	Naval Salvage Vessel	**137**	Support Jack Up	**216**	Tanker
59	Torpedo Recovery Vessel	**138**	Sealer	**217**	Asphalt/Bitumen Tanker
60	Naval Research Vessel	**139**	Trans Shipment Vessel	**218**	Chemical Tanker
61	Naval Patrol Vessel	**140**	Floating Linkspan	**219**	Crude Oil Tanker
62	Troopship	**141**	Crane Jack Up	**220**	Inland Tanker
63	Radar Vessel	**142**	Pumping Platform	**221**	Fruit Juice Tanker
64	Sailing Vessel	**143**	Air Cushion Vessel	**222**	Bunkering Tanker
65	Yacht	**144**	Power Station Vessel	**223**	Wine Tanker
66	Museum Ship	**145**	Supply Jack Up	**224**	Oil Products Tanker
67	Exhibition Ship	**146**	Radar Platform	**225**	Oil/Chemical Tanker
68	Floating Hotel/Restaurant	**147**	Jacket Launching Pontoon	**226**	Water Tanker
69	Theatre Vessel	**148**	Pipe Layer Platform	**227**	Tank Barge
70	Hydrofoil	**149**	Pipe Burying Vessel	**228**	Edible Oil Tanker
71	Hovercraft	**150**	Air Cushion Patrol Vessel	**229**	Lpg/Chemical Tanker
72	Salvage/Rescue Vessel	**151**	Air Cushion Work Vessel	**230**	Shuttle Tanker
73	Offshore Safety Vessel	**152**	Pearl Shells Carrier	**231**	Co2 Tanker

74	Standby Safety Vessel	**153**	Steam Supply Pontoon	**232**	Lng Tanker
75	Icebreaker	**154**	Incinerator	**233**	Lpg Tanker
76	Inland Tug	**155**	Jack Up Barge	**234**	Gas Carrier
77	Pusher Tug	**156**	Desalination Pontoon		
78	Tender	**157**	Grain Elevating Pontoon		
79	Crew Boat	**158**	Passengers Ship		